University of Alberta

IMPROVED MARKOV CHAIN MODELING OF THE RAYLEIGH FADING CHANNEL

by

Robert W. Carruthers ©

A thesis submitted to the Faculty of Graduate Studies and Research in partial fulfillment of the requirements for the degree of **Master of Science**.

Department of Electrical & Computer Engineering

Edmonton, Alberta
Spring 2007

Library and
Archives Canada

Published Heritage
Branch

395 Wellington Street
Ottawa ON K1A 0N4
Canada

Bibliothèque et
Archives Canada

Direction du
Patrimoine de l'édition

395, rue Wellington
Ottawa ON K1A 0N4
Canada

Your file Votre référence
ISBN: 978-0-494-29942-5
Our file Notre référence
ISBN: 978-0-494-29942-5

NOTICE:
The author has granted a non-exclusive license allowing Library and Archives Canada to reproduce, publish, archive, preserve, conserve, communicate to the public by telecommunication or on the Internet, loan, distribute and sell theses worldwide, for commercial or non-commercial purposes, in microform, paper, electronic and/or any other formats.

The author retains copyright ownership and moral rights in this thesis. Neither the thesis nor substantial extracts from it may be printed or otherwise reproduced without the author's permission.

AVIS:
L'auteur a accordé une licence non exclusive permettant à la Bibliothèque et Archives Canada de reproduire, publier, archiver, sauvegarder, conserver, transmettre au public par télécommunication ou par l'Internet, prêter, distribuer et vendre des thèses partout dans le monde, à des fins commerciales ou autres, sur support microforme, papier, électronique et/ou autres formats.

L'auteur conserve la propriété du droit d'auteur et des droits moraux qui protège cette thèse. Ni la thèse ni des extraits substantiels de celle-ci ne doivent être imprimés ou autrement reproduits sans son autorisation.

In compliance with the Canadian Privacy Act some supporting forms may have been removed from this thesis.

While these forms may be included in the document page count, their removal does not represent any loss of content from the thesis.

Conformément à la loi canadienne sur la protection de la vie privée, quelques formulaires secondaires ont été enlevés de cette thèse.

Bien que ces formulaires aient inclus dans la pagination, il n'y aura aucun contenu manquant.

Canada

to my parents

Abstract

A significant source of signal degradation in wireless systems is multipath fading. Fading can be described stochastically, most often as a Rayleigh process. The multivariate Rayleigh is unknown or intractable, a fact which has motivated research into modeling the multipath fading process with Markov chains. The amplitude-based finite state Markov chain has been explored as a fading channel model in a wide number of papers in the literature. It has been found to accurately model the first-order statistics of the fading channel, but not the autocorrelation function. In order to improve on the limitations of the amplitude-based Markov chain model, a new state-space is studied in detail, one that is based on both the amplitude and rate-of-change of the fading process. This new state-space is used as the basis for Markov chain models of the Rayleigh fading process, as well as the underlying complex Gaussian process. It is found that Markov chains based on the new state-space offer significant improvements over the amplitude-based state-space of previous models.

Acknowledgements

I wish to express my thanks to my supervisor Dr. Norman C. Beaulieu for suggesting this research topic to me, as well as his guidance, feedback, and financial support throughout the research process. Thanks also to Jeremiah, David, Amir, Niranjan, Reza, Pavel, and all the other member of the *i*CORE Wireless Communications Laboratory, for their assistance in matters both great and small.

Thanks to my friends, past and present, for making my many years at the University of Alberta enjoyable ones.

Finally, thanks to my parents, for their support and encouragement in everything I do.

This thesis was financially supported though the Natural Sciences and Engineering Research Council of Canada (NSERC) and the Alberta Informatics Circle of Research Excellence (*i*CORE).

Table of Contents

1 Introduction **1**

1.1 Introduction 1

1.2 Thesis Outline 4

1.2.1 Summary of Chapter 2 4

1.2.2 Summary of Chapter 3 5

1.2.3 Summary of Chapter 4 6

1.2.4 Summary of Chapter 5 7

1.3 Contributions 7

1.4 Notation 8

2 Background **10**

2.1 Introduction 10

2.2 Statistical Theory 10

2.2.1 Introduction 10

2.2.2 Gaussian Distributions 11

2.2.3 Rayleigh Distributions 11

2.2.4 Joint Distributions with Derivatives 13

2.2.5 Stochastic Processes 17

2.2.6 Conclusion 19

2.3 Modeling the Wireless Channel 19

2.3.1 Introduction 19

2.3.2 Deriving the Fading Model 20
2.3.3 3-D Scattering Model 24
2.3.4 Ricean Fading Model 24
2.3.5 Nakagami-m Fading Channel 27
2.4 Markov Chains 28
2.4.1 Introduction 28
2.4.2 Markov Chain Model Elements 28
2.4.3 Invariant Probability 31
2.4.4 Autocorrelation 32
2.5 Conclusion 33

3 The History of Markov Modeling for Fading Channels **34**
3.1 Introduction 34
3.2 Early Markov Chain Models 35
3.2.1 Gilbert-Elliott Model 35
3.2.2 Fritchman 36
3.3 Markov Chain Models of the Fading Channel 38
3.3.1 Introduction 38
3.3.2 Swarts and Ferreira 38
3.3.3 Wang and Moayeri 39
3.3.4 Wang and Chang 43
3.3.5 Zorzi, Rao, and Milstein 44
3.3.6 Zhang and Kassam 46
3.3.7 Tan and Beaulieu 48
3.3.8 Bergamo, Maniezzo, Giavanardi, Mazzini, and Zorzi 51
3.3.9 Hueda and Rodríguez 53
3.3.10 Lin and Tseng 54
3.3.11 Conclusion 56
3.4 Markov Chain Models in Practice 56

3.4.1 Introduction . . . 56
3.4.2 Liu and El Zarki . . . 58
3.4.3 Babich . . . 59
3.4.4 Galluccio, Licandro, Morabito, and Schembra . . . 60
3.4.5 Rossi, Badia, and Zorzi . . . 60
3.4.6 Conclusion . . . 63
3.5 Conclusion . . . 63

4 Markov Chain Modeling of the Complex Gaussian Fading Process 65
4.1 Introduction . . . 65
4.2 First-Order Markov Chain Model . . . 66
4.2.1 Introduction . . . 66
4.2.2 Computing the Markov Chain Model . . . 66
4.2.3 Model Analysis . . . 71
4.2.4 3-DISORA Markov Chain Model . . . 80
4.2.5 Modeling the Complex Gaussian Fading Envelope . . . 83
4.2.6 Conclusion . . . 93
4.3 Second-Order Markov Chain Model . . . 94
4.3.1 Introduction . . . 94
4.3.2 Computing the Markov Chain Model . . . 94
4.3.3 Model Analysis . . . 97
4.3.4 Conclusion . . . 102
4.4 Conclusion . . . 102

5 Markov Chain Modeling of the Rayleigh Fading Envelope Process 104
5.1 Introduction . . . 104
5.2 First-Order Markov Chain Model . . . 105
5.2.1 Introduction . . . 105
5.2.2 Computing the Markov Chain Model . . . 105
5.2.3 Model Analysis . . . 108

5.2.4 Conclusion 121
5.3 Second-Order Markov Chain Model 122
5.3.1 Introduction 122
5.3.2 Computing the Markov Chain Model 123
5.3.3 Model Analysis 125
5.3.4 Conclusion 130
5.4 Conclusion 130

6 Conclusions **132**
6.1 Introduction 132
6.2 Review of Contributions 133
6.3 Suggestions for Future Work 136

A Numerical Integration of Multivariate Gaussian Distributions **139**

B Numerical Integration of the Joint Distribution of Correlated Rayleigh Random Variables and Their Derivatives **142**
B.1 Two Correlated Rayleigh Random Variables 142
B.2 Three Correlated Rayleigh Random Variables 145

References **147**

List of Tables

4.1 Numerical verification of the stationarity of the first-order Markov chain model of the ISORA Gaussian fading process. 74
4.2 Numerical verification of the stationarity of the second-order Markov chain model of the ISORA Gaussian fading process. 98

5.1 Numerical verification of the stationarity of the first-order Markov chain model of the ISORA Rayleigh fading process. 111
5.2 Numerical verification of the stationarity of the second-order Markov chain model of the ISORA Rayleigh fading process. 126

List of Figures

1.1 Illustration of urban signal scattering. 3

2.1 Rayleigh PDF. 22
2.2 Power spectra of the electric field component. 22
2.3 3-DISORA model autocorrelation compared to ISORA model autocorrelation. 25
2.4 First-order distribution of the Ricean channel model as parameter K increases. 26
2.5 First-order distribution of the Nakagami-m fading channel model for different values of parameter m. 27

3.1 Diagram of the Fritchman state-space partitioning scheme. 37
3.2 Transition diagram of the Fritchman model with one error state. 37
3.3 Example of uniform partitioning of the amplitude of the Rayleigh fading channel for $N = 8$ states. 40
3.4 Example of equiprobable partitioning of the amplitude of the Rayleigh fading channel for $N = 8$ states. 42
3.5 Measured signal, two-layer Markov chain model simulated signal, and single-layer Markov chain simulated signal envelopes from Lin and Tseng [1]. 57
3.6 Example of the partitioning scheme from Rossi, Badia, and Zorzi [2], for $k = 6$. 62

4.1 The first-order distribution of the Markov chain model of the Gaussian fading process, for various values of n. 73

4.2 Autocorrelation of the Markov chain model of the ISORA Gaussian fading process for increasing values of m, $n = 10$, and $f_DT = 0.10$. 76

4.3 Autocorrelation of the Markov chain model of the ISORA Gaussian fading process for increasing values of m, $n = 15$, and $f_DT = 0.10$. 76

4.4 Autocorrelation of the Markov chain model of the ISORA Gaussian fading process for increasing values of n, $m = 5$, and $f_DT = 0.10$. 77

4.5 Autocorrelation of the Markov chain model of the ISORA Gaussian fading process for increasing values of n, $m = 10$, and $f_DT = 0.10$. 77

4.6 ISORA Gaussian Markov chain model autocorrelation for various values of sample spacing T (sec), $n = 10$, $m = 10$, and $f_D = 100$ Hz. 78

4.7 ISORA Gaussian Markov chain model autocorrelation for various values of sample spacing T (sec), $n = 15$, $m = 10$, and $f_D = 100$ Hz. 78

4.8 ISORA Gaussian Markov chain model autocorrelation for various values of sample spacing T (sec), $n = 15$, $m = 5$, and $f_D = 100$ Hz. 79

4.9 ISORA Gaussian Markov chain model autocorrelation for various values of sample spacing T (sec), $n = 10$, $m = 5$, and $f_D = 100$ Hz. 79

4.10 Autocorrelation of the Markov chain model of the 3-DISORA Gaussian fading channel, compared to the autocorrelation of the ISORA Markov chain model, for $n = 10$, $m = 3$, and $f_DT = 0.10$. 81

4.11 Autocorrelation of the Markov chain model of the 3-DISORA Gaussian fading channel, compared to the autocorrelation of the ISORA Markov chain model, for $n = 10$, $m = 5$, and $f_DT = 0.10$. 81

4.12 Autocorrelation of the Markov chain model of the 3-DISORA Gaussian fading channel, compared to the autocorrelation of the ISORA Markov chain model, for $n = 15$, $m = 3$, and $f_DT = 0.10$. 82

4.13 Autocorrelation of the Markov chain model of the 3-DISORA Gaussian fading channel, compared to the autocorrelation of the ISORA Markov chain model, for $n = 15$, $m = 5$, and $f_D T = 0.10$. 82

4.14 The first-order distribution of the Markov chain model of the envelope fading process, based on the Markov chain model of the Gaussian fading process, for various values of n. 86

4.15 Autocorrelation of the Markov chain model of the ISORA Rayleigh fading envelope process, based on the Markov chain model of the complex Gaussian fading process, for increasing values of m, $n = 10$, and $f_D T = 0.10$. . 88

4.16 Autocorrelation of the Markov chain model of the ISORA Rayleigh fading envelope process, based on the Markov chain model of the complex Gaussian fading process, for increasing values of m, $n = 15$, and $f_D T = 0.10$. . 88

4.17 Autocorrelation of the Markov chain model of the ISORA Rayleigh fading envelope process, based on the Markov chain model of the complex Gaussian fading process, for increasing values of n, $m = 5$, and $f_D T = 0.10$. 89

4.18 Autocorrelation of the Markov chain model of the ISORA Rayleigh fading envelope process, based on the Markov chain model of the complex Gaussian fading process, for increasing values of n, $m = 10$, and $f_D T = 0.10$. . 89

4.19 Autocorrelation of the Markov chain model of the ISORA Rayleigh fading envelope process, based on the Markov chain model of the complex Gaussian fading process, for various values of sample spacing T (sec), $n = 10$, $m = 10$, and $f_D = 100$ Hz. 91

4.20 Autocorrelation of the Markov chain model of the ISORA Rayleigh fading envelope process, based on the Markov chain model of the complex Gaussian fading process, for various values of sample spacing T (sec), $n = 15$, $m = 5$, and $f_D = 100$ Hz. 91

4.21 Autocorrelation of the Markov chain model of the ISORA Rayleigh fading envelope process, based on the Markov chain model of the complex Gaussian fading process, for various values of sample spacing T (sec), $n = 10$, $m = 5$, and $f_D = 100$ Hz. 92

4.22 Fading profile showing the sample spacing resulting at $f_D T = 0.18$. 92

4.23 Autocorrelation of the second-order Markov chain model of the ISORA Gaussian fading process for various values of T (sec), $n = 5$, $m = 3$, and $f_D = 100$ Hz. 100

4.24 Autocorrelation of the second-order Markov chain model of the ISORA Gaussian fading process for various values of T (sec), $n = 5$, $m = 5$, and $f_D = 100$ Hz. 100

4.25 Autocorrelation of the second-order Markov chain model of the ISORA Gaussian fading process for various values of T (sec), $n = 6$, $m = 3$, and $f_D = 100$ Hz. 101

4.26 Autocorrelation of the Markov chain model of the ISORA Rayleigh fading envelope process, based on a second-order Markov chain model of the complex Gaussian fading process, for various values of sample spacing T (sec), $n = 5$, $m = 3$, and $f_D = 100$ Hz. 101

5.1 The first-order distribution of the Markov chain model of the Rayleigh fading process, for various values of n. 110

5.2 Autocorrelation of the Markov chain model of the ISORA Rayleigh fading process for increasing values of m, $n = 10$, and $f_D T = 0.10$. 112

5.3 Autocorrelation of the Markov chain model of the ISORA Rayleigh fading process for increasing values of m, $n = 15$, and $f_D T = 0.10$. 112

5.4 Autocorrelation of the Markov chain model of the ISORA Rayleigh fading process for increasing values of m, $n = 20$, and $f_D T = 0.10$. 113

5.5 Autocorrelation of the Markov chain model of the ISORA Rayleigh fading process for increasing values of n, $m = 5$, and $f_D T = 0.10$. 113

5.6 Autocorrelation of the Markov chain model of the ISORA Rayleigh fading process for increasing values of n, $m = 10$, and $f_D T = 0.10$. 114
5.7 Autocorrelation of the Markov chain model of the ISORA Rayleigh fading process for increasing values of n, $m = 15$, and $f_D T = 0.10$. 114
5.8 ISORA Rayleigh Markov chain model autocorrelation for various values of sample spacing T (sec), $n = 10$, $m = 5$, and $f_D = 100$ Hz. 117
5.9 ISORA Rayleigh Markov chain model autocorrelation for various values of sample spacing T (sec), $n = 10$, $m = 10$, and $f_D = 100$ Hz. 117
5.10 ISORA Rayleigh Markov chain model autocorrelation for various values of sample spacing T (sec), $n = 10$, $m = 15$, and $f_D = 100$ Hz. 118
5.11 ISORA Rayleigh Markov chain model autocorrelation for various values of sample spacing T (sec), $n = 15$, $m = 5$, and $f_D = 100$ Hz. 118
5.12 ISORA Rayleigh Markov chain model autocorrelation for various values of sample spacing T (sec), $n = 15$, $m = 10$, and $f_D = 100$ Hz. 119
5.13 ISORA Rayleigh Markov chain model autocorrelation for various values of sample spacing T (sec), $n = 15$, $m = 15$, and $f_D = 100$ Hz. 119
5.14 ISORA Rayleigh Markov chain model autocorrelation for various values of sample spacing T (sec), $n = 20$, $m = 5$, and $f_D = 100$ Hz. 120
5.15 ISORA Rayleigh Markov chain model autocorrelation for various values of sample spacing T (sec), $n = 20$, $m = 10$, and $f_D = 100$ Hz. 120
5.16 ISORA Rayleigh Markov chain model autocorrelation for various values of sample spacing T (sec), $n = 20$, $m = 15$, and $f_D = 100$ Hz. 121
5.17 Autocorrelation of the second-order Markov chain model of the ISORA Rayleigh fading channel for various values of T (sec), $n = 5$, $m = 4$, and $f_D = 100$ Hz. 127
5.18 Autocorrelation of the second-order Markov chain model of the ISORA Rayleigh fading channel for various values of T (sec), $n = 5$, $m = 10$, and $f_D = 100$ Hz. 127

5.19 Autocorrelation of the second-order Markov chain model of the ISORA Rayleigh fading channel for various values of T (sec), $n = 10$, $m = 4$, and $f_D = 100$ Hz. 128
5.20 Autocorrelation of the second-order Markov chain model of the ISORA Rayleigh fading channel for various values of T (sec), $n = 10$, $m = 10$, and $f_D = 100$ Hz. 128

6.1 Example of the proposed two-tiered Markov chain model transition scheme. 138

Acronyms

Acronyms	**Definition**
3-DISORA	3-dimensional ISORA
AFSMC	amplitude-based finite-state Markov chain
ARQ	automatic repeat request
BER	bit-error rate
CH-ARQ	concatenated hybrid ARQ
FEC	forward error correction
GBN	Go-back-N
ISORA	isotropic scattering, omnidirectional receiving antenna
LOS	line of sight
MRC	maximal ratio combining
MSE	mean-squared error
PDF	probability density function
RCPC	rate-compatible punctured convolutional
RS	Reed-Solomon
SNR	signal-to-noise ratio
SR	selective-repeat

List of Symbols

Symbol	**Definition**
b_0	mean received signal power
b_2	complex Gaussian quadrature second moment
$\mathrm{Det}[C]$	determinant of matrix C
$\mathrm{E}[x]$	expectation of x
$\mathrm{Erf}[z]$	error function
${}_2F_1(a, b; c; z)$	Gaussian Hypergeometric function
$F(x)$	cumulative distribution function
$F_R(x)$	Rayleigh cumulative distribution function
$\mathbf{f}$	Markov chain output vector
f	frequency
f_c	carrier frequency
f_D	Doppler frequency
$f(x)$	probability density function
$f_G(x)$	Gaussian probability density function
$f_m(r)$	Nakagami-m probability density function
$f_R(r)$	Rayleigh probability density function
$f_{Ri}(r)$	Ricean probability density function
$f_\gamma(\gamma)$	exponential probability density function
$H(\cdot)$	entropy
$I(\cdot;\cdot)$	average mutual information

$I_0(x)$	modified Bessel function of the first kind of order zero
$I_D(x)$	indicator function for domain D
$J_0(x)$	Bessel function of the first kind of order zero
k	discrete time
n	number of amplitude states
m	number of rate states
P	Markov chain transition matrix
P_{ij}	element of matrix P at row i and column j
$P_e(\gamma)$	probability of symbol error
$\Pr[x]$	probability function
$Q(\cdot,\cdot)$	Marcum Q function
R	Rayleigh random variable
R'	Rayleigh random variable time derivative
$R(k)$	Markov chain autocorrelation function
$R_G(\tau)$	Gaussian autocorrelation function
$R_R(\tau)$	Rayleigh autocorrelation function
$S_{E_z}(f)$	fading power spectrum
s_d	first-order amplitude/rate state
T	sample spacing
t	continuous time
T_c, T_s	complex Gaussian quadrature components
T_c', T_s'	complex Gaussian quadrature component time derivatives
$\mathbf{T_c}, \mathbf{T_s}$	Gaussian random vectors
w_d	second-order amplitude/rate state
Δ_C	determinant of matrix C
$\boldsymbol{\delta}$	amplitude threshold vector
$\Gamma(z)$	Gamma function
$\boldsymbol{\gamma}$	rate threshold vector
μ_X	mean of random variable X

$\boldsymbol{\mu}_{\mathbf{X}}$	mean vector of random vector $\mathbf{X}$
$\boldsymbol{\phi}_{\mathbf{0}}$,	Markov chain initial occupancy vector
$\boldsymbol{\pi}$	invariant probability vector
Σ	covariance matrix
σ_X^2	variance of random variable X
τ	continuous time separation
$\mathbf{0}$	zero vector
$\lfloor x \rfloor$	floor function
$\|\mathbf{x}\|$	norm of vector $\mathbf{x}$

Chapter 1

Introduction

1.1 Introduction

People don't like being tethered down by their communications devices. This desire for freedom of movement has resulted in the increasing popularity of wireless communications products, from older cordless telephones through to the current cellular technology and wireless internet revolution. Because of wireless technology, people are communicating in ways that they could only have dreamed of in the past.

The increasing usage of wireless products creates interesting problems for wireless engineers. Wireless spectrum is a limited resource, so as the demand for wireless products increases, engineers must find ways to allow for more products to use the available spectrum without causing any degradation in the quality of communications offered. Along with the increasing number of devices making use of the wireless spectrum, users are demanding more in the types of wireless services offered, such as wireless internet access and multimedia capable cell phones, both of which involve considerably more data than traditional voice communications. All of this means that engineers must continually work to make wireless communications as fast and efficient as possible.

An important step towards efficient use of the wireless spectrum is to accurately compensate for wireless noise. There are many sources of noise in the wireless spectrum, but one of the most significant noise sources is what is called multipath fading. Fading is the result of a signal arriving at a receiver via many different paths. This is possible because a wireless signal can be "scattered" by reflecting off of solid objects, like buildings, cars, or even other people. Thus, the process is also sometimes referred to as multipath scattering. This multipath scattering process is demonstrated in Fig. 1.1

The result of this signal scattering is that the same signal arrives at the receiver with different angles of arrival, time delays, and phase shifts. At the receiver, the signal can undergo constructive or destructive combination. When destructive combination occurs, the signal arrives at the receiver with low power, and is said to be in a fade. This fading cannot be predicted, making it a random process, which can only be described statistically.

There are two classes used to describe the type of fading experienced over a particular wireless channel [3]. The first is due to the time delays of the multipath signal. This leads to *time dispersion*, which causes frequency selective fading. This means that signal components at different frequencies will experience different fading values at the same point in time. If the time dispersion is small enough, then we can say that all frequencies experience the same fading value. This is referred to as flat fading. Throughout this thesis, we will be assuming a flat fading channel.

The second fading class is due to the Doppler spread, which is the broadening in frequency a signal can experience. This is called *frequency dispersion* and it leads to time selective fading, meaning the fading value changes over time. Time selective fading can be split into fast or slow fading, depending on the speed of the fading compared to the duration of a transmitted symbol. In this thesis, we make no assumptions about whether the fading is fast or slow.

Because the fading on a wireless channel can only be described statistically, mathematical analysis can often be difficult, or even impossible. This has lead researchers to propose alternative models of the fading channel. One such model is based on Markov chains. Mathematically, Markov chains are very simple to use, since they are completely defined by only one matrix and two vectors. Virtually all previous research on the subject has employed amplitude-based finite-state Markov chains (AFSMCs) to model the fad-

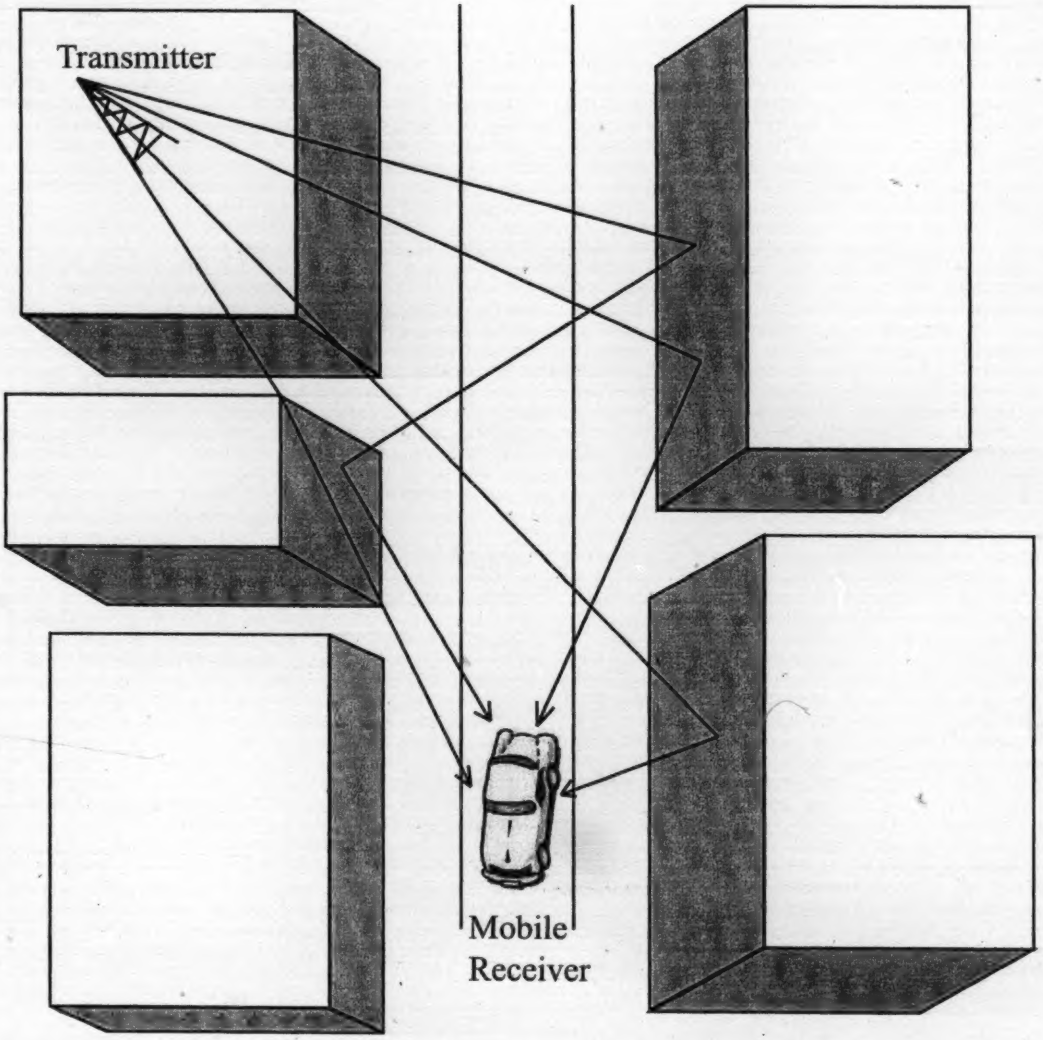
Transmitter
Mobile
Receiver

Fig. 1.1. Illustration of urban signal scattering.

ing channel, typically with little success, although some positive results have been found using them in automatic repeat request (ARQ) analyses. In general, though, AFSMC models have failed to adequately capture the statistics of the fading channel over anything but short time frames. Recently, however, Bergamo, et.al. [4] proposed a new state-space for Markov chain modeling of the fading channel, one that includes both the amplitude and the rate-of-change of the fading process. They presented only a limited analysis of the new state-space, but their results suggest that the new state-space might be able to capture the fading channel statistics that the AFSMCs were unable to. In this thesis, we will be examining Markov chains based on this new state-space in much greater detail, studying whether they can improve on previous Markov chain models of the fading channel.

1.2 Thesis Outline

1.2.1 Summary of Chapter 2

Chapter 2 presents the background topics for this thesis. The background is split into three sections. Section 2.2 presents some basic but important statistical theory. It begins by discussing a series of probability distributions that will be used throughout the thesis, specifically, the single and multivariate Gaussian, and the single and bivariate Rayleigh distributions. As we discussed in the Introduction, the goal of this thesis is to study a Markov chain model that includes a state-space based on the amplitude and rate-of-change of the fading channel. Thus, we proceed to present joint Gaussian and Rayleigh distributions that include the random variables and their derivatives. We conclude the first topic by presenting some important information about stochastic processes.

In Section 2.3 we discuss stochastic models of the fading channel. We focus particular attention on the commonly used isotropic scattering, omnidirectional receiving antenna (ISORA) fading channel model with fading amplitude modeled as a Rayleigh distribution. The ISORA model assumes 2-dimensional isotropic scattering, which is not aways a valid assumption, so we continue and present a variation of the ISORA model more appropriate for 3-dimensional isotropic scattering environments. We also briefly discuss the Ricean and Nakagami-m fading channel amplitude models, although they are not really considered in the Markov chain analysis to come.

The final background topic, Markov chains, is discussed in Section 2.4. We start by presenting the three elements needed to fully define a Markov chain model; the transition matrix P, the initial occupancy vector ϕ_0, and the output vector $\mathbf{f}$. We then discuss the important concept of Markov chain invariance. Statistical models of the fading channel are stationary, meaning their statistics only depend on the time difference between points, not the specific times themselves. In terms of Markov chain models, an invariant Markov chain will be stationary. Finally, we derive an expression for the autocorrelation of a Markov chain model, needed because the autocorrelation function is an important tool in analyzing the suitability of a Markov chain in modeling the fading channel.

1.2.2 Summary of Chapter 3

In Chapter 3, we present a survey of important literature on the topic of Markov chain modeling of the fading channel. As we alluded to in the Introduction, this has been a topic of active research by a number of researchers over the past 13 years, although the number of successes has been small. We start in Section 3.2 by presenting some pivotal early Markov chain models of communications channels, in particular, the well-known Gilbert-Elliott model. Though not proposed for fading channel modeling, they offer a crucial starting point in the development of this topic as a research area.

In Section 3.3, we present literature on the development of the Markov chain model of the fading channel, starting with Swarts and Ferreira [5], who were the first to propose a Markov chain fading channel model, through to Tan and Beaulieu [6], who presented the first real statistical analysis of the Markov chain fading channel model, and beyond. Though we can't discuss every single paper in the literature that has considered this topic, we do discuss all the major developmental papers on the topic.

In Section 3.4, we present some papers that have made use of the Markov chain model of the fading channel in practical analyses. The applications are all in the area of data packet analysis, and ARQ applications appear to have the best success at achieving useful results using the Markov chain model.

1.2.3 Summary of Chapter 4

In Chapter 4, we begin our analysis of Markov chain models of the ISORA Rayleigh fading channel using the new amplitude/rate-of-change state-space. In this chapter, we propose a Markov chain model of the Rayleigh fading channel that is derived by first modeling the underlying complex Gaussian process, then transforming that model into a Markov chain model of the fading envelope.

In Section 4.2, we examine a Markov chain model of the ISORA Rayleigh fading channel based on a *first-order* Markov chain model of the underlying Gaussian process. In Section 4.2.2, we present a method to calculate the elements of a Markov chain model based on the statistics of the ISORA Gaussian fading process, and in Section 4.2.3, we analyze the resulting model by comparing its first-order distribution and autocorrelation function to those of the theoretical ISORA Gaussian fading process. Based on some of the observations we make in this analysis, in Section 4.2.4, we present and analyze a first-order Markov chain model of the 3-D isotropic scattering fading model, focusing particularly on changes in the Markov chain model autocorrelation function when we alter the theoretical model under consideration. Finally, in Section 4.2.5, we present a method to transform a Markov chain model of the complex Gaussian fading process into a Markov chain model of the envelope Rayleigh fading process, and analyze the resulting model in terms of its first-order distribution and autocorrelation function, as before.

In Section 4.3, we examine a Markov chain model of the ISORA Rayleigh fading channel based on a *second-order* Markov chain model of the underlying Gaussian process. In Section 4.3.2, we expand on the methods of Section 4.2.2 to calculate the elements of a second-order Markov chain model of the Gaussian fading process. In Section 4.3.3, we analyze the resulting Markov chain model, focusing particularly on the effects of increasing the Markov chain order, in terms of both the Gaussian model and the transformed Rayleigh model.

1.2.4 Summary of Chapter 5

In Chapter 5, we study a Markov chain model of the ISORA Rayleigh fading channel with the expanded amplitude/rate-of-change state-space, in which the Markov chain model elements are calculated based directly on the statistics of the ISORA Rayleigh fading process, as opposed to the underlying Gaussian process, as considered in Chapter 4.

In Section 5.2, we consider a *first-order* Markov chain model of the ISORA Rayleigh fading process. In Section 5.2.2, we present a method to calculate the elements of a Markov chain model based directly on the statistics of the Rayleigh fading process. In Section 5.2.3, we analyze the resulting Markov chain model in terms of its first-order distribution and autocorrelation function, focusing particularly on the differences between this model and the Gaussian envelope model analyzed in Chapter 4.

In Section 5.3, we consider a *second-order* Markov chain model of the ISORA Rayleigh fading process. In Section 5.3.2, we extend the methods presented in Section 5.2.2 to calculate the elements of a second-order Markov chain directly from the Rayleigh fading statistics. In Section 5.3.3, we analyze the resulting Markov chain model, considering the effects of increasing the Markov chain order on the autocorrelation function, as well as comparing the results to those obtained when studying the Gaussian envelope model in Chapter 4.

1.3 Contributions

The contributions of this thesis are as follows:

- In Chapter 2, we derive an expression for the joint distribution of two correlated Rayleigh random variables and their derivatives, $f_R(r_1, r_2, r'_1, r'_2)$.

- In Chapter 3, we present a survey of important papers in the literature on the development of Markov chain models of the fading channel, as well is their use in practice.

- In Chapter 4, we propose and analyze a Markov chain model of the ISORA Rayleigh fading process based on a Markov chain model of the underlying Gaussian fading process, with an amplitude/rate-of-change state-space, using both first- and second-order Markov chains.

- In Chapter 5, we give precise analytical expressions for the transition probabilities of a Markov chain model of the ISORA Rayleigh fading process with an amplitude/rate-of-change state-space, in which the Markov chain model elements are calculated directly from the ISORA Rayleigh fading statistics.

- In Chapter 5, we perform a detailed analysis of a first-order Markov chain model of the ISORA Rayleigh fading process, with an amplitude/rate-of-change state-space, in which the Markov chain model elements are calculated directly from the ISORA Rayleigh fading statistics, including considering the effects of varying the number of rate states, as well as varying the sample spacing.

- In Chapter 5, we propose and analyze a second-order Markov chain model of the ISORA Rayleigh fading process, with an amplitude/rate-of-change state-space, in which the Markov chain model elements are calculated directly from the ISORA Rayleigh fading statistics, including determining which calculation method gives the best model for different sample spacing values.

1.4 Notation

Throughout this thesis, the probability of event A is denoted $\Pr[A]$, and the expectation is $\mathrm{E}[A]$. Occasionally, the expectation is also denoted as $\langle A \rangle$. In general, a random variable is identified by a capital letter, for example X, while a specific value of that random variable is identified by the equivalent lowercase letter x. A probability density function (PDF) will be denoted by $f(x)$ while the equivalent distribution function is the uppercase $F(x)$.

A matrix will be identified by a capital letter, for example transition matrix P. It should be clear from the context whether a capital letter is referring to a random variable or a matrix. Vectors are identified in bold, like output vector $\mathbf{f}$. They will usually be lowercase, although occasionally uppercase will be used. A scalar is denoted by a regular lowercase letter, such as mean signal power b_0. Indices of a vector are denoted in two ways; $\mathbf{f}_d$ and $\mathbf{f}[d]$ will both denote the d-th element of vector $\mathbf{f}$. The exception to this rule is the initial occupancy vector $\boldsymbol{\phi}_\mathbf{0}$, where, in this case, the subscript represents time. The d-th element of the initial occupancy vector is denoted $\boldsymbol{\phi}_\mathbf{0}[d]$.

Throughout the literature, fading is often discussed in terms of its normalized Doppler frequency $f_D T$, where f_D is the Doppler frequency in Hz, and T is the sample spacing in seconds. In this thesis, it is more convenient to consider variations in sample spacing T, so we always take the Doppler frequency to have the constant value $f_D = 100$ Hz. Note that this is simply a conceptual convenience, the results in this thesis are valid for any Doppler frequency. For example, if we express results for $T = 0.5\text{e-}3$ and $f_D = 100$ Hz, these same results would be valid for $T = 1.0\text{e-}3$ and $f_D = 50$ Hz.

It should also be noted that the ISORA model refers specifically to the 2-dimensional isotropic scattering model with an omnidirectional receiving antenna proposed by Clarke [7] and presented in detail in Section 2.3.2. The 3-dimensional isotropic scattering model with an omnidirectional antenna will be referred to as the 3-DISORA model.

Chapter 2

Background

2.1 Introduction

In this chapter, We present the background topics of this thesis. In Section 2.2, we review some important statistical concepts. We first discuss some useful Gaussian and Rayleigh distributions, then review some basic theory of stochastic processes. In Section 2.3, we discuss the development of some common stochastic models of the wireless fading channel, focusing particularly on the commonly used ISORA Rayleigh model. Section 2.4 discusses the use of Markov chains as statistical models, and Section 2.5 concludes the chapter.

2.2 Statistical Theory

2.2.1 Introduction

In this section, we present some statistical concepts of particular use in this thesis. Section 2.2.2 presents the Gaussian and multivariate Gaussian distributions, while Section 2.2.3 discusses the Rayleigh and bivariate Rayleigh distributions. In Section 2.2.4, we extend all these distributions to include the derivatives of the Gaussian or Rayleigh random variables. Section 2.2.5 reviews some important concepts of stochastic processes, and Section 2.2.6 concludes this section.

2.2.2 Gaussian Distributions

One of the most frequently used statistical distributions is the Gaussian (or Normal) distribution. It takes is name from Carl Friedrich Gauss, a German mathematician in the early 19th century. Random variable X is called Gaussian if it has the probability distribution [8]

$$f_G(x) = \frac{1}{\sqrt{2\pi\sigma_X^2}} e^{-(x-\mu_X)^2/2\sigma_X^2} \tag{2.1}$$

where μ_X is the mean of X, and σ_X^2 is its variance. Sometimes, σ_X is referred to as the standard deviation.

This definition can be easily extended to the multivariate case. Define random vector $\mathbf{X} = [X_1, X_2, \ldots, X_n]^T$. It is Gaussian if it has joint distribution

$$f_G(\mathbf{x}) = \frac{1}{\sqrt{(2\pi)^n \Delta_\Sigma}} e^{-\frac{1}{2}(\mathbf{x}-\boldsymbol{\mu})^T \Sigma^{-1} (\mathbf{x}-\boldsymbol{\mu})} \tag{2.2}$$

where $\boldsymbol{\mu}$ is the mean vector with $\boldsymbol{\mu}_i$ equal to the mean of X_i, Σ is the covariance matrix, and $\Delta_\Sigma = \mathrm{Det}[\Sigma]$, the determinant of matrix Σ. Note that covariance matrix Σ is made up of elements $\Sigma_{ij} = C_{ij} - \boldsymbol{\mu}_i \boldsymbol{\mu}_j$, where matrix C is the correlation matrix with elements defined as $C_{ij} = \mathrm{E}[X_i X_j]$.

2.2.3 Rayleigh Distributions

Another important distribution to be familiar with is the Rayleigh distribution, which takes its name from Lord Rayleigh, a Nobel prize winning physicist at the turn of the 20th century. If we define X_1 and X_2 to be independent, zero-mean, equal variance Gaussian random variables, then the envelope of the quadrature addition of them, $R = \sqrt{X_1^2 + X_2^2}$, will have the distribution

$$f_R(r) = \begin{cases} \frac{r}{\sigma_X^2} e^{-r^2/2\sigma_X^2}, & r \geq 0 \\ 0\,, & r < 0 \end{cases} \tag{2.3}$$

where σ_X^2 is the variance of the Gaussian random variables X_1 and X_2. This is the Rayleigh distribution.

We will quickly sketch the derivation of this distribution. First, we use (2.2) to write the joint distribution of X_1 and X_2 as

$$f_G(x_1, x_2) = \frac{1}{2\pi\sigma_X^2} e^{-\frac{x_1^2+x_2^2}{2\sigma_X^2}}. \tag{2.4}$$

We then use the transformation of variables

$$\begin{aligned} x_1 &= r\cos\theta \\ x_2 &= r\sin\theta \end{aligned}$$

with Jacobian r to write

$$\begin{aligned} f_R(r,\theta) &= \frac{1}{2\pi\sigma_X^2} e^{-\frac{(r\cos\theta)^2+(r\sin\theta)^2}{2\sigma_X^2}} \times r \\ &= \frac{r}{2\pi\sigma_X^2} e^{-r^2/2\sigma_X^2}. \end{aligned}$$

Finally, we get the distribution of R by integrating out θ, which gives us

$$\begin{aligned} f_R(r) &= \int_0^{2\pi} \frac{r}{2\pi\sigma_X^2} e^{-r^2/2\sigma_X^2}\, d\theta \\ &= \frac{r}{\sigma_X^2} e^{-r^2/2\sigma_X^2}. \end{aligned}$$

Clearly, R can only take positive values, so this distribution is only valid for $R \geq 0$.

Also of interest is the distribution of R^2. We sketch that derivation here as well. Define random variable $\gamma = R^2$. Since R must be positive, there is no ambiguity in rewriting this as $R = \sqrt{\gamma}$, with $\frac{dR}{d\gamma} = \frac{1}{2\sqrt{\gamma}}$. Substituting this transform into (2.3), we get

$$\begin{aligned} f_\gamma(\gamma) &= \frac{(\sqrt{\gamma})}{\sigma_X^2} e^{-(\sqrt{\gamma})^2/2\sigma_X^2} \times \frac{1}{2\sqrt{\gamma}} \\ &= \frac{1}{2\sigma_X^2} e^{-\gamma/2\sigma_X^2}. \end{aligned}$$

Thus, R^2 has an exponential distribution, with parameter $1/2\sigma_X^2$.

A more-or-less identical process to the Rayleigh derivation above can give us the bivariate Rayleigh distribution. Define four zero-mean Gaussian random variables X_1, X_2, X_3, X_4, and the envelope transformations $R_1 = \sqrt{X_1^2 + X_2^2}$ and $R_2 = \sqrt{X_3^2 + X_4^2}$. We require R_1 and R_2 to have marginal distributions equal to the Rayleigh distribution above, so it must be true that X_1 and X_2 are independent and have equal variance, and X_3 and X_4 must also be independent and have equal variance. In general, all other correlation values can be arbitrary, but, since this joint distribution will be used in the context of describing the fading channel, Jakes [9] reports that the physical channel imposes the following correlation constraints,

$$\langle X_1^2 \rangle = \langle X_2^2 \rangle = \langle X_3^2 \rangle = \langle X_4^2 \rangle = \mu \tag{2.5a}$$

$$\langle X_1 X_2 \rangle = \langle X_3 X_4 \rangle = 0 \tag{2.5b}$$

$$\langle X_1 X_3 \rangle = \langle X_2 X_4 \rangle = \mu_1 \tag{2.5c}$$

$$\langle X_1 X_4 \rangle = -\langle X_2 X_3 \rangle = \mu_2. \tag{2.5d}$$

By using (2.2) to write the joint distribution of X_1, X_2, X_3, and X_4, the envelope transformation of variables brings us to the joint distribution

$$f_R(r_1, r_2, \theta_1, \theta_2) = \frac{r_1 r_2}{(2\pi\mu)^2(1-\lambda^2)} e^{-\frac{r_1^2 + r_2^2 - 2r_1 r_2 \lambda \cos(\theta_2 - \theta_1 - \phi)}{2\mu(1-\lambda^2)}} \tag{2.6}$$

where $\tan\phi = \frac{\mu_2}{\mu_1}$ and $\lambda^2 = \frac{\mu_1^2+\mu_2^2}{\mu^2}$. After integrating out θ_1 and θ_2, we arrive at the bivariate Rayleigh distribution

$$f_R(r_1, r_2) = \frac{r_1 r_2}{\mu^2(1-\lambda^2)} e^{-\frac{r_1^2+r_2^2}{2\mu(1-\lambda^2)}} I_0\left(\frac{r_1 r_2}{\mu} \frac{\lambda}{1-\lambda^2}\right) \tag{2.7}$$

where $I_0(\cdot)$ is the modified Bessel function of the first kind of order zero given by [10, eq. 9.6.12]

$$I_0(z) = \sum_{q=0}^{\infty} \frac{(\frac{1}{4}z^2)^q}{(q!)^2}. \tag{2.8}$$

2.2.4 Joint Distributions with Derivatives

Of more importance to the upcoming analysis than the distributions in the previous two sections are the joint distributions of Gaussian and Rayleigh random variables and their derivatives. In this section, we will find expressions for the joint distribution of a single

Gaussian or Rayleigh random variable and its derivative, as well as two correlated Gaussian or Rayleigh random variables and their derivatives. The final derivation of the joint distribution of two correlated Rayleigh random variables and their derivatives is, to the best of the author's knowledge, new.

Because assuming a general correlation structure leads to unnecessarily complex expressions, the distributions derived here are derived specifically for the ISORA Rayleigh fading channel. As we will justify in Section 2.3.2, the ISORA Rayleigh fading process models fading as the envelope of a complex Gaussian process. Define T_c and T_s as the quadrature components of this complex Gaussian process. Allow subscripts 1 and 2 to refer to the components at times t and $t + \tau$, respectively. Rice [11] gives the correlation structure of the quadrature Gaussian components as

$$\langle T_{c_1} T_{c_2} \rangle = \langle T_{s_1} T_{s_2} \rangle = g(\tau) \tag{2.9a}$$

$$\langle T_{c_1} T_{s_2} \rangle = -\langle T_{s_1} T_{c_2} \rangle = h(\tau) \tag{2.9b}$$

$$\langle T_{c_1} T'_{c_2} \rangle = \langle T_{s_1} T'_{s_2} \rangle = -\langle T'_{c_1} T_{c_2} \rangle = -\langle T'_{s_1} T_{s_2} \rangle = g'(\tau) \tag{2.9c}$$

$$\langle T_{c_1} T'_{s_2} \rangle = \langle T'_{s_1} T_{c_2} \rangle = -\langle T'_{c_1} T_{s_2} \rangle = -\langle T_{s_1} T'_{c_2} \rangle = h'(\tau) \tag{2.9d}$$

$$\langle T'_{c_1} T'_{c_2} \rangle = \langle T'_{s_1} T'_{s_2} \rangle = -g''(\tau) \tag{2.9e}$$

$$\langle T'_{c_1} T'_{s_2} \rangle = -\langle T'_{s_1} T'_{c_2} \rangle = -h''(\tau) \tag{2.9f}$$

where

$$g(\tau) = R_G(\tau) = b_0 J_0(2\pi f_D \tau) \tag{2.10}$$

$$h(\tau) = 0 \tag{2.11}$$

and $J_0(\cdot)$ is the Bessel function of the first kind of order zero given by [10, eq. 9.1.12]

$$J_0(z) = \sum_{q=0}^{\infty} \frac{(-\frac{1}{4}z^2)^q}{(q!)^2}. \tag{2.12}$$

Expressions for $g'(\tau)$ and $g''(\tau)$ can be found by using [10, eq. 9.1.27] to get

$$g'(\tau) = -2\pi f_D b_0 J_1(2\pi f_D \tau) \tag{2.13}$$

$$g''(\tau) = 2\pi^2 f_D^2 b_0 \left(J_2(2\pi f_D \tau) - J_0(2\pi f_D \tau) \right). \tag{2.14}$$

The moments can be found by evaluating (2.9) at $\tau = 0$ to obtain

$$\langle T_c^2 \rangle = \langle T_s^2 \rangle = g(0) = b_0 \tag{2.15a}$$

$$\langle T_c T_s \rangle = h(0) = 0 \tag{2.15b}$$

$$\langle T_c T_c' \rangle = \langle T_s T_s' \rangle = g'(0) = 0 \tag{2.15c}$$

$$\langle T_c T_s' \rangle = -\langle T_c' T_s \rangle = h'(0) = 0 \tag{2.15d}$$

$$\langle T_c'^2 \rangle = \langle T_s'^2 \rangle = -g''(0) = b_2 \tag{2.15e}$$

$$\langle T_c' T_s' \rangle = -h''(0) = 0 \tag{2.15f}$$

where $b_2 = 2\pi^2 f_D^2 b_0$.

Since the derivative of a Gaussian random variable is itself Gaussian [12], we can use moments (2.15a), (2.15c), and (2.15e) in (2.2) to immediately write joint distributions $f_G(T_c, T_c')$ and $f_G(T_s, T_s')$ as

$$f_G(T, T') = \frac{1}{\sqrt{2\pi b_0}} e^{-T^2/2b_0} \frac{1}{\sqrt{2\pi b_2}} e^{-T'^2/2b_2}. \tag{2.16}$$

Thus, in terms of the correlation structure of the fading channel, a Gaussian random variable and its derivative are independent.

The extension to two Gaussian random variables and their derivatives is also simple. Define $\mathbf{T_c} = [T_{c_1}, T_{c_1}', T_{c_2}, T_{c_2}']^T$ and $\mathbf{T_s} = [T_{s_1}, T_{s_1}', T_{s_2}, T_{s_2}']^T$ to be two independent Gaussian random vectors, each having the correlation structure given by (2.9), which also establishes the independence of these two vectors. Joint distributions $f_G(\mathbf{T_c})$ and $f_G(\mathbf{T_s})$ will be given by (2.2), with $\boldsymbol{\mu} = \mathbf{0}$, where $\mathbf{0}$ is the zero vector, and with covariance matrix

$$\Sigma = \begin{pmatrix} b_0 & 0 & g(\tau) & g'(\tau) \\ 0 & b_2 & -g'(\tau) & -g''(\tau) \\ g(\tau) & -g'(\tau) & b_0 & 0 \\ g'(\tau) & -g''(\tau) & 0 & b_2 \end{pmatrix}. \tag{2.17}$$

To find the joint distribution of a Rayleigh random variable and its derivative, we refer to Jakes [9]. By forming $f_G(T_c, T_c', T_s, T_s') = f_G(T_c, T_c') f_G(T_s, T_s')$, which is true because of the independence of T_c and T_s, and applying the transformation of variables

$$T_c = r\cos\theta \tag{2.18a}$$

$$T_c' = r'\cos\theta - r\theta'\sin\theta \tag{2.18b}$$

$$T_s = r\sin\theta \tag{2.18c}$$

$$T_s' = r'\sin\theta + r\theta'\cos\theta \tag{2.18d}$$

we can integrate out θ and θ' to get

$$f_R(r, r') = \frac{r}{b_0} e^{-r^2/2b_0} \frac{1}{\sqrt{2\pi b_2}} e^{-r'^2/2b_2}. \tag{2.19}$$

As in the Gaussian case, a Rayleigh random variable and its derivative are independent.

In a basically similar pattern, we can derive the expression for two correlated Rayleigh random variables and their derivatives. Since $\mathbf{T_c}$ and $\mathbf{T_s}$ are independent, we can write

$$f_G(T_{c_1}, T_{c_1}', T_{c_2}, T_{c_2}'; T_{s_1}, T_{s_1}', T_{s_2}, T_{s_2}') = f_G(\mathbf{T_c}) f_G(\mathbf{T_s}). \tag{2.20}$$

We apply envelope transformations

$$T_{c_1} = r_1\cos\theta_1 \tag{2.21a}$$

$$T_{c_1}' = r_1'\cos\theta_1 - r_1\theta_1'\sin\theta_1 \tag{2.21b}$$

$$T_{c_2} = r_2\cos\theta_2 \tag{2.21c}$$

$$T_{c_2}' = r_2'\cos\theta_2 - r_2\theta_2'\sin\theta_2 \tag{2.21d}$$

$$T_{s_1} = r_1\sin\theta_1 \tag{2.21e}$$

$$T_{s_1}' = r_1'\sin\theta_1 + r_1\theta_1'\cos\theta_1 \tag{2.21f}$$

$$T_{s_2} = r_2\sin\theta_2 \tag{2.21g}$$

$$T_{s_2}' = r_2'\sin\theta_2 + r_2\theta_2'\cos\theta_2 \tag{2.21h}$$

with Jacobian $r_1 r_2$ to (2.20). After integrating out the four θ variables, considerable algebra brings us to the result

$$f_R(r_1, r_2, r_1', r_2') = \frac{r_1 r_2}{(2\pi)^2} \int_0^{2\pi} \frac{\mathrm{Exp}\left[-\frac{1}{2M}(\mathbf{v}^T D_1 \mathbf{v} - \mathbf{v}^T D_2 \mathbf{v})\right]}{\sqrt{M_{22}^2 - c^2 M_{24}^2}} d\phi \tag{2.22a}$$

$$D_1 = \begin{pmatrix} M_{11} & M_{13}c & M_{12} & M_{14}c \\ M_{13}c & M_{11} & -M_{14}c & -M_{12} \\ M_{12} & -M_{14}c & M_{22} & M_{24}c \\ M_{14}c & -M_{12} & M_{24}c & M_{22} \end{pmatrix} \tag{2.22b}$$

$$D_2 = \frac{s^2}{M_{22}^2 - c^2 M_{24}^2} \begin{pmatrix} M_{14}^2 M_{22} & -M_{14}^2 M_{24}c & M_{14}M_{22}M_{24} & M_{14}M_{24}^2 c \\ -M_{14}^2 M_{24}c & M_{14}^2 M_{22} & -M_{14}M_{24}^2 c & -M_{14}M_{22}M_{24} \\ M_{14}M_{22}M_{24} & -M_{14}M_{24}^2 c & M_{22}M_{24}^2 & M_{24}^3 c \\ M_{14}M_{24}^2 c & -M_{14}M_{22}M_{24} & M_{24}^3 c & M_{22}M_{24}^2 \end{pmatrix} \tag{2.22c}$$

where $\mathbf{v} = [r_1, r_2, r_1', r_2']^T$, $c = \cos\phi$, $s = \sin\phi$, $M = \text{Det}[\Sigma]$, and the M_{ij}'s are cofactors of covariance matrix Σ (2.17) for row i and column j. This notation and derivation approach is due to Rice [13], but the result in (2.22) is, to the best of the author's knowledge, new.

2.2.5 Stochastic Processes

A good reference on the topic of probability and stochastic processes is the textbook by Papoulis and Pillai [8]. In traditional probability, random variable X takes values depending on distribution $F_X(x) = \Pr[X \le x]$. Stochastic processes simply introduce an element of time variation to this definition. Thus, a stochastic process is identified as $X(t)$, which can be considered a traditional random variable for specific values of time t, where the value of $X(t)$ depends on the distribution

$$F_X(x;t) = \Pr[X(t) \le x]. \tag{2.23}$$

This is called the first-order distribution of the stochastic process and it can vary with t.

We can also consider the joint distribution of the stochastic process at two different times. This is called the second-order distribution and is defined as

$$F_X(x_1, x_2; t_1, t_2) = \Pr[X(t_1) \le x_1, X(t_2) \le x_2]. \tag{2.24}$$

As in the first-order expression, this distribution can vary with t_1 and t_2. These definitions can be extended to the n-th-order distribution, which would be defined as the joint distribution of the stochastic process at n different times.

To completely define a stochastic process, we need to know the n-th-order distribution for all values of n, x_i, and t_i, however, this can't reasonably be done, in general. Thus, a stochastic process is usually specified in terms of its mean and autocorrelation function.

The mean $\mu_X(t)$ depends only on the first-order distribution of the stochastic process and is defined as the expected value of $X(t)$ via

$$\mu_X(t) = \mathrm{E}[X(t)] = \int_{-\infty}^{\infty} x f_X(x;t) dx \tag{2.25}$$

where $f_X(x;t)$ is the first-order density of $X(t)$ defined as

$$f_X(x;t) = \frac{\partial F_X(x;t)}{\partial x}. \tag{2.26}$$

The autocorrelation function $R_X(t_1, t_2)$ depends on the second-order distribution of the stochastic process and is defined as the expected value of the product $X(t_1)X(t_2)$ using

$$R_X(t_1,t_2) = \mathrm{E}[X(t_1)X(t_2)] = \int_{-\infty}^{\infty}\int_{-\infty}^{\infty} x_1 x_2 f_X(x_1,x_2;t_1,t_2) dx_1 dx_2 \tag{2.27}$$

where $f_X(x_1, x_2; t_1, t_2)$ is the second-order density of $X(t)$ defined as

$$f_X(x_1,x_2;t_1,t_2) = \frac{\partial^2 F_X(x_1,x_2;t_1,t_2)}{\partial x_1 \partial x_2}. \tag{2.28}$$

A property of stochastic processes that is important to the work presented throughout the remainder of this thesis is the concept of stationarity. While there are many different categories of stationarity (first-order, second-order, n-th-order), there are two types of particular importance, strict sense stationarity and wide sense stationarity.

A stochastic process $X(t)$ is strict sense stationary if all its statistical properties are invariant to a time shift of the origin. To put it another way, for any value of c it must be true that $f_X(x;t) = f_X(x;t+c)$, $f_X(x_1,x_2;t_1,t_2) = f_X(x_1,x_2;t_1+c,t_2+c)$, and so on for all n-th-order distributions.

Since the n-th-order distribution of a stochastic process is hard or impossible to know in general, strict sense stationarity can be difficult to prove. In those cases, a relaxed condition, called wide sense stationarity, can be used. For a stochastic process to be wide sense stationary, it must have a constant mean

$$\mu_X(t) = \mu_X \tag{2.29}$$

and its autocorrelation function must only depend on the time difference $\tau = t_2 - t_1$, giving

$$R_X(t_1, t_2) = R_X(t_1, t_1 + \tau) = R_X(\tau). \tag{2.30}$$

Thus, a wide sense stationary process will have stationary first- and second-order distributions, but may not be stationary at higher-order distributions. Any strict sense stationary process is also wide sense stationary, but the converse is not generally true.

2.2.6 Conclusion

In this section, we have presented some important statistical theory. In particular, Section 2.2.2 presented some useful Gaussian distributions, and Section 2.2.3 presented the derivation of some important Rayleigh distributions. In Section 2.2.4, we derived expressions, one of them new, for the joint distributions of Gaussian or Rayleigh random variables and their derivatives, and Section 2.2.5 reviewed some information about stochastic processes.

2.3 Modeling the Wireless Channel

2.3.1 Introduction

Wireless spectrum is a limited resource. As the number of devices making use of the wireless spectrum to communicate increases, it becomes crucial that these devices be designed to make the most efficient use of the available spectrum. An important tool in the design of efficient devices is to have an accurate method of modeling the noise experienced over wireless channels. Wireless channel noise is random, so it is frequently modeled as a stochastic process.

In Section 2.3.2, we present the ISORA model for Rayleigh amplitude fading, which is the fading model of primary interest in this thesis. Section 2.3.3 discusses an alternate model that is more appropriate for 3-D isotropic scattering environments, and Sections 2.3.4 and 2.3.5 discuss the Ricean and Nakagami-m amplitude fading models respectively.

2.3.2 Deriving the Fading Model

A frequently used model of the wireless channel is the model originally proposed by Clarke [7]. It models the wireless channel as a wide sense stationary stochastic process, and thus, the model is specified by stationary first- and second-order distributions. The first-order distribution of this model is the Rayleigh distribution, while the second-order distribution is the bivariate Rayleigh. In determining the autocorrelation function of the second-order distribution, this model assumes a 2-dimensional isotropic scattering environment, along with an omnidirectional receiving antenna, so we refer to it as the ISORA model for Rayleigh amplitude fading.

Based on field recordings of the amplitude variation of the envelope of a signal propagated over the wireless channel, Jakes [9] makes the assumption that at any point a received signal consists of a number of horizontally traveling plane waves, where both amplitude and angle of arrival are random, and the phases of the waves are independent of the amplitude and uniformly distributed from 0 to 2π. Under this assumption, for a vertically polarized transmitted signal, the electric field component can be written as

$$E_z = E_0 \sum_{n=1}^{N} C_n \cos(\omega_c t + \omega_n t + \phi_n) \tag{2.31}$$

or as

$$E_z = T_c(t) \cos \omega_c t - T_s(t) \sin \omega_c t \tag{2.32}$$

where

$$T_c(t) = E_0 \sum_{n=1}^{N} C_n \cos(\omega_n t + \phi_n) \tag{2.33}$$

$$T_s(t) = E_0 \sum_{n=1}^{N} C_n \sin(\omega_n t + \phi_n). \tag{2.34}$$

For large N, the central limit theorem can be used to state that at any value of t, $T_c(t)$ and $T_s(t)$ are approximately uncorrelated, zero-mean Gaussian random variables with equal variance $b_0 = 3E_0^2/4$, assuming an omnidirectional receiving antenna. So, $T_c(t)$ and $T_s(t)$ have distributions $f_G(T_c)$ and $f_G(T_s)$ respectively, where $f_G(x)$ is the Gaussian distribution (2.1) with variance $\sigma_X^2 = b_0$, the mean signal power. Specifically,

$$f_G(x) = \frac{1}{\sqrt{2\pi b_0}} e^{-x^2/2b_0}. \tag{2.35}$$

The envelope of E_z is $R = \sqrt{T_c^2 + T_s^2}$. We saw in Section 2.2.3 that the envelope of the quadrature addition of two independent zero-mean, equal variance Gaussian random variables has the Rayleigh distribution (2.3). Since the variance of T_c and T_s is b_0, R has the distribution

$$f_R(r) = \begin{cases} \frac{r}{b_0} e^{-r^2/2b_0}, & r \geq 0 \\ 0\,, & r < 0 \end{cases} \tag{2.36}$$

which has mean $\mu_R = \sqrt{\pi b_0/2}$ and is plotted in Fig. 2.1. Thus, for a sufficiently large N (i.e. high scattering environment), the amplitude of a received signal undergoes fading with a first-order Rayleigh distribution. This distribution doesn't depend on time t, so the first-order model of the fading channel is stationary.

Next, we find an expression for the autocorrelation of the wireless channel. In [7] and [9], under the assumption that the transmitted signal is vertically polarized, undergoes 2-D isotropic scattering, and is received by an omnidirectional antenna, the power spectra of E_z is found to be

$$S_{E_z}(f) = \begin{cases} \frac{b_0}{\pi f_D} \frac{1}{\sqrt{1 - \left(\frac{f - f_c}{f_D}\right)^2}}, & f_c - f_D \leq f \leq f_c + f_D \\ 0\,, & \text{otherwise} \end{cases} \tag{2.37}$$

where f_c is the carrier frequency and f_D is the maximum Doppler frequency, both in Hz. This spectrum is plotted in Fig. 2.2.

We previously saw the complex Gaussian correlation structure for the fading channel, due to Rice [11], as (2.9) in Section 2.2.4. The specific expressions for the autocorrelation, $g(\tau)$, and cross-correlation, $h(\tau)$, of the quadrature components of the complex Gaussian

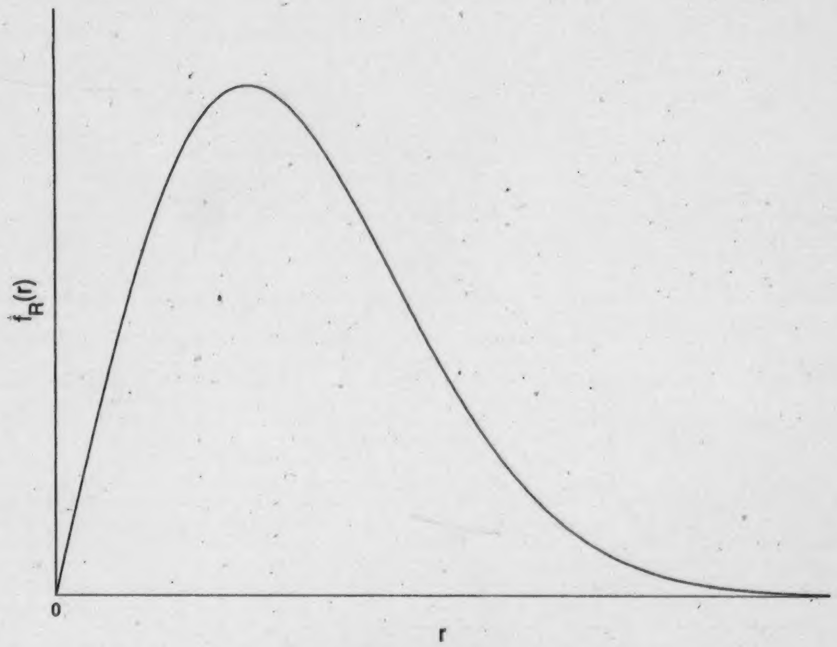

Fig. 2.1. Rayleigh PDF.

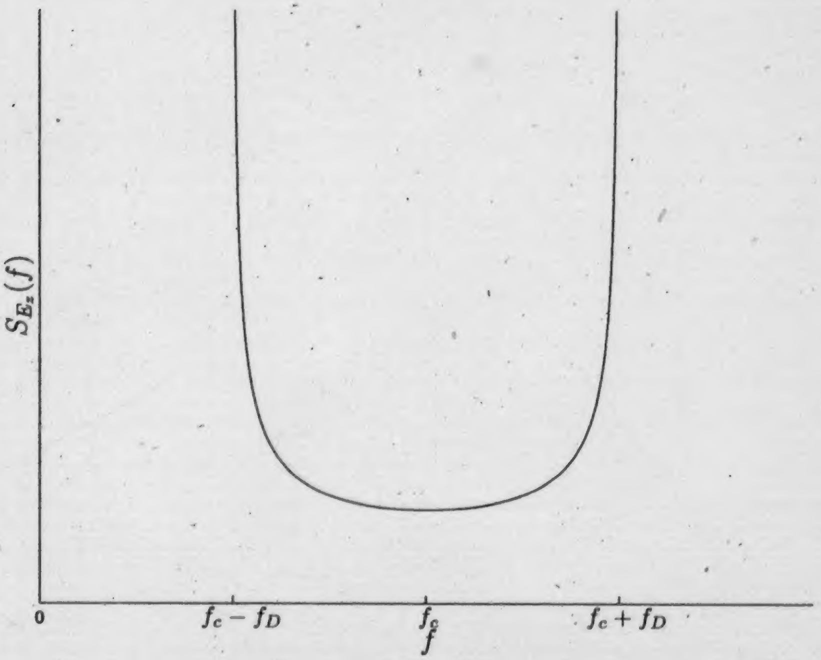

Fig. 2.2. Power spectra of the electric field component.

process are calculated in terms of the power spectrum using equations

$$g(\tau) = \int_{f_c-f_D}^{f_c+f_D} S_{E_z}(f)\cos 2\pi(f-f_c)\tau df \tag{2.38}$$

$$h(\tau) = \int_{f_c-f_D}^{f_c+f_D} S_{E_z}(f)\sin 2\pi(f-f_c)\tau df. \tag{2.39}$$

From these, the autocorrelation and cross-correlation can be found to be

$$g(\tau) = R_G(\tau) = b_0 J_0(2\pi f_D \tau) \tag{2.40}$$

$$h(\tau) = 0 \tag{2.41}$$

where $J_0(\cdot)$ is the Bessel function of the first kind of order zero (2.12).

In [14], it is shown that these correlation values can be used to find the autocorrelation of the envelope R to be

$$R_R(\tau) = \frac{\pi b_0}{2} {}_2F_1\left(-\frac{1}{2}, -\frac{1}{2}; 1; J_0(2\pi f_D \tau)^2\right) \tag{2.42}$$

where ${}_2F_1(\cdot,\cdot;\cdot;\cdot)$ is the Gaussian Hypergeometric function defined as [10, eq. 15.1.1]

$${}_2F_1(a,b;c;z) = \frac{\Gamma(c)}{\Gamma(a)\Gamma(b)} \sum_{q=0}^{\infty} \frac{\Gamma(a+q)\Gamma(b+q)}{\Gamma(c+q)} \frac{z^q}{q!} \tag{2.43}$$

and the gamma function $\Gamma(z)$ is given by [10, eq. 6.1.1]

$$\Gamma(z) = \int_0^\infty t^{z-1} e^{-t} dt, \quad Re[z] > 0. \tag{2.44}$$

Since (2.42) only depends on time difference τ, the ISORA model of the second-order distribution of the fading channel is stationary.

So, the ISORA Rayleigh fading model of the wireless channel is specified in two ways. First, in terms of the independent Gaussian quadrature components $T_c(t)$ and $T_s(t)$ via first-order distribution (2.35) and autocorrelation (2.40), or in terms of the Rayleigh fading envelope $R(t)$ with first-order distribution (2.36) and autocorrelation (2.42). Both specifications will be used throughout this thesis.

2.3.3 3-D Scattering Model

The ISORA model discussed in the previous section assumes 2-dimensional isotropic scattering with no line of sight (LOS) between the transmitter and receiver. This model is most appropriate for outdoor urban environments, for example, modeling the fading experienced by a receiver in a car driving down a city street or a by person walking down a sidewalk. However, in some environments, particularly indoor, a 3-dimensional scattering assumption is much more appropriate.

Like the ISORA model, the received signal is modeled as a complex Gaussian process with independent, zero-mean, equal variance quadrature components. Clarke and Khoo [15] derive the Doppler spectrum and autocorrelation function in the case of 3-D isotropic scattering, assuming an omnidirectional receiving antenna. They find that the Doppler spectrum is flat for $f_c - f_D \leq f \leq f_c + f_D$ and zero outside this range. This leads to the 3-D isotropic scattering model autocorrelation expression

$$g(\tau) = b_0 \mathrm{sinc}(2\pi f_D \tau) \tag{2.45}$$

where the sinc function is defined as

$$\mathrm{sinc}(x) = \begin{cases} 1\,, & x = 0 \\ \frac{\sin x}{x}, & \text{otherwise} \end{cases}. \tag{2.46}$$

This model of the second-order distribution of the fading channel will be referred to as the 3-DISORA model.

Fig. 2.3 shows the 3-DISORA autocorrelation and the traditional ISORA autocorrelation. While similar in shape, the 3-DISORA model's oscillations lag behind those of the ISORA autocorrelation. It also decays faster than the ISORA model.

2.3.4 Ricean Fading Model

When the signal received by an antenna is made up of a high number of uniformly scattered signals, the first-order distribution of the fading envelope can be modeled as a Rayleigh distribution, as we saw in Section 2.3.2. The Rayleigh fading model is no longer valid

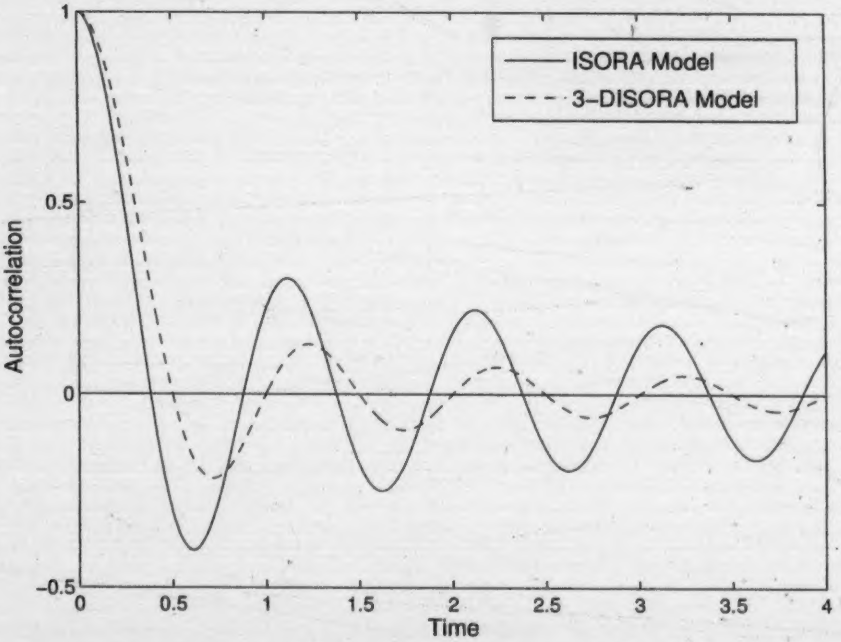

Fig. 2.3. 3-DISORA model autocorrelation compared to ISORA model autocorrelation.

when the received signal has a significant LOS component. Intuitively, we would expect that a dominant LOS component in the received signal would result in fades that are less deep than those seen in the Rayleigh fading model, since the scattering makes up a smaller component of the received signal.

Parsons [16] gives the joint density function of the envelope and phase of a scattered signal with dominant component r_s as

$$f(r,\theta) = \frac{r}{2\pi b_0} e^{-\frac{r^2+r_s^2-2rr_s\cos\theta}{2b_0}}. \tag{2.47}$$

By integrating out θ, we get the density of the envelope expressed as

$$f_{Ri}(r) = \frac{r}{b_0} e^{-\frac{r^2+r_s^2}{2b_0}} I_0\left(\frac{rr_s}{b_0}\right) \tag{2.48}$$

where $I_0(\cdot)$ is the modified Bessel function of the first kind of order zero (2.8). This problem is equivalent to the sinusoidal wave plus random noise examined by Rice [17], so (2.48) is referred to as the Ricean distribution, making this the Ricean model of the first-order amplitude fading distribution.

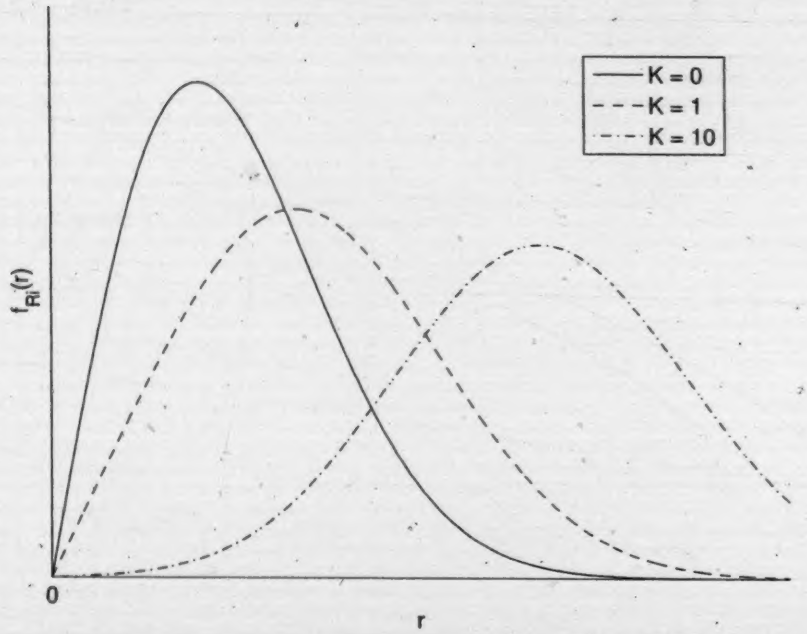

Fig. 2.4. First-order distribution of the Ricean channel model as parameter K increases.

In the literature, the Ricean model is typically described in terms of the K parameter, defined as

$$K = \frac{r_s^2}{2b_0} \tag{2.49}$$

which can be interpreted as the ratio of the power in the dominant LOS component to the power in the scattering component. Note that the Rayleigh distribution is a particular instance of the Ricean distribution, when $K = 0$. Fig. 2.4 shows the Ricean density function for different values of K. As expected, as K is increased, the probability that the envelope amplitude r is large increases, so there is less chance of a fade occurring, and the fades that do occur aren't as deep.

When used in practice, a value for the K parameter must be estimated to give the best match to the fading channel being modeled. The subject of K parameter estimation has been studied in [18], [19], [20], and [21] among others.

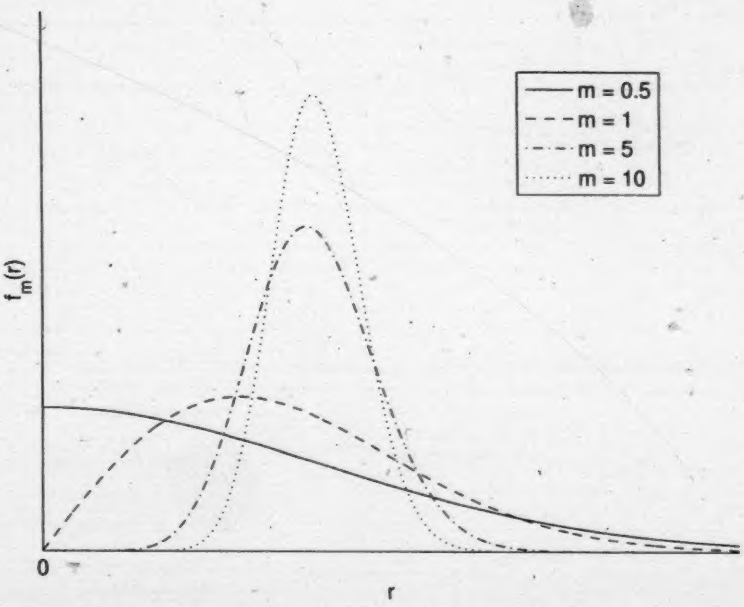

Fig. 2.5. First-order distribution of the Nakagami-m fading channel model for different values of parameter m.

2.3.5 Nakagami-m Fading Channel

The Rayleigh amplitude fading model is only appropriate when the received signal is made up of a large number of uniform scatters. A distribution that can model a wider range of fading conditions is the Nakagami-m distribution. Empirical studies have shown that this distribution is appropriate for modeling the fading channel [22], [23]. The density function of the Nakagami-m distribution is [22]

$$f_m(r) = \begin{cases} \frac{2}{\Gamma(m)} \left(\frac{m}{\Omega}\right)^m r^{2m-1} e^{-mr^2/\Omega}, & r \geq 0 \\ 0\,, & r < 0 \end{cases} \tag{2.50}$$

where Ω is the second moment, $\Omega = \mathrm{E}[R^2]$, m is the fading figure, defined as

$$m = \frac{\Omega^2}{\mathrm{E}[(R^2 - \Omega)^2]}, \quad m \geq \frac{1}{2} \tag{2.51}$$

and $\Gamma(\cdot)$ is the Gamma function, defined by (2.44). A plot of the Nakagami-m distribution for various values of parameter m is shown in Fig. 2.5. Note that when $m = 1$, the

Nakagami-m distribution is the same as the Rayleigh distribution, and when $m = \frac{1}{2}$, it is a one-sided Gaussian distribution. As m is increased, the probability of envelope r being in a fade decreases, so the Nakagami-m model is appropriate for fading environments where the fade depth isn't as deep as predicted by the Rayleigh model.

Like the Ricean channel model, when the Nakagami-m model is used in practice, a value for the m parameter must be estimated. The subject of m parameter estimation has been studied in such papers as [24] and [25].

2.4 Markov Chains

2.4.1 Introduction

A Markov process is a simple stochastic process where the outcome at any instant in time depends only on the outcome in the preceding time instant. In other words, if we know the present state of a Markov process, the past will have no influence on the state it will be in at the next time period. The Markov process takes its name from Andrej Andreevic Markov, who introduced the discrete-time, finite state version, called a Markov chain, at the turn of the 20th century. Though later extended to include countably infinite states, we will be focusing on the traditional finite-state Markov chain in this section and throughout the remainder of this thesis.

In Section 2.4.2, we identify the elements necessary to fully define a Markov chain model. Section 2.4.3 discusses the important concept of invariant probabilities of a Markov chain, and Section 2.4.4 presents the derivation of an expression for the autocorrelation of a Markov chain, which will be an important tool in the analysis of Markov chain models of the fading channel to come in later chapters.

2.4.2 Markov Chain Model Elements

In this section, we present some basic discussion of the elements needed to define a Markov chain model of a random process. Detailed treatments of Markov chains and their applications can be found in such sources as [8], [26], [27], [28], and [29].

By definition [26], the stochastic process X_k is a Markov chain if, for any discrete time k,

$$\Pr[X_k = i_k | X_{k-1} = i_{k-1}, \ldots, X_1 = i_1, X_0 = i_0] = \Pr[X_k = i_k | X_{k-1} = i_{k-1}] \qquad (2.52)$$

where i_k is the state at time k. So, the probability of entering state i_k at time k depends only on the state at time $k - 1$. The history of the Markov chain prior to that point has no influence.

Assume that state-space S is made up of N states, $S = \{s_1, \ldots, s_N\}$. As a notational convention, we will interpret $X_k = j$ to mean the same as $X_k = s_j$. Allowing the index to represent the state will simplify the notation. Define a *time homogeneous* Markov chain to be one in which

$$\Pr[X_k = j | X_{k-1} = i] = p(i, j) \qquad (2.53)$$

where the transition probability does not depend on k. All Markov chains considered here are of this type.

The first Markov chain model element we define is the $N \times N$ transition matrix P, where the element at row i and column j, P_{ij}, is defined by (2.53). Transition matrix P identifies the probabilities of all possible transitions the Markov chain can make. Since the elements of the transition matrix are probabilities, it must be true that $0 \leq P_{ij} \leq 1$. Also, all row sums of P must equal 1, since

$$\begin{aligned}
\sum_{j=1}^{N} P_{ij} &= \sum_{j=1}^{N} \Pr[X_k = j | X_{k-1} = i] \\
&= \sum_{j=1}^{N} \frac{\Pr[X_k = j, X_{k-1} = i]}{\Pr[X_{k-1} = i]} \\
&= \frac{\Pr[X_{k-1} = i]}{\Pr[X_{k-1} = i]} = 1
\end{aligned}$$

using the Total Probability Theorem [8], since the sum from $j = 1, \ldots, N$ represents a complete partition of the state-space.

The second element needed to define a Markov chain model is called the initial occupancy vector, and is denoted by ϕ_0. This vector represents the distribution of the Markov chain at time 0. Accordingly, we set

$$\phi_0[d] = \Pr[X_0 = d] \tag{2.54}$$

where d is the vector index. Since it represents a probability distribution, the sum of all elements of ϕ_0 must equal 1.

By initializing the Markov chain with probability vector ϕ_0, the distribution at any time k can be expressed as

$$\phi_k{}^T = \phi_0{}^T P^k. \tag{2.55}$$

To prove this, we first prove that $\Pr[X_k = j|X_0 = i] = P_{ij}^k$, which can be proven by induction. To do this, we first find that

$$\begin{aligned}
\Pr[X_2 = j|X_0 = i] &= \sum_{q=1}^{N} \Pr[X_2 = j, X_1 = q|X_0 = i] \\
&= \sum_{q=1}^{N} \Pr[X_1 = q|X_0 = i]\Pr[X_2 = j|X_1 = q, X_0 = i] \\
&= \sum_{q=1}^{N} \Pr[X_1 = q|X_0 = i]\Pr[X_2 = j|X_1 = q] \\
&= \sum_{q=1}^{N} P_{iq}P_{qj} \\
&= P_{ij}^2.
\end{aligned}$$

Now, assume the expression is true for $k - 1$. Then,

$$\begin{aligned}
\Pr[X_k = j | X_0 = i] &= \sum_{q=1}^{N} \Pr[X_k = j, X_{k-1} = q | X_0 = i] \\
&= \sum_{q=1}^{N} \Pr[X_{k-1} = q | X_0 = i] \Pr[X_k = j | X_{k-1} = q, X_0 = i] \\
&= \sum_{q=1}^{N} \Pr[X_{k-1} = q | X_0 = i] \Pr[X_k = j | X_{k-1} = q] \\
&= \sum_{q=1}^{N} P_{iq}^{k-1} P_{qj} \\
&= P_{ij}^{k}.
\end{aligned}$$

Now, we can examine (2.55). The d-th element of ${\phi_0}^T P^k$ can be written as

$$\begin{aligned}
\sum_{i=1}^{N} \phi_0[i] P_{id}^{k} &= \sum_{i=1}^{N} \Pr[X_0 = i] \Pr[X_k = d | X_0 = i] \\
&= \sum_{i=1}^{N} \Pr[X_0 = i, X_k = d] \\
&= \Pr[X_k = d] = \phi_k[d]. \qquad (2.56)
\end{aligned}$$

Thus, given ϕ_0 and P, the distribution of the Markov chain at any time k can be found using (2.55).

The final element needed to define a Markov chain model is vector $\mathbf{f}$, which we call the output vector. The output vector defines the value of the Markov chain in each state of the state-space S. Specifically, $\mathbf{f}[d]$ will represent the value of state s_d.

By computing values for the transition matrix P, initial occupancy vector ϕ_0, and output vector $\mathbf{f}$, a Markov chain model of a stochastic process will be completely defined.

2.4.3 Invariant Probability

An important property of Markov chains for the present work is the invariant probability property. In simple terms, a probability vector π is called invariant over transition matrix

P if

$$\pi^T = \pi^T P. \tag{2.57}$$

The invariant vector π represents a probability distribution that doesn't change after one time period. Mathematically, it can also be viewed as the left eigenvector of matrix P corresponding to an eigenvalue of 1.

If the initial occupancy vector ϕ_0 is chosen equal to the invariant vector, then the first-order distribution of the Markov process will remain unchanged at all time instants. In this case, the Markov process is referred to as *stationary*.

2.4.4 Autocorrelation

In this section, we derive an expression for the autocorrelation of a Markov chain model. This is a necessary tool in the analysis of fading channel models performed in later chapters.

Recall from Section 2.2.5 that the autocorrelation of a stochastic process is the expected value of the product $X(t_1)X(t_2)$ at times t_1 and t_2. In the case of a Markov process, the times are discrete values k_1 and k_2. Also, random variables X_{k_1} and X_{k_2} represent states, not values of the states, so output vector $\mathbf{f}$ must also be included, resulting in the autocorrelation of a Markov chain being expressed as

$$\begin{aligned}
\mathrm{E}[\mathbf{f}(X_{k_1})\mathbf{f}(X_{k_2})] &= \sum_{x_{k_1}=0}^{N}\sum_{x_{k_2}=0}^{N} \mathbf{f}[x_{k_1}]\mathbf{f}[x_{k_2}]\mathrm{Pr}[X_{k_1} = x_{k_1}, X_{k_2} = x_{k_2}] \\
&= \sum_{l=0}^{N}\sum_{q=0}^{N} \mathbf{f}[l]\mathbf{f}[q]\mathrm{Pr}[X_{k_1} = l, X_{k_2} = q] \\
&= \sum_{l=0}^{N}\sum_{q=0}^{N} \mathbf{f}[l]\mathbf{f}[q]\mathrm{Pr}[X_{k_2} = q | X_{k_1} = l]\mathrm{Pr}[X_{k_1} = l] \\
&= \sum_{l=0}^{N}\sum_{q=0}^{N} \mathbf{f}[l]\mathbf{f}[q]P_{lq}^{k_2-k_1}({\phi_0}^T P^{k_1})[l].
\end{aligned}$$

If we assume that ϕ_0 is invariant over transition matrix P, this can be further simplified to

$$\mathrm{E}[\mathbf{f}(X_{k_1})\mathbf{f}(X_{k_2})] = \sum_{l=0}^{N}\sum_{q=0}^{N} \mathbf{f}[l]\mathbf{f}[q]P_{lq}^{k}\phi_0[l]$$

where $k = k_2 - k_1$. If we define $\mathbf{a} = \mathbf{f}.*\phi_0$ to be the element-by-element multiplication of $\mathbf{f}$ and ϕ_0, and set $\mathbf{b} = \mathbf{f}$, then we can write the final expression for the autocorrelation of a Markov chain as

$$E[\mathbf{f}(X_{k_1})\mathbf{f}(X_{k_2})] = R(k) = \mathbf{a}^T P^k \mathbf{b}. \tag{2.58}$$

This expression is similar to the autocorrelation expression used by Tan and Beaulieu [6], but generalized to be valid for any invariant ϕ_0, not just equiprobable ones.

2.5 Conclusion

In this chapter, we presented the background material necessary for the remainder of the thesis. In Section 2.2, we discussed some useful statistical theory concepts. Single and multivariate Gaussian distribution expressions were shown in Section 2.2.2, and the single and bivariate Rayleigh distributions were derived in Section 2.2.3. All these expressions were expanded to the joint distributions of Gaussian or Rayleigh random variables and their derivatives in Section 2.2.4. Section 2.2.5 then discussed some important information on stochastic processes.

In Section 2.3, we presented the development of some of the common statistical models of the wireless fading channel. Section 2.3.2 discussed the development of the frequently used ISORA Rayleigh fading model, and Section 2.3.3 expanded this model to be more appropriate for 3-D isotropic scattering environments. Section 2.3.4 detailed the Ricean fading channel model, which models wireless channels with a dominant LOS component, and Section 2.3.5 discussed the Nakagami-m channel model, which can model a wider range of fading conditions.

The final important background topic was Markov chains, presented in Section 2.4. Section 2.4.2 presented the three elements necessary to define a Markov chain model. Section 2.4.3 discussed the important concept of invariance, and an expression for the autocorrelation of a Markov chain was derived in Section 2.4.4.

Chapter 3

The History of Markov Modeling for Fading Channels

3.1 Introduction

The modeling of communications channels with Markov chains is an idea that has been studied in the literature for many years. As far back as the 1960's, researchers such as Gilbert [30] and Elliott [31] were proposing Markov chains as models for burst-noise over wireline and fixed radio channels. Research into modeling general wireless channels with Markov chains is more contemporary, with the first papers on the subject appearing in the literature in the early 1990's.

This chapter presents a survey of the literature on the subject of Markov chain modeling of wireless channels. In Section 3.2, we discuss some of the earliest papers on the subject, in particular the well-known Gilbert-Elliot model and extensions by Fritchman [32]. Section 3.3 surveys the literature on Markov chain modeling of the fading channel, and Section 3.4 discusses some papers that have employed Markov chain fading channel models in practice. Section 3.5 concludes this chapter.

3.2 Early Markov Chain Models

3.2.1 Gilbert-Elliott Model

Gilbert [30] first proposed the use of a Markov chain to model a burst-noise binary channel. His model consisted of two states, an error-free transmission state, and a state where the probability of error-free transmission was h.

Gilbert considered the symmetric binary channel, which is the classical model of a noisy binary channel in information theory. If the input digit at time n is x_n, then the output of the noisy channel is $y_n = x_n + z_n$, where z_n is the random noise digit, which is added (modulo 2) to the input digit. Thus, z_n takes either the value 0 or 1. In the two state channel model, state G is the error-free state, where $z_n = 0$. In state B, $z_n = 0$ with probability h and $z_n = 1$ with probability $1 - h$. Gilbert always takes $h = 0.5$.

Gilbert proposed two methods to determine the Markov chain model parameters, both based on channel noise measurements. The first method involved studying the trigram statistics of the measured channel. For the second method, Gilbert noted that the run lengths of the Markov chain states will have a geometric distribution. Under the assumption that the various noises on a real channel are unrelated, the times between noise events will also have a geometric distribution. Thus, the proposed method consisted of fitting the expression

$$u(K) = AJ^K + (1 - A)L^K \tag{3.1}$$

to the zero run length distribution of the channel measurements. The model parameters were determined from the fitted values for A, J, and L.

Elliott [31] used Gilbert's Markov chain model to study the error probabilities of error correcting codes, and the probability of retransmission of error detecting codes. Since the complex error structure with memory on communication channels makes accurate prediction of code performance difficult, codes had previously been evaluated in terms of discrete, memory-less channels. This was an analytically simple method of evaluation, but gave little information about the performance of the codes in real channels, where statistical dependencies exist. Thus, Gilbert's simple channel model allowed for the code performance to be estimated for a channel with error dependencies. Elliott generalized Gilbert's model by replacing the error-free state G with a state where the probability of correct transmission was k and the probability of error was $1 - k$. This new state still represented the "good" state in the two state model, so $k > h$.

As an example of the performance analysis method, Elliott studied the Bose-Chaudhuri code on a telephone network. By comparing the error rate analysis results to simulated results, he found that the analysis method generally agreed to within an order of magnitude in all but a few extreme circumstances.

3.2.2 Fritchman

Fritchman [32], like Elliott, considered the problem of evaluation of error-detecting and correcting codes. He recognized, however, that the two-state Gilbert-Elliott model lacked the flexibility to be applied to a broad class of channels. So, Fritchman proposed an N-state Markov chain model. Like the Gilbert-Elliott model, Fritchman restricted the model to a binary channel, where the transmitted signal was either received correctly, or in error. However, he generalized the Gilbert-Elliott model by including k error-free states and $N-k$ error states. A diagram of this scheme can be seen in Fig. 3.1. The Gilbert model can be considered a special case of this model. Fritchman also proposed a method to determine the transition matrix for this model based on the error-free-run and error-cluster distributions of a channel.

As examples of the proposed model, Fritchman determined parameters for two sample radio links. In both cases, only a single error state was used, meaning that the transition probabilities were fully specified by the error-free-run distribution. A transition diagram of this single error scheme can be found in Fig. 3.2. In one of the sample radio links, three error-free states were used, and the model was seen to fit the error-free-run distribution very well. In the second case, only two error-free states were used, but the model still fit the error-free-run distribution well. The error cluster distribution, however, was not modeled as well.

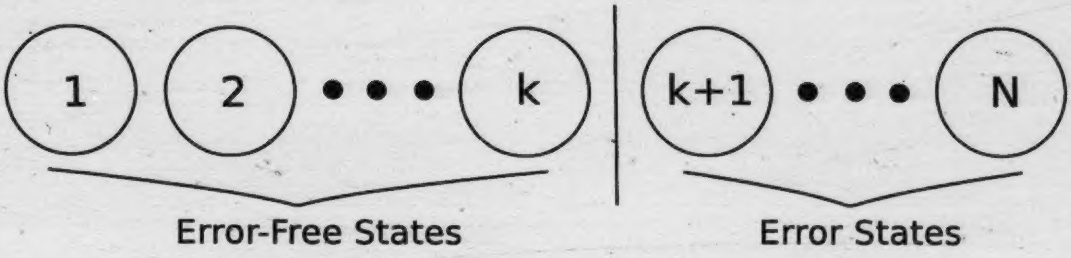
1
2
k
k+1
N
Error-Free States
Error States

Fig. 3.1. Diagram of the Fritchman state-space partitioning scheme.

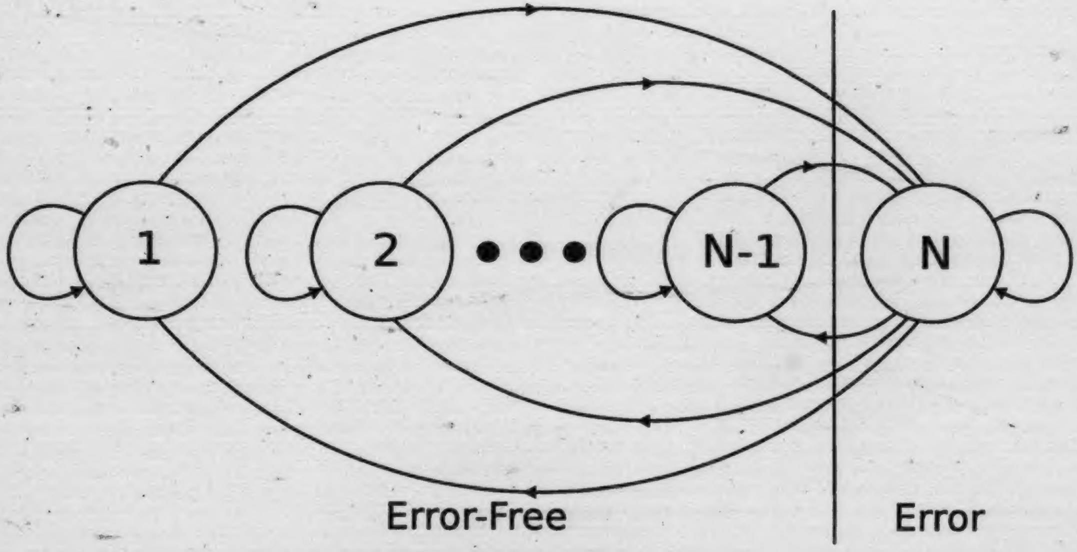
1
2
N-1
N
Error-Free
Error

Fig. 3.2. Transition diagram of the Fritchman model with one error state.

3.3 Markov Chain Models of the Fading Channel

3.3.1 Introduction

Since the early 1990's, many researchers have studied the use of Markov chains as a way of modeling the wireless fading channel. As it was for Gilbert, Elliott, and Fritchman, the motivation behind using Markov chains is to find a simple model for mathematically complex problems. In Section 2.3.2, we saw that the fading channel is commonly modeled as a Rayleigh process. This can lead to complicated analyses, particularly in multivariate problems, because multivariate Rayleigh distributions are not well known. A Markov chain is a mathematically simple tool, and could lead to reduced complexity in many problems.

In this section, we review works in the literature that have proposed Markov chain models specifically for use in modeling the wireless fading channel. The models discussed in this section include many different approaches to the subject. Some expand on the Gilbert-Elliott symmetric binary channel model, some are based on the envelope amplitude of the received signal, while others are based on the received signal-to-noise ratio (SNR). Some approaches model the fading signal itself, while others seek to model some function of the fading, such as the bit-error rate (BER). In each case, we present the model used, and discuss its benefits and short-comings.

3.3.2 Swarts and Ferreira

The first report to propose a Markov chain model of the fading channel amplitude was Swarts and Ferreira [5]. They proposed a hidden Markov model [33] in which the underlying Markov process was the fading amplitude and the visible process was soft-decision decoder output. They validated their model by computing the soft burst and soft burst interval distributions of the model and comparing them to simulator results. We focus our discussion here on the underlying fading model.

To define the state-space, the fading amplitude was linearly quantized into N intervals, making this an amplitude-based model. This resulted in N states, each consisting of an equal amplitude range, up to some maximum amplitude value. An example of this type of state-space partitioning scheme is shown in Fig. 3.3, for $N = 8$ states.

Because the fading channel model was the hidden portion of a hidden Markov model, the output vector f was not addressed in the model. Swarts and Ferreira also made the claim that the initial occupancy vector ϕ_0 is not important. An accurate Markov chain model of the fading channel will necessarily have to be stationary, and we saw in Section 2.4.3 that correctly choosing ϕ_0 plays a crucial role in creating a stationary Markov chain model, so Swarts and Ferreira were wrong on this point. They were, however, correct when they stated that in the long-term, the starting point will have no effect, since the Markov chain will approach stationarity. This renders any observations made before stationarity is achieved as useless, though, which isn't considered in the model at all.

To determine the transition matrix, Swarts and Ferreira calculated the average transition statistics of a fading channel simulator. To simulate the fading channel, two Gaussian processes were generated using the Polar method [34], then filtered using identical first-order low-pass Butterworth filters and combined in quadrature to produce a Rayleigh process. They presented a figure that claimed to relate the filter cut-off frequency to the fading rate, but no source for this relation was given. This filtering method results in a computationally simple fading simulator, but there are limitations to this method, as discussed by Stüber [35]. The autocorrelation of the Gaussian components after low-pass filtering is exponential, much different than the desired Bessel function (2.40). The low-pass filter has the effect of basically modeling the fading as a Markov process. Thus, the good fit of model and simulation results given by Swarts and Ferreira is no surprise, since they were essentially using a Markov chain to model a Markov process.

3.3.3 Wang and Moayeri

Wang and Moayeri [36] attempted to extend the Gilbert-Elliott model of a symmetric binary channel to include a higher number of states, as well as provide a more analytically sound Markov chain channel model than Swarts and Ferreira. They proposed an AFSMC model

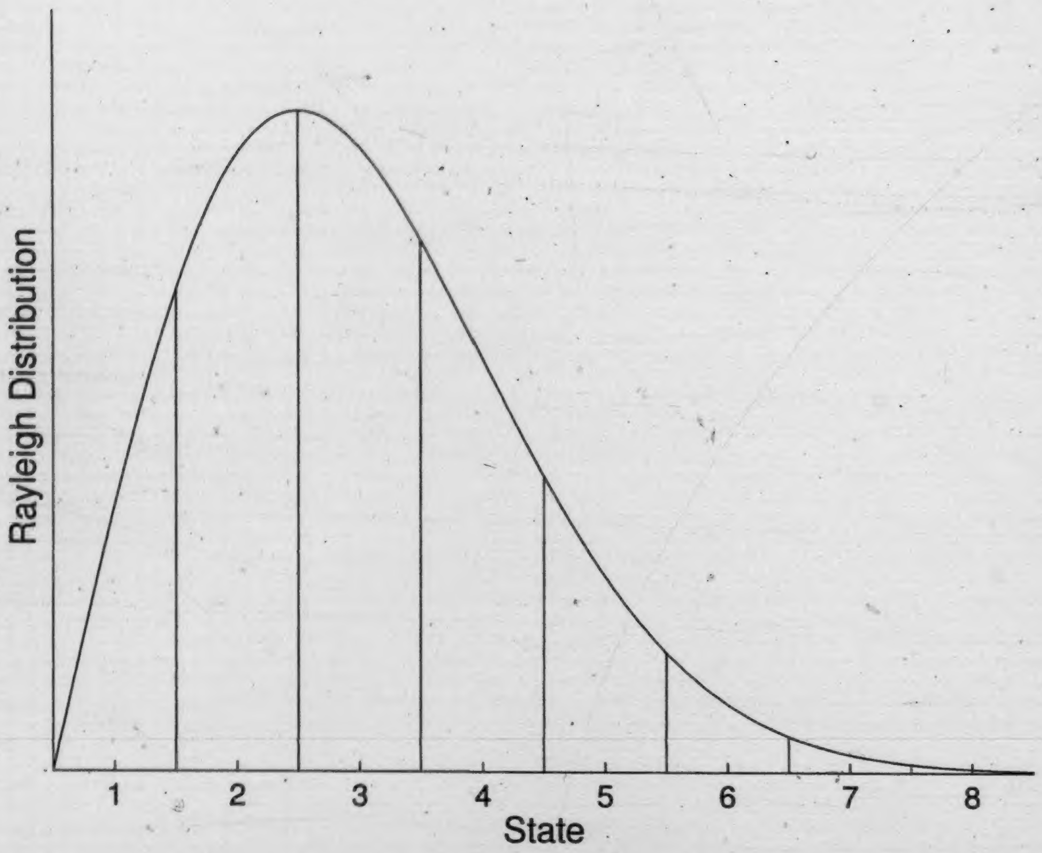

Fig. 3.3. Example of uniform partitioning of the amplitude of the Rayleigh fading channel for $N = 8$ states.

with N states, where each state represented a crossover probability of a symmetric binary channel. After identifying a set of constraints on the Markov chain channel model, they attempted to determine the model parameters by optimizing the channel, first in terms of maximizing capacity, and then in terms of minimizing distortion. They achieved some unreasonable results using this method, and instead tried to choose the model parameters to represent a real channel.

Wang and Moayeri thus chose to model the traditional ISORA Rayleigh fading channel. Like Swarts and Ferreira, the state-space was chosen to represent a partitioning of the fading signal amplitude, however, they selected the thresholds between states in such a way as to result in an equiprobable state-space. This meant that all elements of the initial occupancy vector ϕ_0 were equal to $1/N$. A diagram of this partitioning can be seen in Fig. 3.4 for $N = 8$ states. Since each state represented the crossover probability of a symmetric binary channel, output vector **f** was instead replaced with crossover probability vector **e**, which served a similar purpose.

To determine the transition probabilities, they first made the assumption that transitions only occur between neighboring states, that is,

$$P_{ij} = 0, \quad \forall |i - j| > 1. \tag{3.2}$$

The remaining values were calculated based on the level crossing rate of the ISORA Rayleigh fading model, which is expressed in [9]. To verify the model, Wang and Moayeri determined the transition probabilities of a sum-of-sinusoids simulator [37] and compared them to the transition probabilities found using the level crossing rate. They found an excellent match between the two.

Wang and Moayeri's model validation is a problem. By comparing the transition probabilities of a sum-of-sinusoids simulator to the model transition probabilities, all they really confirmed is that the sum-of-sinusoids simulator accurately models the level crossing rate of the ISORA Rayleigh fading channel. No other validation is offered that would verify whether or not the model is accurately modeling the fading channel. In fact, the sum-of-sinusoids simulator itself is known to have limitations in accurately simulating the fading

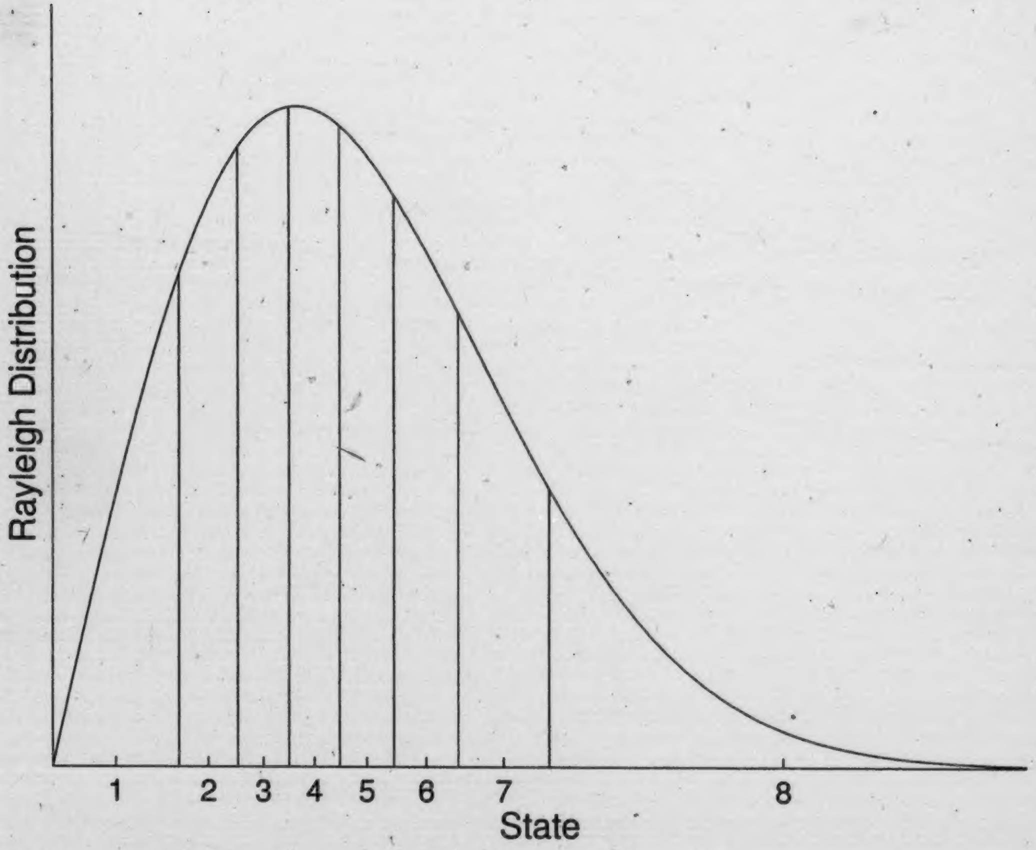

Fig. 3.4. Example of equiprobable partitioning of the amplitude of the Rayleigh fading channel for $N = 8$ states.

channel, in particular, it is not stationary [38].

3.3.4 Wang and Chang

Wang and Chang [39] attempted to verify the first-order Markovian assumption for the Rayleigh fading channel. To do this, they developed a metric based on the mutual information between states in the Markov chain. They used this metric to show that, given the information corresponding to the previous symbol, the amount of uncertainty remaining in the current symbol should be negligible. Thus, a second-order AFSMC would not provide any more meaningful information than a first-order AFSMC does and, they claim, the first-order Markovian assumption would be verified.

Wang and Chang did not consider any particular Markov chain model, and instead chose to attempt to verify the Markovian assumption based on the statistics of the ISORA Rayleigh fading channel model. They first gave an expression for the joint trivariate Rayleigh distribution, where the underlying Gaussian branches are independent with autocorrelation (2.40). This distribution was used in their metric.

They define R_i to be the received signal amplitude at time i. Then the information about R_i provided by the previous symbols R_{i-1} and R_{i-2} can be quantified by the average mutual information $I(R_i; R_{i-1}R_{i-2})$, which can be decomposed as [40]

$$I(R_i; R_{i-1}R_{i-2}) = I(R_i; R_{i-1}) + I(R_i; R_{i-2}|R_{i-1}). \tag{3.3}$$

So, Wang and Chang express the significance of R_{i-2}, given R_{i-1}, as the ratio of the average conditional mutual information $I(R_i; R_{i-2}|R_{i-1})$ and the average mutual information $I(R_i; R_{i-1}R_{i-2})$. Based on the joint trivariate Rayleigh distribution, these two mutual information values are expressed as

$$I(R_3; R_1|R_2) = \iiint f(r_1, r_2, r_3) \log \frac{f(r_3, r_1|r_2)}{f(r_1|r_2)f(r_3|r_2)} dr_1 dr_2 dr_3 \tag{3.4}$$

and

$$I(R_3; R_2R_1) = \iiint f(r_1, r_2, r_3) \log \frac{f(r_1, r_2, r_3)}{f(r_3)f(r_1, r_2)} dr_1 dr_2 dr_3 \tag{3.5}$$

where r_1, r_2, r_3 are Rayleigh random variables at three consecutive time periods, correlated as in the ISORA Rayleigh fading channel model. Wang and Chang numerically evaluated these integrals and compared the results to approximations of the mutual information ratio based on sum-of-sinusoids simulator results, for very slowly fading channels with normalized Doppler frequency $f_D T < 0.002$. They concluded that for the current channel symbol, the effect of symbols beyond the immediately previous one was negligible, thus, the Markovian assumption was validated.

Tan and Beaulieu [6] found problems with this mutual information metric. In particular, the average conditional mutual information $I(R_i; R_{i-2}|R_{i-1})$ approaches zero when the first and third samples are independent, as discussed by Wang and Chang, but also when the first, second, and third samples are highly correlated. This second case is the situation encountered by Wang and Chang in their modeling of very slowly fading channels.

Tan and Beaulieu also pointed out that the consideration of $I(R_i; R_{i-1}R_{i-2})$, as Wang and Chang did, can only be used to justify whether a second-order Markov chain will offer improvements over a first-order Markov chain. To really verify the Markovian assumption, the analysis would have to be performed on $I(R_i; R_{i-1}R_{i-2} \cdots R_{-\infty})$, which is, in general, a much more difficult problem.

3.3.5 Zorzi, Rao, and Milstein

Zorzi, Rao, and Milstein [41] made use of an AFSMC model of the fading channel to study the throughput performance of the Go-back-N (GBN) and selective-repeat (SR) ARQ protocols [42], [43]. Like the Gilbert-Elliot model, the channel was divided into two states, an error-free state and an error-guaranteed state. The two states were defined by using a threshold value to partition the fading amplitude of the received signal. Signal amplitudes above the threshold represented the error-free, or transmission success, state, while amplitudes below the threshold represented the error, or transmission failure, state. The channel sample spacing was chosen large enough that each state in the Markov chain represented successful/failed transmission of a data block.

8

Zorzi, Rao, and Milstein began by using the mutual information metric of Wang and Chang [39] to show that the Markovian assumption continued to be true when applied to their data block success/failure state space, as opposed to the fading amplitude state-space studied by Wang and Chang. They found that the metric suggested that the Markovian assumption was true for slow fading, but not for fast fading.

The transition matrix for this model was a simple 2 × 2 matrix

$$M = \begin{pmatrix} p & q \\ r & s \end{pmatrix} \tag{3.6}$$

where the marginal probability that a packet is in error is

$$\varepsilon = 1 - \frac{r}{1-p+r}. \tag{3.7}$$

Zorzi, Rao, and Milstein proposed a method to compute the elements of the transition matrix based on the average block error rate, ε, and the average length of an error burst, $1/r$, of the Rayleigh fading channel. In particular, they found that

$$\varepsilon = 1 - e^{-b} \tag{3.8}$$

and

$$r = \frac{Q(\theta, \rho\theta) - Q(\rho\theta, \theta)}{e^{b} - 1} \tag{3.9}$$

where ρ is the usual fading channel correlation, $\rho = J_0(2\pi f_D T)$, b is the fading amplitude threshold value dividing the data block success/failure states,

$$\theta = \sqrt{\frac{2b}{1-\rho^2}} \tag{3.10}$$

and $Q(\cdot,\cdot)$ is the Marcum Q function [44] defined as

$$Q(a,b) = \int_b^{\infty} x e^{-\frac{x^2+a^2}{2}} I_0(ax)\,dx \tag{3.11}$$

where $I_0(\cdot)$ is the modified Bessel function of the first kind of order zero (2.8). They also considered calculating the transition probabilities based on simulator output, using the sum-of-sinusoids simulator.

Zorzi, Rao and Milstein then studied the performance of the GBN protocol in slow fading, and compared the throughput results using the Markov chain model to simulation results. The throughput analysis involved five consecutive time slots of the Markov chain, and they found that a first-order Markov chain well matched the simulation results. They continued and used the Markov chain to study the performance of GBN and SR ARQ protocols under a number of fading scenarios. They claimed good agreement between the Markov chain analyses and simulation results, but did not include the simulation results in any of the plots.

The use of the Wang and Chang mutual information metric not withstanding, this model, though simple, was the first instance of a first-order Markov chain model successfully being used in a fading channel analysis. The limitation of this work is that the GBN and SR ARQ analyses only involved a small number of sample points, which immediately casts the applicability of this model to a wider range of problems in doubt. Also, because it is modeling the effect of the fading channel on successful packet delivery, and not the fading channel itself, it is still unclear from this work whether a Markov chain can accurately model the amplitude of the ISORA Rayleigh fading channel.

3.3.6 Zhang and Kassam

Zhang and Kassam [45] directly followed up the work of Wang and Moayeri [36] and proposed an AFSMC model of the Rayleigh fading channel where the state-space partitioning was performed on the received SNR. Each state represented a BER. They determined the number of states, as well as the partition values between the states, based on the fading rate of the channel. The model was verified using computer simulations.

To define the state-space, Zhang and Kassam partitioned the received SNR into K states, denoted s_i, $i = 1, \ldots, K$. The state thresholds were denoted $\Gamma_1, \Gamma_2, \ldots, \Gamma_{K+1}$, where $\Gamma_1 = 0$ and $\Gamma_{K+1} = \infty$. They proposed a method of choosing the threshold values based on the average time duration of each state. In particular, they derived

$$c_k = \frac{\mathrm{Exp}\left[-\frac{\Gamma_k}{\gamma_0}\right] - \mathrm{Exp}\left[-\frac{\Gamma_{k+1}}{\gamma_0}\right]}{\sqrt{\frac{2\pi\Gamma_k}{\gamma_0}}\mathrm{Exp}\left[-\frac{\Gamma_k}{\gamma_0}\right] + \sqrt{\frac{2\pi\Gamma_{k+1}}{\gamma_0}}\mathrm{Exp}\left[-\frac{\Gamma_{k+1}}{\gamma_0}\right]} \cdot \frac{1}{f_D T}, \quad k = 1, \ldots, K \tag{3.12}$$

where γ_0 is the average SNR and c_k is the average time duration of state k. By requiring that $c_k = c$ for all k, solving this set of equations for a particular value of K gave the state thresholds and the average state time duration c.

To define the initial occupancy vector, Zhang and Kassam recognized that in a Rayleigh fading environment, the received instantaneous SNR, γ, has an exponential distribution with density

$$f_\gamma(\gamma) = \frac{1}{\gamma_0} e^{-\frac{\gamma}{\gamma_0}}, \quad \gamma \geq 0 \tag{3.13}$$

which we saw in Section 2.2.3. Thus, ϕ_0 was found via

$$\phi_0[k] = \int_{\Gamma_k}^{\Gamma_{k+1}} f_\gamma(\gamma) d\gamma. \tag{3.14}$$

Instead of modeling the Rayleigh fading channel amplitude, each state in Zhang and Kassam's model represented the average BER for that state. Thus, the specific output vector values were dependant on the modulation scheme. Assuming the probability of symbol error as a function of SNR is given by $P_e(\gamma)$, the average probability of symbol error for each state was computed as

$$\mathbf{f}[k] = \frac{\int_{\Gamma_k}^{\Gamma_{k+1}} P_e(\gamma) f_\gamma(\gamma) d\gamma}{\phi_0[k]}. \tag{3.15}$$

To determine the transition matrix, Zhang and Kassam first made the same assumption as Wang and Moayeri, namely that

$$P_{ij} = 0, \quad \forall |i - j| > 1 \tag{3.16}$$

i.e. transitions only occur between neighboring states. Also like Wang and Moayeri, they determined the remaining transition probabilities based on the level-crossing rate of the Rayleigh fading process.

Verification of the model was performed more-or-less the same as was done by Wang and Moayeri. Transition probabilities were measured based on sum-of-sinusoids simulator output and compared to transition probabilities based on the model calculations. They found that the agreement between the two was very good.

Zhang and Kassam proposed an interesting method to determine the number of states and the threshold values based on the channel statistics, as opposed to the somewhat arbitrary choices of other models. However, since this work follows the work of Wang and Moayeri so closely, it succumbs to all the same limitations of that work. The assumption that transitions only occur between neighboring states doesn't really seem necessary, although the Doppler frequency was always chosen low enough that this assumption was still reasonable. Basing the transition matrix on the level crossing rate has the same problems recounted in Section 3.3.3, plus, no real performance comparison is performed between the model and a real or simulated fading channel.

3.3.7 Tan and Beaulieu

Tan and Beaulieu [6] performed a detailed analysis of the stochastic properties of a first-order AFSMC model of the fading channel. Motivated by the successful results of Zorzi, Rao, and Milstein [41], they studied the suitability of a Markov chain model in the cases of analysis of a short time frame application, and analysis of a longer time frame application. Unlike Zorzi, Rao, and Milstein, however, they modeled the amplitude of the fading channel itself, not a channel property dependant on the fading.

The state-space of Tan and Beaulieu's model was defined as follows. The received signal amplitude up to a finite maximum value M was partitioned into N states. The threshold values defining the states were denoted τ_i, where $\tau_0 = 0$ and $\tau_N = M$. The partitioning was equiprobable, like that used by Wang and Moayeri [36] and shown in Fig. 3.4. This resulted in an initial occupancy vector where all entries had the same value. In order to compensate for the fact that the partitioning was performed only up to finite value

M, they found the threshold values by solving

$$\int_{\tau_{i-1}}^{\tau_i} f_R(r)dr = \frac{F_R(M)}{N}, \quad i = 1, \ldots, N \tag{3.17}$$

where $f_R(r)$ is the usual Rayleigh density (2.3), and $F_R(M)$ is the Rayleigh distribution

$$F_R(M) = \int_0^M f_R(r)dr < 1. \tag{3.18}$$

The initial occupancy vector ϕ_0 was found by solving

$$\phi_0[i] = \frac{1}{F_R(M)} \int_{\tau_{i-1}}^{\tau_i} f_R(r)dr. \tag{3.19}$$

The scaling by $F_R(M)$ has the effect that, despite the amplitude partitioning only being performed up to a finite value, the sum of the initial occupancy vector will still be 1, as required.

The output vector f was chosen so that each state represented its midpoint amplitude value. Specifically,

$$\mathbf{f}[i] = \tau_{i-1} + \frac{\tau_i - \tau_{i-1}}{2}. \tag{3.20}$$

Unlike previous work, where the transition matrix was generally found by simulation analysis or with a simple fading channel statistic, Tan and Beaulieu followed Wang and Chang [39] in using the joint bivariate Rayleigh distribution, which gives a direct relationship between two consecutive fading channel points. The correlation between the two points was based on the traditional ISORA Rayleigh fading channel model. More specifically, if R_n is the Markov chain state at time n, then the probability of transition from state i to state j was found using the conditional distribution

$$\begin{aligned} P_{ij} &= \Pr[R_n = j | R_{n-1} = i] \\ &= \int_{\tau_{j-1}}^{\tau_j} \int_{\tau_{i-1}}^{\tau_i} f_{R_2|R_1}(r_2|r_1)dr_1dr_2 \\ &= \frac{\int_{\tau_{j-1}}^{\tau_j} \int_{\tau_{i-1}}^{\tau_i} f_{R_1R_2}(r_1, r_2)dr_1dr_2}{\int_{\tau_{i-1}}^{\tau_i} f_R(r)dr} \end{aligned} \tag{3.21}$$

where $f_{R_1R_2}(r_1, r_2)$ is the joint bivariate Rayleigh distribution. Like the initial occupancy vector, each row was scaled by its row-sum in order to compensate for the finite maximum amplitude M.

To analyze the model, Tan and Beaulieu performed a stochastic analysis on the Markov chain, comparing its first-order distribution and autocorrelation function to those of the ISORA Rayleigh fading channel model. To confirm the first-order distribution, they numerically compared the limiting probability distribution to the initial distribution to establish stationarity. Though no specific values were reported, they claimed that the Markov chain models were stationary. This confirmed the first-order distribution because the initial occupancy vector was calculated based on the first-order distribution of the ISORA Rayleigh channel model.

Plots were shown comparing the autocorrelation function of the Markov chain to that of the ISORA Rayleigh fading channel, for both slow and medium fading scenarios and various numbers of amplitude states N. In all cases, they found that the shape was very different, exhibiting an exponential-like decay, as opposed to the oscillatory-like decay of the theoretical function (2.42).

Tan and Beaulieu concluded by applying the first-order Markov chain model to two applications, a short duration application and a long duration application. The short duration application consisted of the study of the block-error rates of error correcting codes over the Rayleigh fading channel. They found that a first-order Markov chain can be appropriate for these types of applications in slow fading environments, which validates the good results found by Zorzi, Rao, and Milstein [41], since they were studying a short duration application in slow fading. Tan and Beaulieu also suggested that an uncorrelated Markov chain may be more appropriate to model fast fading applications over a short duration. For a long duration application, they studied the fade duration distribution of the fading channel. They found that a first-order Markov chain does not adequately model the ISORA Rayleigh fading channel in these types of applications.

This model and subsequent analysis represents the most thorough study of the stochastic properties of a Markov chain model of the Rayleigh fading channel to date. The main limitations of the study are the fact that partitioning the fading amplitude up to some maximum value M introduces unnecessary error into the model. The error is compensated for to some extent, and M is chosen large enough that $F_R(M)$ is close to 1, so that the error introduced is small, but there is still no apparent reason not to use $M = \infty$. Also, the stationarity of the model is not established in a clear way. It was verified numerically, but no validation is actually presented in the paper. It is very important that a Markov chain model of the fading channel be stationary, and proper validation of this property warrants deeper consideration than given in this analysis.

3.3.8 Bergamo, Maniezzo, Giavanardi, Mazzini, and Zorzi

Due to the significant mismatch of the AFSMC model's autocorrelation function to that of the ISORA Rayleigh fading channel, as reported by Tan and Beaulieu [6], Bergamo et.al. [4] proposed a new state-space for use in Markov chain models of the fading channel. Whereas virtually all previous models employed a state-space defined by the amplitude of the fading channel (or an ulterior metric, such as block-error, based on the amplitude), the new state-space proposed by Bergamo, et.al. consisted of both the amplitude and the rate-of-change of the fading envelope. They used the new Markov chain model to investigate the throughput of a simple GBN ARQ protocol, and compared the results to simulated results, as well as traditional AFSMC model results. They found that the new state-space resulted in a Markov chain model that agreed much better with simulated results than the AFSMC did.

To define the state-space, Bergamo, et.al. partitioned the envelope amplitude into M states, defined by the threshold values e_k, where $e_0 = 0$, and $e_M = \infty$. By setting an infinite upper threshold, they avoided the need to scale the resulting Markov chain elements like Tan and Beaulieu did. Likewise, the envelope rate-of-change was partitioned into S states, defined by the thresholds ϵ_k. The amplitude thresholds were chosen to result in equiprobable amplitude states, as in [6] and [36] and shown in Fig. 3.4. This was accomplished by solving

$$\int_{e_{k-1}}^{e_k} f_R(x)dx = \frac{1}{M}. \tag{3.22}$$

To choose the rate state thresholds, they claimed that numerical results indicated that $S = 3$ gave good results with thresholds $-\epsilon_1 = \epsilon_2 = \epsilon$. Note that each Markov chain state would consist of an amplitude state and a rate state, so there were M^2S^2 states in the state-space.

Bergamo, et.al. did not explicitly address the issue of computing the initial occupancy vector ϕ_0, but they did address the output vector $\mathbf{f}$. Unlike Tan and Beaulieu, where the state output value was set to the median value of each partitioned amplitude range, Bergamo, et.al. used the conditional average of each amplitude interval. Specifically,

$$\mathbf{f}[k] = M \int_{e_{k-1}}^{e_k} x f_R(x) dx. \tag{3.23}$$

No output values were associated with the rate states.

Bergamo, et.al. determined the transition probabilities via numerical analysis of a sum-of-sinusoids simulator. Since fading simulator results only consist of samples of the amplitude of the fading envelope, the rate-of-change of the envelope at time t was approximated by the difference of simulator amplitude samples, $j_t - j_{t-1}$.

To analyze the suitability of the new Markov chain model, Bergamo, et.al. first plotted the autocorrelation of the new model for increasing values of rate threshold ϵ and compared them to the sum-of-sinusoids simulator autocorrelation, as well as the autocorrelation of a traditional AFSMC model. They found that the new Markov chain model autocorrelation lay much closer to the simulator autocorrelation than that of the AFSMC. More interestingly, at small values of ϵ, the Markov chain possessed a decaying-oscillatory autocorrelation function.

Bergamo, et.al. then investigated the throughput of a GBN ARQ protocol using the new Markov chain model. As in the autocorrelation plot, they compared the throughput results to simulator throughput results, as well as those of a tradition AFSMC model. They found that the AFSMC model only matched the simulator results for very small window sizes, consistent with the results of Zorzi, Rao, and Milstein [41]. By contrast, the new Markov chain model predicted the simulator results with reasonably high accuracy for larger window sizes up to $N = 150$, the largest size on the plot. Note that the GBN protocol was studied with $\epsilon = 0.01$, which corresponded to the oscillatory autocorrelation mentioned in the previous paragraph.

This paper makes a strong case for using the new expanded state-space. In the case of a GBN throughput analysis, the new Markov chain performs far better than an AFSMC model. However, the stochastic analysis of the new Markov chain is extremely limited. The first-order and stationary properties are not considered, and the initial occupancy vector is not explicitly considered either. Basing the transition matrix on sum-of-sinusoids simulator output is also a limitation, since it has known issues in accurately simulating the ISORA Rayleigh fading channel [38]. Despite these limitations, the good application results suggest that a more substantial stochastic analysis of this state-space is warranted.

3.3.9 Hueda and Rodríguez

In light of the problems with the Wang and Chang metric [36] pointed out by Tan and Beaulieu [6], Hueda and Rodríguez [46] proposed a new information theoretic test of the Markov property. The Markov chain state-space under consideration was the same as in Zorzi, Rao, and Milstein [41], where a state represents either a successful block transmission, or a failed block transmission. They used the new test to verify the first-order Markovian assumption for block error processes on Rayleigh fading channels.

Hueda and Rodríguez began by proposing the new information theoretic metric in terms of the block errors. They define β_i to be a binary process where $\beta_i = 1$ if received data block i is in error, and $\beta_i = 0$ otherwise. Based on the observations made by Tan and Beaulieu, they defined

$$I(\beta_i; \beta_{i-1}\beta_{i-2}\cdots\beta_{i-\infty}) = H(\beta_i) - H(\beta_i|\beta_{i-1}\beta_{i-2}\cdots\beta_{i-\infty}) \tag{3.24}$$

where $H(\cdot)$ and $H(\cdot|\cdot)$ are the entropy and conditional entropy, respectively [47]. Then, they defined

$$\begin{aligned}\lambda &= \frac{I(\beta_i; \beta_{i-1})}{I(\beta_i; \beta_{i-1}\cdots\beta_{i-\infty})}\\ &= \frac{H(\beta_i) - H(\beta_i|\beta_{i-1})}{H(\beta_i) - H(\beta_i|\beta_{i-1}\cdots\beta_{i-\infty})}.\end{aligned} \tag{3.25}$$

When the process is exactly a Markov process, $\lambda = 1$, but when $\lambda < 1$ and $\lambda \to 1$, it cannot be concluded that the process is Markov for the same reasons Tan and Beaulieu described earlier. Thus, the proposed criterion for a first-order Markov chain model to adequately model the block error process is

$$\psi = \frac{\lambda}{I(\beta_i; \beta_{i-1} \cdots \beta_{i-\infty})} \gg 1, \quad \lambda < 1. \tag{3.26}$$

Since $I(\beta_i; \beta_{i-1} \cdots \beta_{i-\infty}) \leq 1$ and gets smaller as the correlation value of β_i with the past samples decreases, the authors claim it is reasonable to assume that the process is approximately Markov when ψ is sufficiently large.

Hueda and Rodríguez compared the performance of the new metric with that of Wang and Chang's metric in the analysis of the suitability of a first-order Markov chain in modeling the Rayleigh fading channel, as well as a Rayleigh fading channel with maximal ratio combining (MRC) diversity. In the traditional case with no diversity, they found that their metric outperformed that of Wang and Chang, and that it suggested that a first-order Markov chain may be sufficient to model the block errors in slow-to-medium fading ($0.01 < f_D T < 0.1$) in cases where the block error rate is small enough. In the case of Rayleigh fading with MRC diversity, the metric suggested that the accuracy of the first-order Markovian assumption decreases as the diversity order increases.

Although the new metric outperforms that of Wang and Chang, its general accuracy is not established. No actual Markov chain models are considered for any of the scenarios discussed. This doesn't necessarily discount the results, but additional justification is needed to verify the new metric.

3.3.10 Lin and Tseng

Lin and Tseng [1] proposed a two-layer Markov chain model of the fading channel. The upper layer was used to model the small-scale Rayleigh fading, while the lower layer was used to model the large-scale log-normal shadowing. The Markov chain parameters were determined from propagation measurement data. The two-layer Markov chain model was verified by comparing some statistics of the model to those of the measurements. Results were also compared to those of traditional single-layer Markov chains.

Lin and Tseng defined the state-space by partitioning the shadowing envelope into J states and the fading envelope into K states. Threshold values l_k partitioned the shadowing envelope, and values r_k partitioned the fading envelope, where $l_0 = r_0 = 0$ and $l_J = r_K = \infty$. At each time period, the Markov chain state was specified by one shadowing state and one fading state.

The transition matrix structure of this model is more complicated than the usual Markov chain model. One transition matrix was used the describe the transition probabilities between shadowing states. For each of these shadowing states, a different transition matrix was used to describe the transition probabilities of the fading. The particular model computed by Lin and Tseng used a 9×9 shadowing transition matrix, and nine 5×5 fading transition matrices. The specific transition probabilities were determined via numerical analysis of propagation measurement data taken near the campus of National Taipei University of Technology in urban Taipei. A transmission antenna was placed on a floor of one of the buildings, and measurements were taken over a drive of approximately 1.5 km around the campus.

To verify the model, Lin and Tseng compared the PDF, level-crossing rate, and BER of the two-layer model to those of the measurements. They also compared a single-layer Markov chain model using the same statistics. They found that the two-layer model performed better than the single-layer model, and matched the measured statistics quite closely.

While the idea of modeling the fading and shadowing in separate Markov chain processes may have merit, there are a number of limitations to the work of Lin and Tseng. Verifying the two-layer model by saying it outperforms a single-layer model is somewhat disingenuous. The traditional single-layer Markov chains were never meant to model the shadowing process; they have historically been studied in terms of modeling the stationary Rayleigh fading process. The two-layer model was also verified by comparing its PDF and level-crossing rate to that of the measured process. We have already seen that Markov chain models are able to accurately model the first-order distribution of the channel, as well as the level crossing rate. Where Markov chain models currently struggle is in modeling the fading channel autocorrelation function, which Lin and Tseng do not consider. However, based on a qualitative comparison of a two-layer Markov chain simulated signal amplitude and the measured signal, as plotted in their paper and reproduced in Fig. 3.5, we would guess that the autocorrelation structure is being modeled poorly, since the shadowing structures look very different.

3.3.11 Conclusion

In this section, we surveyed the literature on the subject of Markov chain modeling of the Rayleigh fading channel. Despite many different approaches to the subject, as well as differing goals in many cases, a uniform theory begins to emerge. An AFSMC can adequately model the first-order statistics of the ISORA Rayleigh fading channel, but higher-order statistics, in particular, the autocorrelation function, cannot be modeled well. Despite this apparently significant limitation, there is evidence that Markov chain models may still be appropriate in some applications, especially data packet level analysis over a short time frame in slow fading scenarios. There is also evidence that an expanded state-space that involves both the amplitude and rate-of-change of the fading envelope, proposed by Bergamo, et.al. [4], may improve on the Markov chain model's ability to approximate the fading channel autocorrelation function. It is this new state-space that will be studied in detail throughout subsequent chapters of this thesis.

3.4 Markov Chain Models in Practice

3.4.1 Introduction

Despite the limitations of Markov chain models of the fading channel identified in Section 3.3, AFSMCs have found practical use in a number of applications. The most successful uses have primarily been in data packet analysis, and in this section, we review some of the papers in the literature that have employed Markov chains as models for the Rayleigh fading channel. We focus on the particular model used, and consider the validity of the

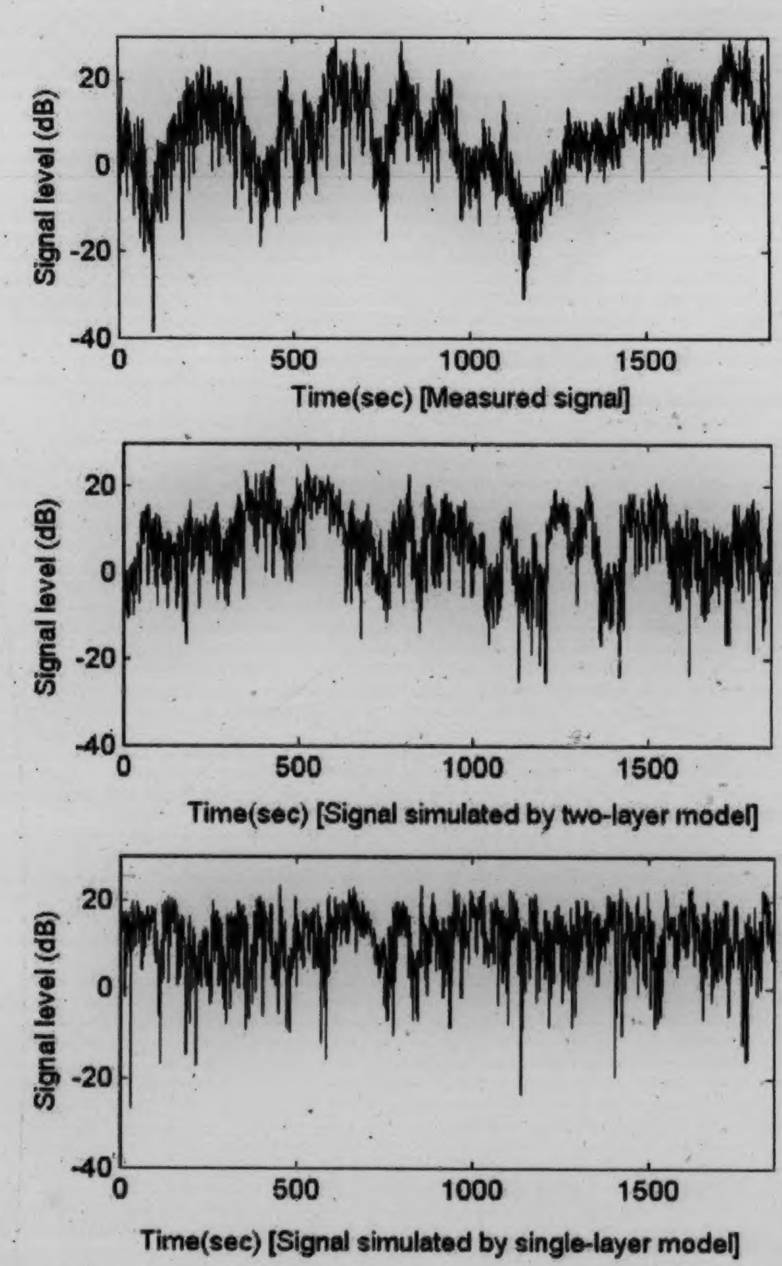

Fig. 3.5. Measured signal, two-layer Markov chain model simulated signal, and single-layer Markov chain simulated signal envelopes from Lin and Tseng [1].

results obtained.

3.4.2 Liu and El Zarki

Liu and El Zarki [48] proposed a hybrid ARQ error control scheme based on the concatenation of a Reed-Solomon (RS) code and a rate-compatible punctured convolutional (RCPC) code for low-bit-rate video transmission over wireless channels. To study the performance of this scheme, they made use of a Markov chain model of the wireless fading channel.

The Markov chain model used was essentially the same as that of Wang and Moayeri [36], except that the partitioning of the states was based on the received SNR, like that of Zhang and Kassam [45], as opposed to the fading envelope amplitude. Also like Zhang and Kassam, each state represented the average BER over the partitioned SNR range.

The received signal was partitioned into Φ states, where the SNR values defining the state thresholds were denoted $0 = x_1 < x_2 < \cdots < x_{\Phi+1} = \infty$. Liu and El Zarki proposed a method to select the thresholds in order to minimize the mean-squared error (MSE) between the BER value for the Markov model and the BER for the Rayleigh fading channel. They defined the MSE as

$$MSE = \sum_{k=1}^{\Phi} \int_{x_k}^{x_{k+1}} (e_k - P_e(\gamma))^2 f_\gamma(\gamma) d\gamma \tag{3.27}$$

where e_k is the BER value in state k, $P_e(\gamma)$ is the probability of error for SNR γ, and $f_\gamma(\gamma)$ is the probability distribution of the SNR. For the Rayleigh fading channel, $f_\gamma(\gamma)$ is exponential (3.13). The result of the MSE minimization is that the state thresholds and BER values were defined by iteratively solving

$$e_k = \frac{\int_{x_k}^{x_{k+1}} P_e(\gamma) f_\gamma(\gamma) d\gamma}{\int_{x_k}^{x_{k+1}} f_\gamma(\gamma) d\gamma} \tag{3.28}$$

and

$$P_e(x_k) = \frac{e_{k-1} + e_k}{2}. \tag{3.29}$$

This expression for e_k happens to be the conditional mean of the BER over each state, which is the expression used by Zhang and Kassam, although the partitioning resulting from this method would likely be different. The initial occupancy vector ϕ_0 and the transition matrix P were both defined like Zhang and Kassam, which in turn were defined like Wang and Moayeri.

Liu and El Zarki used this channel model to study the performance of their proposed concatenated hybrid ARQ (CH-ARQ) scheme. They compared the results to simulations and found that the analysis based on the Markov chain fading channel model agreed reasonably well with the simulated results.

The limitations of the level-crossing rate approach to calculating the Markov chain transition probabilities have been discussed already. However, it is interesting that, despite these limitations, the results found by Liu and El Zarki agree reasonably well with the simulated results. We note, however, that simulation results were only presented for the cases when the mobile speed is 2 km/h, which results in a very low Doppler frequency value. For the cases when the mobile speed is 100 km/h, which gives a much higher Doppler frequency, no simulation results were presented. We've seen previously that Markov chains model slow fading environments acceptably over limited time frames, which the results here validate, but the validity of the higher Doppler frequency analysis is questionable.

3.4.3 Babich

Babich [49] made use of a Markov chain model of the fading channel while studying the performance of hybrid ARQ schemes. He proposed a theoretical method, based on the sphere-packing bound, to evaluate and compare the achievable performance of different schemes.

Babich offered no details on the Markov model used in this work, which makes it difficult to draw any conclusions on the applicability of Markov chain models in the context of this type of analysis. His throughput efficiency plots, which include simulation results, show that the analytic and simulation results agree reasonably closely, although the analytic results, which are based on a Markov model of the fading channel, consistently over-predict the throughput efficiency. The relative data trends are reasonably consistent, though, even if the values aren't exact.

The results of this work seem to suggest that an AFSMC is an appropriate fading channel model for this type of application. However, due to the lack of details about the channel model chosen, it is impossible to tell whether the differences between analytic and simulation results are due to channel model limitations, or due to looseness in the sphere-packing bound used in the analysis.

3.4.4 Galluccio, Licandro, Morabito, and Schembra

Galluccio, et.al. [50] studied adaptive rate video encoding over wireless links. In situations where adaptive forward error correction (FEC) schemes are used, the available bandwidth can vary as the FEC redundancy is changed. The authors studied an analytical framework for adapting video encoding rates to changing channel conditions.

Since the video source can be modeled as a Markov chain, it is convenient to model the wireless channel as a Markov chain as well. The authors did not derive a particular model themselves, instead referring to the literature, particularly Tan and Beaulieu [6] and Wang and Moayeri [36]. Because of this, their channel model suffers all the limitations discussed previously. Although there have been some successes in modeling packet-level applications using AFSMCs, there are no simulation results among the many results presented in this paper, which makes the validity of the Markov chain channel model for this type of application impossible to judge.

3.4.5 Rossi, Badia, and Zorzi

Rossi, Badia, and Zorzi [2] used an N-state Markov chain model of the fading channel to study SR ARQ delay statistics. They derived an exact expression for the ARQ packet delay statistics in a Markov channel. The analysis results were compared to simulation results to verify their accuracy.

A similar study was performed by these authors in [51], where they presented an analytical framework to obtain the delivery delay statistics. However, that work assumed a two-state Markov model of the fading channel, like Zorzi, Rao, and Milstein [41], which may limit the validity. Thus, the authors generalized the problem by expanding the model to arbitrary N states.

Like Zhang and Kassam [45], the authors partitioned the Markov chain in terms of the SNR instead of the fading envelope amplitude. As opposed to the equiprobable partitioning frequently performed in the literature, Rossi, Badia, and Zorzi proposed a partitioning scheme based on the packet error probability function. Since each state of the Markov chain model represented a BER, which is dependant on the SNR of that state, basing the partitioning on the packet error probability function gave the state partitioning that best quantized that function. To specify the SNR threshold values $\Gamma_0, \Gamma_1, \ldots, \Gamma_K$ for a K state Markov chain, the authors first selected two numbers, l_1 and l_{K-1}, such that l_1 was close to 1 and l_{K-1} was close to zero. Then, two threshold values were specified using $\Gamma_1 = P_e^{-1}(l_1)$ and $\Gamma_{K-1} = P_e^{-1}(l_{K-1})$, where $P_e(\cdot)$ is the packet error probability function. After that, $\boldsymbol{\phi}_0[1]$ and $\boldsymbol{\phi}_0[K]$ were found via

$$\boldsymbol{\phi}_0[k] = \int_{\Gamma_{k-1}}^{\Gamma_k} f_\gamma(\gamma) d\gamma \tag{3.30}$$

where $f_\gamma(\gamma)$ is the exponential distribution (3.13) with parameter γ_0, the average SNR of the channel. Finally, the remaining threshold values were found by solving

$$\int_{\Gamma_{k-1}}^{\Gamma_k} f_\gamma(\gamma) d\gamma = \frac{1 - \boldsymbol{\phi}_0[1] - \boldsymbol{\phi}_0[K]}{K-2}. \tag{3.31}$$

An example of this partitioning scheme is shown in Fig. 3.6 for $k = 6$.

Once the partition thresholds were defined, the initial occupancy vector $\boldsymbol{\phi}_0$ was found using (3.30) and the transition matrix was calculated using the correlated bivariate Rayleigh distribution as in Tan and Beaulieu [6]. The output vector, which in this case is a packet error vector, was found, as in Zhang and Kassam, with

$$\mathbf{f}[k] = \frac{\int_{\Gamma_k}^{\Gamma_{k+1}} P_e(\gamma) f_\gamma(\gamma) d\gamma}{\boldsymbol{\phi}_0[k]}. \tag{3.32}$$

Rossi, Badia, and Zorzi proceeded to examine the delivery delay statistics of a SR ARQ protocol using the Markov chain model and compared the results with simulations.

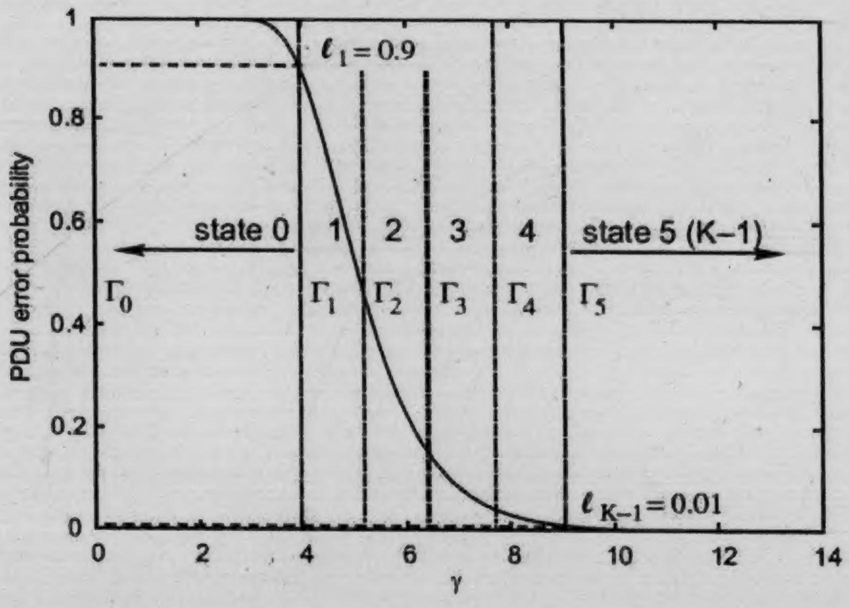

Fig. 3.6. Example of the partitioning scheme from Rossi, Badia, and Zorzi [2], for $k = 6$.

Two Markov chain models were included, one using the new partitioning scheme discussed above, and one using the more common equiprobable partitioning scheme. They found that the new partitioning scheme greatly outperformed the traditional equiprobable scheme, and that the agreement with simulated results was quite good. The match of the Markov model delivery delay statistics to the simulated statistics was not perfect, but it was reasonably close.

An important discovery of this paper is that the partitioning of the state-space can have a significant effect on the goodness of the resulting Markov chain model. The partitioning scheme should be chosen to best reflect the process the Markov chain is being used to model. This paper also demonstrated that, despite the limitations of the AFSMC in modeling the higher-order statistics of the fading channel, good results can still be achieved in packet delay problems.

3.4.6 Conclusion

In this section, we discussed some works from the literature that made use of Markov chains to model the fading channel. We found that, in some cases, too much faith is placed on the previous research and model specifics are not given, nor is the applicability of the Markov chain fading channel model to a given application established or verified. In those cases, the validity of the results obtained is questionable. In other cases, the model specifics are dealt with in some detail. In the situations where simulation results are presented to validate the Markov chain model, agreement is typically reasonable. It would appear that an AFSMC model of the fading channel can give good results in data packet analysis problems, particularly ARQ problems, provided they are not applied naïvely.

3.5 Conclusion

This chapter presented a survey of much of the literature on the subject of Markov chain modeling of communications channels. In Section 3.2, we discussed some early models proposed for wireline and fixed wireless communications. Section 3.3 presented models proposed especially for the fading channel, focusing particularly on first-order AFSMCs. Section 3.4 presented some work from the literature that made use of Markov chain models of the fading channel in practice.

In general, we saw that most of the Markov chain models proposed previously in the literature can successfully model the first-order statistics of the fading channel, but fail to correctly capture the higher-order statistics. However, there have still been some successful applications of Markov chain fading channel models, particularly for ARQ analyses over short time periods in slow fading.

In virtually all models proposed in the literature, the state-space is based on the envelope amplitude of the fading signal, or the SNR. An expanded state-space, proposed by Bergamo, et.al. [4], is based on the amplitude and the rate-of-change of the fading envelope. Results suggest that this state-space may improve the Markov chain models ability to capture the higher-order statistics of the fading model, but a more detailed study is required. It is this state-space that will be analyzed in the remaining chapters of this thesis.

Chapter 4

Markov Chain Modeling of the Complex Gaussian Fading Process

4.1 Introduction

As we discussed in Section 2.3.2, the ISORA model of the Rayleigh fading channel is specified in two ways, as a complex Gaussian process, and as a Rayleigh process. In this chapter, we propose a Markov chain model of the ISORA Rayleigh fading channel, formed by first modeling the underlying complex Gaussian fading process, based on an amplitude/rate-of-change state-space. A Markov chain model of the Rayleigh fading envelope process can then be formed from the Gaussian model. Unlike many of the models we discussed in Chapter 3, the models we derive here will model the amplitude of the fading process.

In Section 4.2, we examine the suitability of a first-order Markov chain in modeling the fading process. We first find and analyze a first-order Markov chain model of the ISORA Gaussian fading process. Then, we propose a method to transform this Gaussian model into a model of the fading envelope, and analyze the resulting model.

In Section 4.3, we examine the suitability of a second-order Markov chain in modeling the fading process. The methods of Section 4.2 are extended to find and analyze a second-order Markov chain model of the ISORA Gaussian fading process, as well as the associated model of the fading envelope process. Section 4.4 concludes the chapter.

4.2 First-Order Markov Chain Model

4.2.1 Introduction

In this section, we examine the ability of a first-order Markov chain to model the complex Gaussian components of the ISORA Rayleigh fading channel, when the state-space is based on the amplitude and rate-of-change of the Gaussian process. In Section 4.2.2, we present a method to calculate the three elements of a Markov chain model, based on the statistics of the ISORA Gaussian fading process, and in Section 4.2.3, we analyze the resulting Markov chain model. Based on the observations made in this analysis, in Section 4.2.4, we consider a Markov chain model of the 3-DISORA Gaussian fading process. In Section 4.2.5, we present a method to create a Markov chain model of the ISORA Rayleigh fading envelope process, based on the Markov chain model of the underlying Gaussian process, and analyze the resulting model. Section 4.2.6 concludes this section.

4.2.2 Computing the Markov Chain Model

In Section 2.4.2, we identified the three elements necessary to define a Markov chain model, namely, the transition matrix P, initial occupancy vector ϕ_0, and output vector $\mathbf{f}$. In this section, we present a method of calculating these three elements in order to model the underlying complex Gaussian process of the ISORA Rayleigh fading channel.

Recall from Section 2.3.2 that the ISORA Rayleigh fading model is the envelope of a complex Gaussian process with quadrature components $T_c(t)$ and $T_s(t)$. Both of these components have first-order distributions $f_G(T_c)$ and $f_G(T_s)$, where (2.35) gives

$$f_G(x) = \frac{1}{\sqrt{2\pi b_0}} e^{-x^2/2b_0}$$

which is a zero-mean Gaussian distribution with variance b_0. Each quadrature component has autocorrelation (2.40)

$$g(\tau) = R_G(\tau) = b_0 J_0(2\pi f_D \tau)$$

and the cross-correlation between the two components is (2.41)

$$h(\tau) = 0$$

thus, the quadrature components are independent and identically distributed. We will focus on modeling Gaussian process $T_c(t)$, with the understanding that the resulting Markov chain also models $T_s(t)$. Since the state-space of the Markov chain models we consider is based on the amplitude and rate-of-change of the Gaussian process, we will be making use of the joint distributions of Gaussian random variables are their derivatives, which we presented in Section 2.2.4.

4.2.2.1 Defining the State-Space

Before finding expressions for the Markov chain model elements, we must define the state-space of the Markov chain, which is based on both the amplitude and rate-of-change of the Gaussian fading component $T_c(t)$. Since a Gaussian random variable and its derivative are independent, as we saw in (2.16), the amplitude space and rate space can be partitioned independently.

Let the state-space be divided into n amplitude states and m rate states. The n amplitude states are defined by the length $n+1$ vector $\boldsymbol{\delta} = [\delta_0, \ldots, \delta_n]$ of threshold values, where $\delta_0 = -\infty$, $\delta_n = \infty$, and $\delta_1, \ldots, \delta_{n-1}$ can be any ascending sequence of real numbers. Likewise, the m rate states are defined by a length $m+1$ vector of threshold values $\boldsymbol{\gamma} = [\gamma_0, \ldots, \gamma_m]$, where $\gamma_0 = -\infty$, $\gamma_m = \infty$, and $\gamma_1, \ldots, \gamma_{m-1}$ is also any ascending sequence of real numbers.

The result of this partitioning is nm states, labeled $\{s_1, \ldots, s_{nm}\}$, where the threshold values defining the border of state s_d are $\{\delta_{i_d-1}, \delta_{i_d}\}$ in the amplitude domain and $\{\gamma_{j_d-1}, \gamma_{j_d}\}$ in the rate domain, with

$$i_d = \text{Quotient}(d, m, 1) + 1 = \left\lfloor \frac{d-1}{m} \right\rfloor + 1 \tag{4.1}$$

$$j_d = \mathrm{Mod}(d, m, 1) = d - m \left\lfloor \frac{d-1}{m} \right\rfloor \tag{4.2}$$

where $\lfloor x \rfloor$ is the floor function, or the largest integer less than or equal to x. Thus, the state-space of the Markov chain model is fully specified by the threshold vectors $\boldsymbol{\delta}$ and $\boldsymbol{\gamma}$.

4.2.2.2 Output Vector f

Vector f represents the output of the Markov chain at each state. Since this Markov chain will be modeling the amplitude of the Gaussian fading process, we employ a method similar to Liu and El Zarki [48] and choose the elements of f to minimize the MSE between the amplitude value of the Markov chain model and the amplitude of the Gaussian fading process over each state.

The MSE is defined as

$$\begin{aligned}
\mathrm{MSE} &= \sum_{d=1}^{nm} \int_{\gamma_{j_d-1}}^{\gamma_{j_d}} \int_{\delta_{i_d-1}}^{\delta_{i_d}} (\mathbf{f}_d - T_c)^2 f_G(T_c, T_c') dT_c dT_c' \\
&= \sum_{d=1}^{nm} \int_{\gamma_{j_d-1}}^{\gamma_{j_d}} \int_{\delta_{i_d-1}}^{\delta_{i_d}} (\mathbf{f}_d - T_c)^2 f_G(T_c) f_G(T_c') dT_c dT_c'
\end{aligned}$$

where i_d and j_d specify the thresholds of the amplitude and rate of state s_d and are found using (4.1) and (4.2), and joint distribution $f_G(T_c, T_c')$ (2.16) can be decomposed into $f_G(T_c)$ and $f_G(T_c')$ because of the independence of T_c and T_c'. To minimize the MSE with respect to $\mathbf{f}_d$, we find the derivatives of the MSE and set them to zero:

$$\frac{\partial \mathrm{MSE}}{\partial \mathbf{f}_d} = \int_{\gamma_{j_d-1}}^{\gamma_{j_d}} \int_{\delta_{i_d-1}}^{\delta_{i_d}} 2(\mathbf{f}_d - T_c) f_G(T_c) f_G(T_c') dT_c dT_c' = 0.$$

By rearranging this expression, we get

$$
\begin{aligned}
\mathrm{f}_d &= \frac{\int_{\gamma_{j_d-1}}^{\gamma_{j_d}} \int_{\delta_{i_d-1}}^{\delta_{i_d}} T_c f_G(T_c) f_G(T'_c) dT_c dT'_c}{\int_{\gamma_{j_d-1}}^{\gamma_{j_d}} \int_{\delta_{i_d-1}}^{\delta_{i_d}} f_G(T_c) f_G(T'_c) dT_c dT'_c} \\
&= \frac{\int_{\delta_{i_d-1}}^{\delta_{i_d}} T_c f_G(T_c) dT_c \cancel{\int_{\gamma_{j_d-1}}^{\gamma_{j_d}} f_G(T'_c) dT'_c}}{\int_{\delta_{i_d-1}}^{\delta_{i_d}} f_G(T_c) dT_c \cancel{\int_{\gamma_{j_d-1}}^{\gamma_{j_d}} f_G(T'_c) dT'_c}} \\
&= \frac{\int_{\delta_{i_d-1}}^{\delta_{i_d}} T_c f_G(T_c) dT_c}{\int_{\delta_{i_d-1}}^{\delta_{i_d}} f_G(T_c) dT_c} \\
&= \frac{\sqrt{\frac{2b_0}{\pi}} \left(e^{-\frac{\delta_{i_d-1}^2}{2b_0}} - e^{-\frac{\delta_{i_d}^2}{2b_0}} \right)}{\mathrm{Erf}\left[\frac{\delta_{i_d}}{\sqrt{2b_0}}\right] - \mathrm{Erf}\left[\frac{\delta_{i_d-1}}{\sqrt{2b_0}}\right]}
\end{aligned}
\tag{4.3}
$$

where $f_G(T_c)$ is given by (2.35) and Erf[·] is the error function [10, eq. 7.1.1] defined as

$$\mathrm{Erf}[z] = \frac{2}{\sqrt{\pi}} \int_0^z e^{-t^2} dt. \tag{4.4}$$

To verify that (4.3) minimizes the MSE, we must ensure that the second derivative of the MSE is positive. We find that

$$\frac{\partial^2 \mathrm{MSE}}{\partial \mathrm{f}_d^2} = 2 \int_{\gamma_{j_d-1}}^{\gamma_{j_d}} \int_{\delta_{i_d-1}}^{\delta_{i_d}} f_G(T_c) f_G(T'_c) dT_c dT'_c > 0 \tag{4.5}$$

because the integral over any range of a Gaussian PDF will always be positive. Thus, the MSE minimizing solution for f is the conditional mean of a Gaussian random variable over each state. Note that, although each Markov chain state consists of an amplitude state and a rate state, no output value is associated with the rate.

4.2.2.3 Initial Occupancy Vector ϕ_0

As we discussed in Section 2.4.2, the initial occupancy vector represents the distribution of the Markov chain at its starting point. When used in conjunction with the transition matrix, it also specifies the distribution of the Markov chain at any point in time. To model the Gaussian fading process over the amplitude/rate state-space, the initial occupancy vector will be calculated to represent a quantized version of $f_G(T_c, T'_c)$, which is given in (2.16).

Thus, to compute $\phi_0[d]$, we first find i_d and j_d using (4.1) and (4.2), respectively. This identifies the amplitude and rate thresholds of state s_d. Then, the probability of starting in this state is calculated as

$$\begin{aligned}\phi_0[d] = \Pr[X_0 = s_d] &= \int_{\gamma_{j_d-1}}^{\gamma_{j_d}} \int_{\delta_{i_d-1}}^{\delta_{i_d}} f_G(T_c, T_c')dT_c dT_c' \\ &= \frac{1}{4}\left(\mathrm{Erf}\left[\frac{\gamma_{j_d}}{\sqrt{2b_2}}\right] - \mathrm{Erf}\left[\frac{\gamma_{j_d-1}}{\sqrt{2b_2}}\right]\right)\left(\mathrm{Erf}\left[\frac{\delta_{i_d}}{\sqrt{2b_0}}\right] - \mathrm{Erf}\left[\frac{\delta_{i_d-1}}{\sqrt{2b_0}}\right]\right). \qquad (4.6)\end{aligned}$$

4.2.2.4 Transition Matrix P

The transition matrix specifies the probabilities of all the state transitions in the Markov chain. Specifically, P_{qh} is the probability that the Markov chain makes the transition to state s_h from state s_q. We saw in Chapter 3 that there have been a number of different approaches to finding the transition matrix of a Markov chain model of the fading channel. The most direct method is to use the joint distribution of two consecutive states, as Tan and Beaulieu [6] did, so we adapt their method to the amplitude/rate state-space under examination here.

Let T_{c_1} and T_{c_1}' represent the amplitude and rate-of-change of the Gaussian fading process at time t, while T_{c_2} and T_{c_2}' represent the amplitude and rate at time $t + T$, where T is the sample spacing of the model. Let X_{k-1} be a random variable representing the state of the Markov chain at time t, and X_k be a random variable representing the state at the next time instant, $t + T$. Then, the transition matrix will be calculated as

$$\begin{aligned}P_{qh} &= \Pr[X_k = s_h | X_{k-1} = s_q] \\ &= \frac{\Pr[X_{k-1} = s_q, X_k = s_h]}{\Pr[X_{k-1} = s_q]} \\ &= \frac{\int_{\gamma_{j_h-1}}^{\gamma_{j_h}} \int_{\delta_{i_h-1}}^{\delta_{i_h}} \int_{\gamma_{j_q-1}}^{\gamma_{j_q}} \int_{\delta_{i_q-1}}^{\delta_{i_q}} f_G(T_{c_1}, T_{c_1}', T_{c_2}, T_{c_2}')dT_{c_1}dT_{c_1}'dT_{c_2}dT_{c_2}'}{\int_{\gamma_{j_q-1}}^{\gamma_{j_q}} \int_{\delta_{i_q-1}}^{\delta_{i_q}} f_G(T_{c_1}, T_{c_1}')dT_{c_1}dT_{c_1}'} \\ &= \frac{\int_{\gamma_{j_h-1}}^{\gamma_{j_h}} \int_{\delta_{i_h-1}}^{\delta_{i_h}} \int_{\gamma_{j_q-1}}^{\gamma_{j_q}} \int_{\delta_{i_q-1}}^{\delta_{i_q}} f_G(T_{c_1}, T_{c_1}', T_{c_2}, T_{c_2}')dT_{c_1}dT_{c_1}'dT_{c_2}dT_{c_2}'}{\phi_0[q]}. \qquad (4.7)\end{aligned}$$

Joint distribution $f_G(T_{c_1}, T_{c_1}', T_{c_2}, T_{c_2}')$ was discussed in Section 2.2.4. It is a multivariate Gaussian (2.2) with mean vector $\boldsymbol{\mu} = 0$, and covariance matrix, assuming sample spacing

T between consecutive points, given by

$$\Sigma = \begin{pmatrix} b_0 & 0 & g(T) & g'(T) \\ 0 & b_2 & -g'(T) & -g''(T) \\ g(T) & -g'(T) & b_0 & 0 \\ g'(T) & -g''(T) & 0 & b_2 \end{pmatrix}. \tag{4.8}$$

There is no closed-form for the numerator of (4.7), so the transition matrix must be calculated numerically. We make use of the algorithm proposed by Genz [52] to perform numerical computation of multivariate Gaussian integrals with arbitrary covariance matrix Σ. Details of this algorithm are discussed in Appendix A.

4.2.3 Model Analysis

To analyze how well a first-order Markov chain models the ISORA Gaussian fading process, we compare the statistics of the Markov chain model to those of the ISORA Gaussian fading model on the basis of three important properties. First, the first-order distribution of the Markov chain should approximate the first-order Gaussian distribution with variance b_0. Second, the Markov chain model must be stationary. Finally, the autocorrelation of the Markov chain model should approximate the ISORA autocorrelation function.

We focus our study on threshold vectors $\boldsymbol{\delta}$ and $\boldsymbol{\gamma}$ that result in equiprobable state-space definitions, meaning all values of the initial occupancy vector are equal to $1/nm$. Because of the independence of the amplitude and rate, which can be seen in joint distribution (2.16), the amplitude state-space and rate state-space can be partitioned separately. Specifically, we can find $\boldsymbol{\delta}[d]$ by solving

$$\int_{\delta_{d-1}}^{\delta_d} \frac{1}{\sqrt{2\pi b_0}} e^{-\frac{T_c^2}{2b_0}} dT_c = \frac{1}{2}\left(\mathrm{Erf}\left[\frac{\delta_d}{\sqrt{2b_0}}\right] - \mathrm{Erf}\left[\frac{\delta_{d-1}}{\sqrt{2b_0}}\right]\right) = \frac{1}{n} \tag{4.9}$$

for $d = 1, \ldots, n-1$. Likewise, $\gamma[d]$ is found by solving

$$\int_{\gamma_{d-1}}^{\gamma_d} \frac{1}{\sqrt{2\pi b_2}} e^{-\frac{T_c'^2}{2b_2}} dT_c' = \frac{1}{2}\left(\mathrm{Erf}\left[\frac{\gamma_d}{\sqrt{2b_2}}\right] - \mathrm{Erf}\left[\frac{\gamma_{d-1}}{\sqrt{2b_2}}\right]\right) = \frac{1}{m} \tag{4.10}$$

for $d = 1, \ldots, m-1$. Note that, without loss of generality, we always take $b_0 = 1$.

4.2.3.1 First-Order Distribution

Fig. 4.1 shows the first-order distribution of the Markov chain model compared to the Gaussian distribution, for various values of n. We can see that the modeling is accurate for all values of n, although at $n = 5$, the model is quite coarse. For $n \geq 10$, the Markov chain models the first-order Gaussian distribution, in general, excellently. However, even at $n = 20$, there remains some coarseness in the modeling of the tails of the Gaussian distribution. This is inherent in the equiprobable state-space definition, as the Gaussian tails have very low probability.

Thus, we see that a Markov chain model with an equiprobable state-space can effectively model the amplitude of the Gaussian fading process. Note that m is not considered here because the number of rate states has no effect on the amplitude distribution of the Markov chain, since output vector f has no dependence on the rate states.

4.2.3.2 Invariance

The figures shown in the first-order distribution analysis are based on the output vector f and the initial occupancy vector ϕ_0, thus, on their own, they only confirm that the Markov chain model starts with a Gaussian distribution. In order to verify that the Markov chain has a Gaussian distribution at all time points, i.e. is stationary, we must verify that ϕ_0 is invariant over transition matrix P.

We described the concept of Markov chain invariance in Section 2.4.3. In order to prove invariance, we must prove that ${\phi_0}^T = {\phi_0}^T P$, or, to put it another way, we must prove that $\phi_{k-1} = \phi_k$. Recall from Section 4.2.2 that, when defining the transition matrix for this Markov chain model, we made the substitution

$$\Pr[X_{k-1} = s_q, X_k = s_h] = \int_{\gamma_{j_h-1}}^{\gamma_{j_h}} \int_{\delta_{i_h-1}}^{\delta_{i_h}} \int_{\gamma_{j_q-1}}^{\gamma_{j_q}} \int_{\delta_{i_q-1}}^{\delta_{i_q}} f_G(T_{c_1}, T'_{c_1}, T_{c_2}, T'_{c_2}) dT_{c_1} dT'_{c_1} dT_{c_2} dT'_{c_2}$$

where $f_G(T_{c_1}, T'_{c_1}, T_{c_2}, T'_{c_2})$ is the multivariate Gaussian distribution (2.2) with covariance

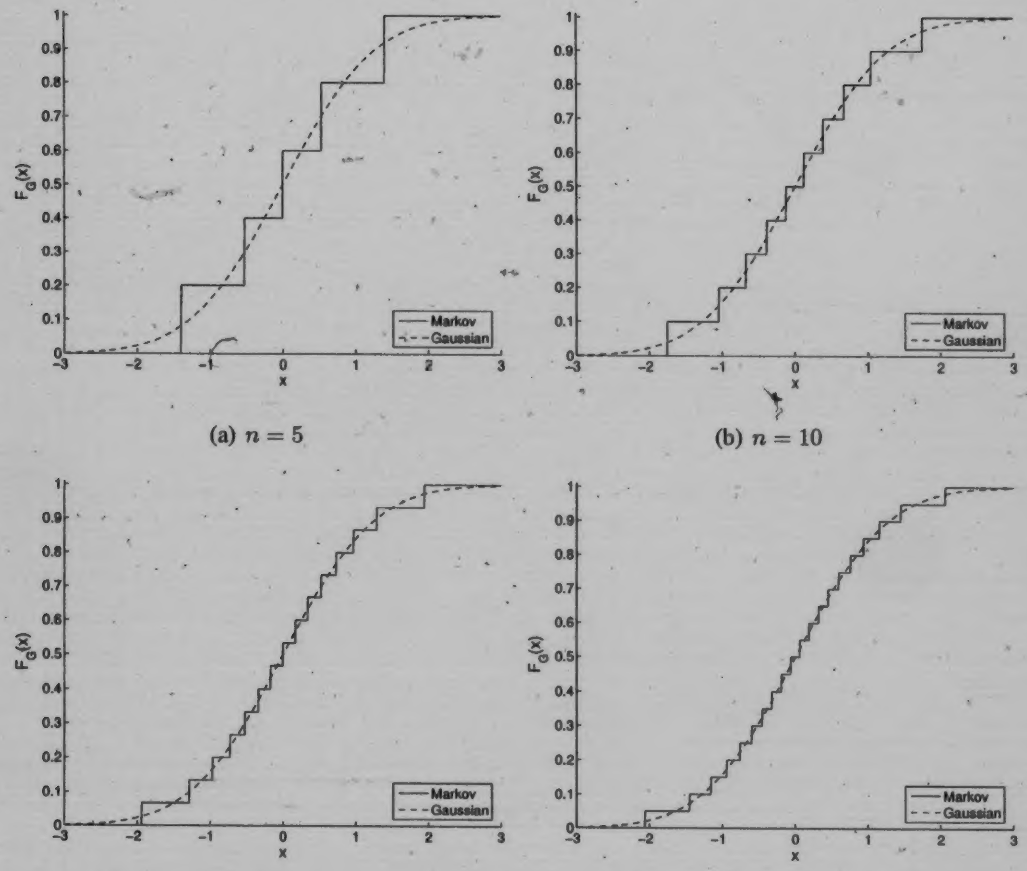

(a) $n = 5$ (b) $n = 10$

(c) $n = 15$ (d) $n = 20$

Fig. 4.1. The first-order distribution of the Markov chain model of the Gaussian fading process, for various values of n.

TABLE 4.1

Numerical verification of the stationarity of the first-order Markov chain model of the ISORA Gaussian fading process.

		$\lVert\phi_1 - \phi_0\rVert$		
n	m	$f_D T = 0.10$	$f_D T = 0.05$	$f_D T = 0.01$
10	5	5.49×10^{-6}	4.73×10^{-6}	3.12×10^{-6}
10	10	8.60×10^{-6}	6.89×10^{-6}	4.70×10^{-6}
15	5	6.42×10^{-6}	5.07×10^{-6}	4.46×10^{-6}
15	10	9.59×10^{-6}	7.38×10^{-6}	7.23×10^{-6}

matrix (4.8). If we consider the marginal distributions of this expression, we get

$$\Pr[X_{k-1} = s_q] = \int_{\gamma_{j_q-1}}^{\gamma_{j_q}} \int_{\delta_{i_q-1}}^{\delta_{i_q}} f_G(T_{c_1}, T'_{c_1}) dT_{c_1} dT'_{c_1}$$

$$\Pr[X_k = s_h] = \int_{\gamma_{j_h-1}}^{\gamma_{j_h}} \int_{\delta_{i_h-1}}^{\delta_{i_h}} f_G(T_{c_2}, T'_{c_2}) dT_{c_2} dT'_{c_2}.$$

Based on covariance matrix (4.8), we can immediately see that $f_G(T_{c_1}, T'_{c_1})$ and $f_G(T_{c_2}, T'_{c_2})$ are identical and are, in fact, given by (2.16), the distribution used to calculate ϕ_0. Thus,

$$\phi_{k-1}[d] = \Pr[X_{k-1} = s_d] = \Pr[X_0 = s_d] = \Pr[X_k = s_d] = \phi_k[d] \tag{4.11}$$

so, the Markov chain is invariant, making the Markov chain model stationary.

Unfortunately, this proof assumes the multivariate Gaussian integral is known exactly, which is not true. We can only approximate the integral values through numerical methods. To verify that this does not significantly affect the stationarity of the Markov chain model, we numerically compute $\lVert\phi_1 - \phi_0\rVert$, the norm of the difference of the Markov chain distribution at two consecutive points, for a number of different model parameters. Table 4.1 displays the results of these calculations. We can see that the difference between ϕ_0 and ϕ_1 is small for all parameters. The differences are on the order of the error in the numerical integration values, which is not a surprising result. Thus, even considering the approximations in the transition probabilities, the Markov chain model can still be considered stationary.

4.2.3.3 Autocorrelation

Figs. 4.2-4.5 show the autocorrelation of the Markov chain model of the ISORA Gaussian fading process compared to the theoretical ISORA autocorrelation function (2.40). In Figs. 4.2 and 4.3, we see the autocorrelation of the Markov chain model for increasing m and constant n, with $f_D T = 0.10$. We can see that the Markov chain model has a decaying-oscillatory autocorrelation function of very similar shape to that of the theoretical function. However, the Markov chain autocorrelation has a slower oscillation frequency than the theoretical, and decays faster. This oscillatory behavior was reported by Bergamo, et.al. [4], although they were modeling the ISORA Rayleigh process, not the underlying Gaussian process as we are here. Their results showed quite small oscillations, while the autocorrelation functions we see here have large oscillation magnitudes, at least for the first few extrema. In both Figs. 4.2 and 4.3, we can see that increasing m increases the magnitude of the oscillations, but doesn't have any significant effect on the oscillation frequency or decay rate. Figs. 4.4 and 4.5 contain the same data, but reorganized to show the autocorrelation of the Markov chain model for increasing n and constant m. We can see that increasing n has only a minimal effect on the autocorrelation of the Markov chain model, slightly increasing the magnitude of the oscillations, but, like m, has no significant effect on the oscillation frequency or decay rate.

Figs. 4.6-4.9 show the effects of variations in the sample spacing T on the autocorrelation of the Markov chain model of the ISORA Gaussian fading process. We can see that the shape of the Markov chain autocorrelation remains basically the same at all values of T tested. As the sample spacing is increased, there is a slight slowing in the oscillation frequency. More significant is the effect the sample spacing has on the oscillation magnitudes. In Figs. 4.6 and 4.7, where the Markov chain model has a larger number of rate states, we can see that decreasing the sample spacing from the large sample spacing $T = 2.0$e-3 to the medium sample spacing $T = 0.5$e-3 causes the oscillation magnitudes to increase. Interestingly, decreasing the sample spacing beyond this point causes the oscillation magnitudes to decrease, to the point where the extrema of the autocorrelation function for $T = 0.1$e-

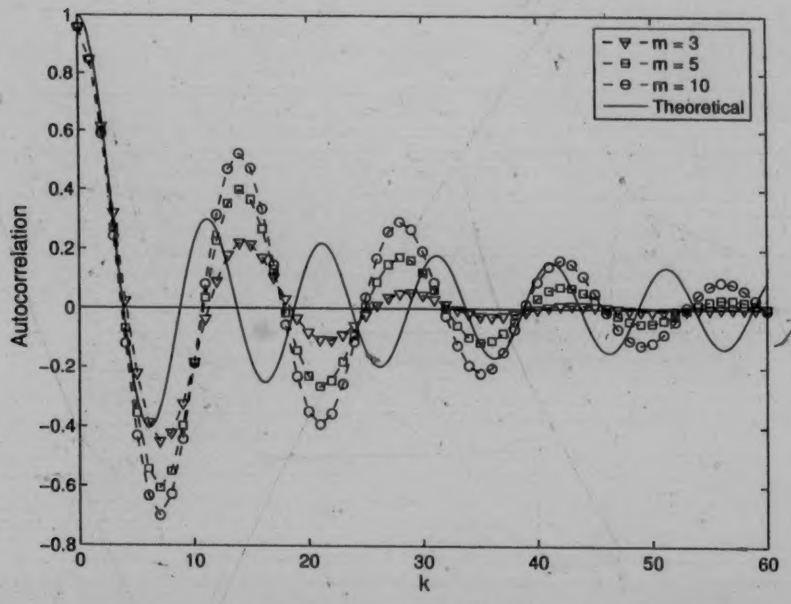

Fig. 4.2. Autocorrelation of the Markov chain model of the ISORA Gaussian fading process for increasing values of m, $n = 10$, and $f_D T = 0.10$.

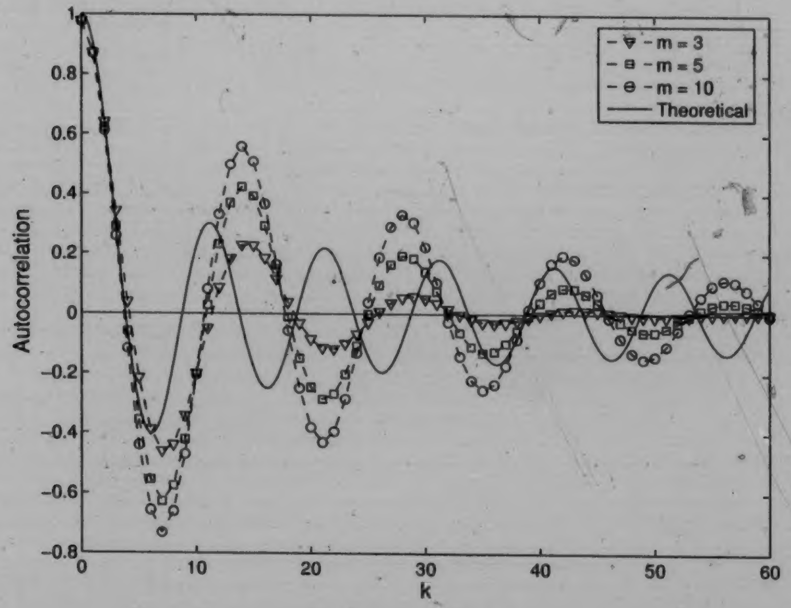

Fig. 4.3. Autocorrelation of the Markov chain model of the ISORA Gaussian fading process for increasing values of m, $n = 15$, and $f_D T = 0.10$.

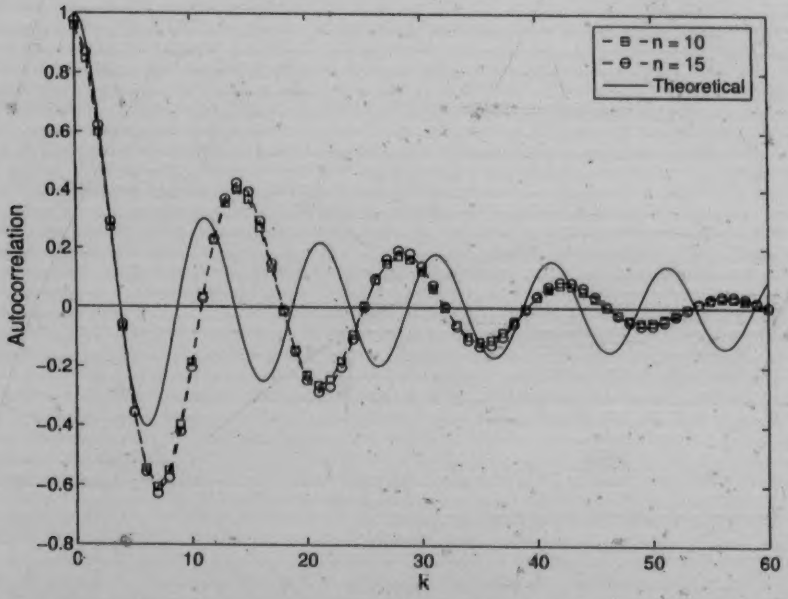

Fig. 4.4. Autocorrelation of the Markov chain model of the ISORA Gaussian fading process for increasing values of n, $m = 5$, and $f_D T = 0.10$.

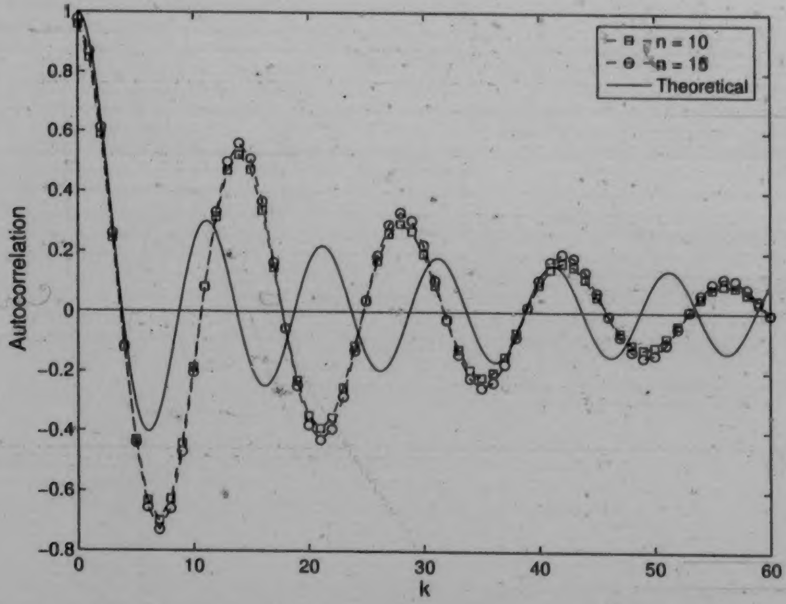

Fig. 4.5. Autocorrelation of the Markov chain model of the ISORA Gaussian fading process for increasing values of n, $m = 10$, and $f_D T = 0.10$.

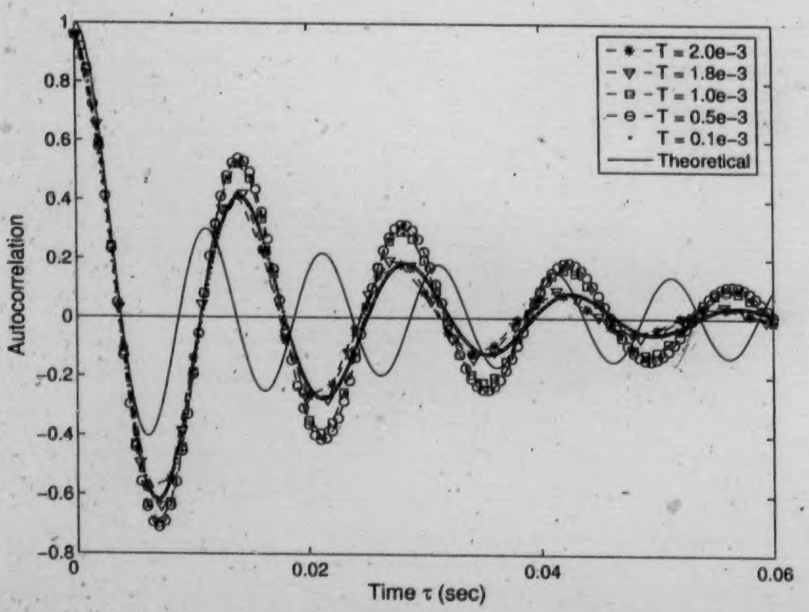

Fig. 4.6. ISORA Gaussian Markov chain model autocorrelation for various values of sample spacing T (sec), $n = 10$, $m = 10$, and $f_D = 100$ Hz.

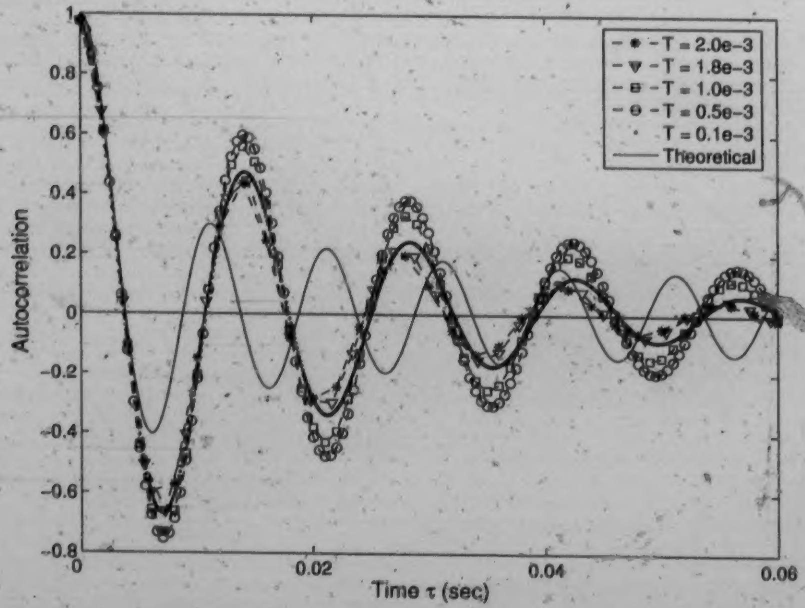

Fig. 4.7. ISORA Gaussian Markov chain model autocorrelation for various values of sample spacing T (sec), $n = 15$, $m = 10$, and $f_D = 100$ Hz.

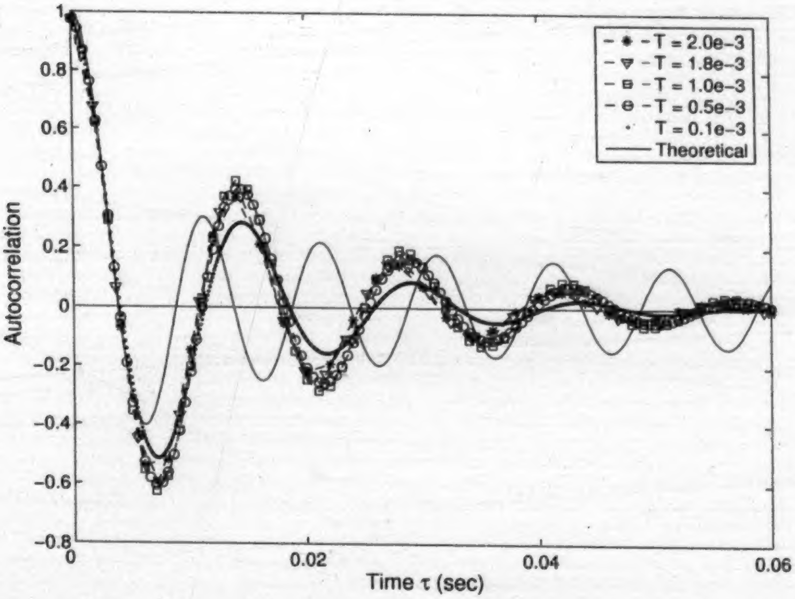

Fig. 4.8. ISORA Gaussian Markov chain model autocorrelation for various values of sample spacing T (sec), $n = 15$, $m = 5$, and $f_D = 100$ Hz.

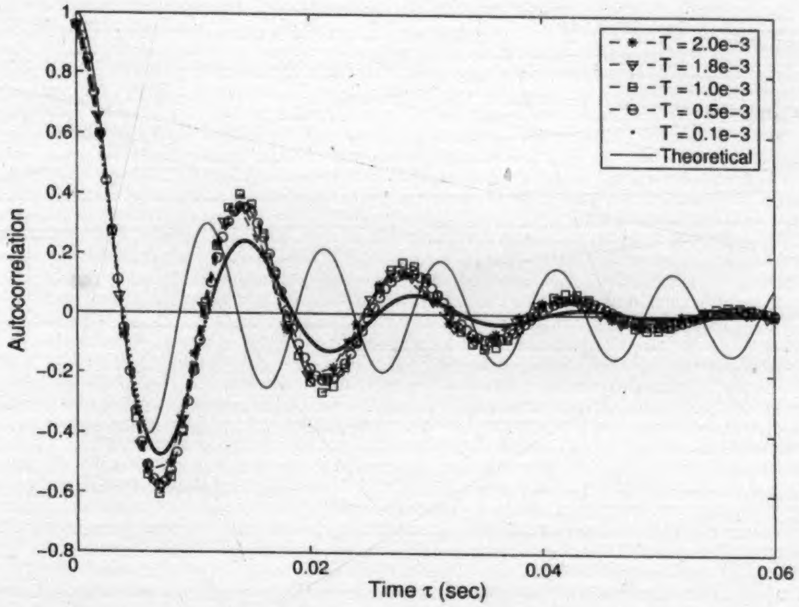

Fig. 4.9. ISORA Gaussian Markov chain model autocorrelation for various values of sample spacing T (sec), $n = 10$, $m = 5$, and $f_D = 100$ Hz.

3 are roughly the same as those for T = 2.0e-3. Figs. 4.8 and 4.9 show the effect of the sample spacing on the Markov chain model autocorrelation function for models with a smaller number of rate states. It remains true that decreasing the sample spacing causes a slight slowing in the oscillation frequency. However, with a smaller number of rate states, the sample spacing has much less of an effect on the oscillation magnitudes. In fact, the extrema for the large to medium sample spacings are all very close together. Decreasing the sample spacing to $T = 0.1$e-3 continues to cause a notable decrease in the oscillation magnitudes, though.

4.2.4 3-DISORA Markov Chain Model

During the analysis of the Markov chain model of the ISORA Gaussian fading process, we saw that the Markov chain model had an autocorrelation function that exhibited a slower oscillation frequency than that of the ISORA model, while decaying faster. In Section 2.3.3, we discussed the 3-DISORA model, which is a fading channel model appropriate for use in 3-dimensional isotropic scattering environments when the receiving antenna is omnidirectional. We saw that the autocorrelation function of that model, given by (2.45), has oscillations that lag behind those of the ISORA model, and decay faster. Thus, there is reason to think that a Markov chain model with an amplitude/rate-of-change state-space may be able to model the 3-DISORA fading channel more closely than the ISORA fading channel.

The Markov chain model of the 3-DISORA fading process is computed exactly as discussed in Section 4.2.2, with the exception that $g(T)$ and its derivatives, used in the calculation of covariance matrix Σ (4.8), are found using (2.45) instead of (2.40). Thus, the first-order distribution of this model will be identical to the Gaussian model analyzed in Section 4.2.3, and the invariance proof will also still apply. So, we focus on the autocorrelation of the model.

Figs. 4.10-4.13 show the autocorrelation of the Markov chain model of the 3-DISORA Gaussian fading process, compared to the theoretical 3-DISORA autocorrelation function.

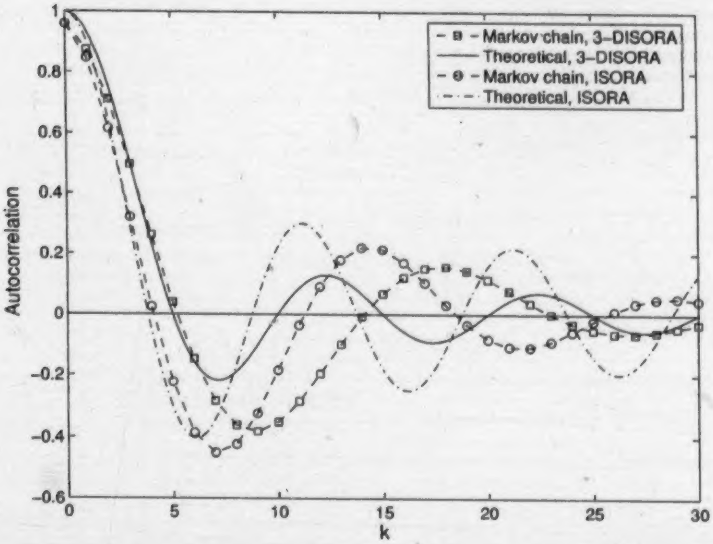

Fig. 4.10. Autocorrelation of the Markov chain model of the 3-DISORA Gaussian fading channel, compared to the autocorrelation of the ISORA Markov chain model, for $n = 10$, $m = 3$, and $f_D T = 0.10$.

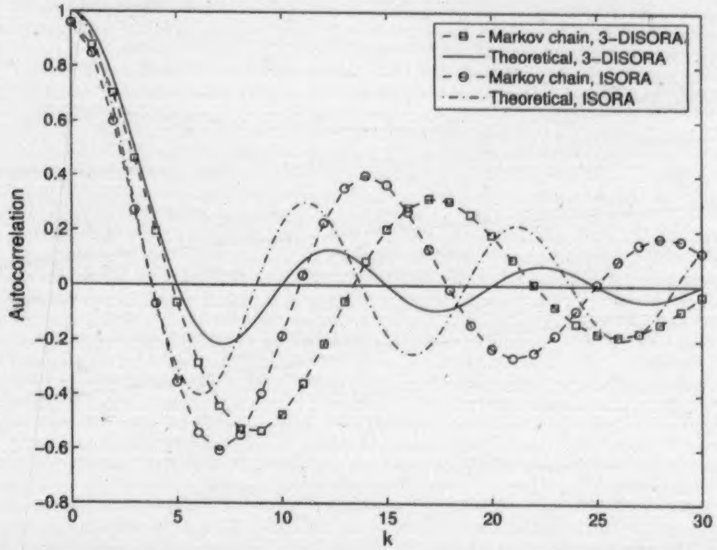

Fig. 4.11. Autocorrelation of the Markov chain model of the 3-DISORA Gaussian fading channel, compared to the autocorrelation of the ISORA Markov chain model, for $n = 10$, $m = 5$, and $f_D T = 0.10$.

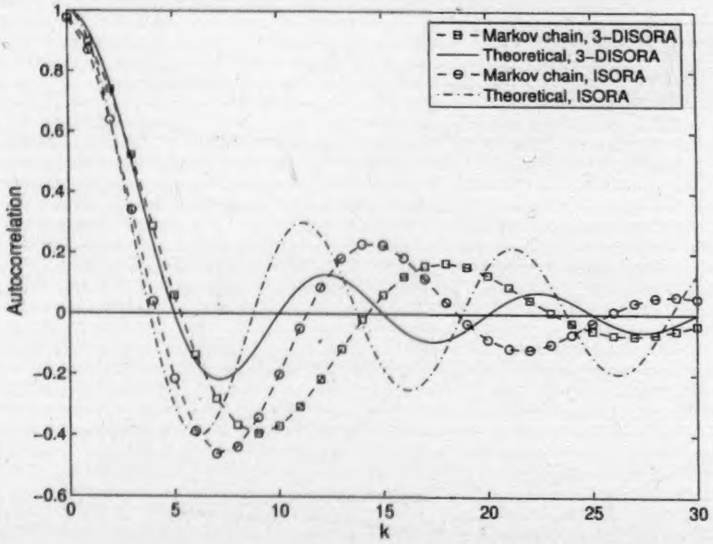

Fig. 4.12. Autocorrelation of the Markov chain model of the 3-DISORA Gaussian fading channel, compared to the autocorrelation of the ISORA Markov chain model, for $n = 15$, $m = 3$, and $f_D T = 0.10$.

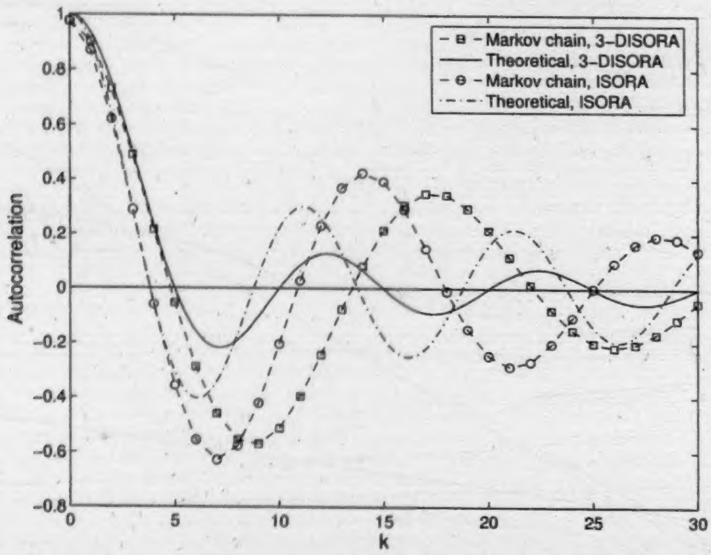

Fig. 4.13. Autocorrelation of the Markov chain model of the 3-DISORA Gaussian fading channel, compared to the autocorrelation of the ISORA Markov chain model, for $n = 15$, $m = 5$, and $f_D T = 0.10$.

An equivalent ISORA Gaussian fading process Markov chain model autocorrelation function is also included for comparison. We can see that in all cases, the autocorrelation of the Markov chain model of the 3-DISORA process oscillates slower than the theoretical function, and decays faster. In fact, it appears to decay at the same rate as the autocorrelation of the Markov chain model of the ISORA process. When comparing the autocorrelation of the Markov chain models of the 3-DISORA and ISORA channels, we see that the oscillations of the 3-DISORA Markov chain model lag behind those of the ISORA Markov chain model, much like the oscillations of the theoretical 3-DISORA autocorrelation lag behind those of the theoretical ISORA model. A first-order Markov chain with an amplitude/rate-of-change state-space appears to model the 3-DISORA Gaussian fading process as well as it did the ISORA Gaussian fading process. No improvement in the goodness of the model is evident upon switching to a fading channel model that oscillates differently than the ISORA model.

4.2.5 Modeling the Complex Gaussian Fading Envelope

In Section 2.3.2, we found that the amplitude of a fading signal can be modeled as the envelope of a complex Gaussian process, making the amplitude of the fading signal a Rayleigh process. We developed and analyzed first-order Markov chain models of the ISORA Gaussian fading process in Sections 4.2.2 and 4.2.3. In this section, we show how to form a Markov chain model of the ISORA Rayleigh fading envelope process based on a Markov chain model of the underlying Gaussian process, and we study its first-order distribution and autocorrelation function.

4.2.5.1 Computing the Markov Chain Model

To form a Markov chain model of the ISORA Rayleigh fading envelope process based on a Markov chain model of the underlying Gaussian process, we will form a new Markov chain that essentially represents two Markov chains operating concurrently. This method is appropriate because the fading amplitude is modeled as the envelope of two independent, identically distributed quadrature Gaussian processes. It is the independence of the quadrature components that permits this envelope combining method. If the quadrature components were dependent in any way, this method would not be suitable.

Define $A \otimes B$ to be the Kronecker product,

$$A \otimes B = \begin{pmatrix} A_{11}B & A_{12}B & \cdots & A_{1h}B \\ A_{21}B & A_{22}B & \cdots & A_{2h}B \\ \vdots & \vdots & \ddots & \vdots \\ A_{q1}B & A_{q2}B & \cdots & A_{qh}B \end{pmatrix} \tag{4.12}$$

where A and B can be matrices or vectors. Thus, we can define the initial occupancy vector of the Markov chain model of the ISORA Rayleigh fading envelope process as

$$\phi_{0R} = \phi_0 \otimes \phi_0 \tag{4.13}$$

where ϕ_0 is the initial occupancy vector of the Markov chain model of the ISORA Gaussian fading process studied previously. Likewise, the transition matrix of the Markov chain model of the ISORA Rayleigh fading envelope process can be defined as

$$P_R = P \otimes P \tag{4.14}$$

where P is the transition matrix of the Markov chain model of the ISORA Gaussian fading process.

The amplitude of the Rayleigh fading process is the envelope of the quadrature addition of the Gaussian fading processes, so, to find the output vector of the Markov chain model of the ISORA Rayleigh fading envelope process, we must first define the following algebraic expression. If $\mathbf{x} = [x_1, \ldots, x_j]^T$ and $\mathbf{y} = [y_1, \ldots, y_k]^T$, define $\mathbf{x} \odot \mathbf{y}$ as

$$\mathbf{x} \odot \mathbf{y} = \begin{bmatrix} \sqrt{x_1^2 + y_1^2} \\ \vdots \\ \sqrt{x_1^2 + y_k^2} \\ \sqrt{x_2^2 + y_1^2} \\ \vdots \\ \sqrt{x_2^2 + y_k^2} \\ \vdots \\ \sqrt{x_j^2 + y_1^2} \\ \vdots \\ \sqrt{x_j^2 + y_k^2} \end{bmatrix} \tag{4.15}$$

which is a variation on the Kronecker product. Thus, the output vector of the Markov chain model of the ISORA Rayleigh fading envelope process can be defined as

$$\mathbf{f_R} = \mathbf{f} \odot \mathbf{f} \tag{4.16}$$

where $\mathbf{f}$ is the output vector of the Markov chain model of the ISORA Gaussian fading process. So, a Markov chain model of the envelope fading process can be defined based on a Markov chain model of the complex Gaussian fading process by applying transformations (4.13), (4.14), and (4.16).

4.2.5.2 Model Analysis

To begin, we look at the first-order distribution of the Markov chain model of the ISORA Rayleigh fading envelope process. Note that when we refer to n and m, we are referring to the number of amplitude and rate states in the Markov chain model of the underlying Gaussian process, not the number of states in the Markov chain model of the envelope process. Fig. 4.14 shows the first-order distribution of the Markov chain model compared to the first-order distribution of the fading envelope, which we saw in Section 2.3.2 to be the Rayleigh distribution (2.36). We can see that the modeling of the first-order Rayleigh

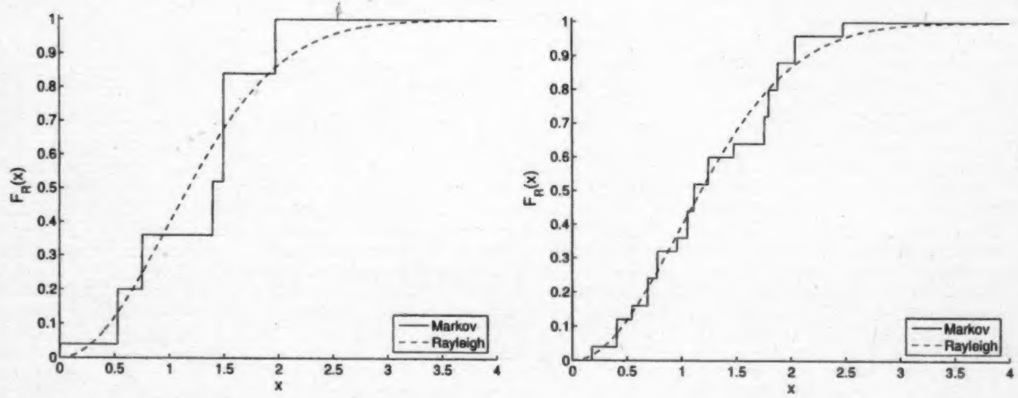

(a) $n = 5$

(b) $n = 10$

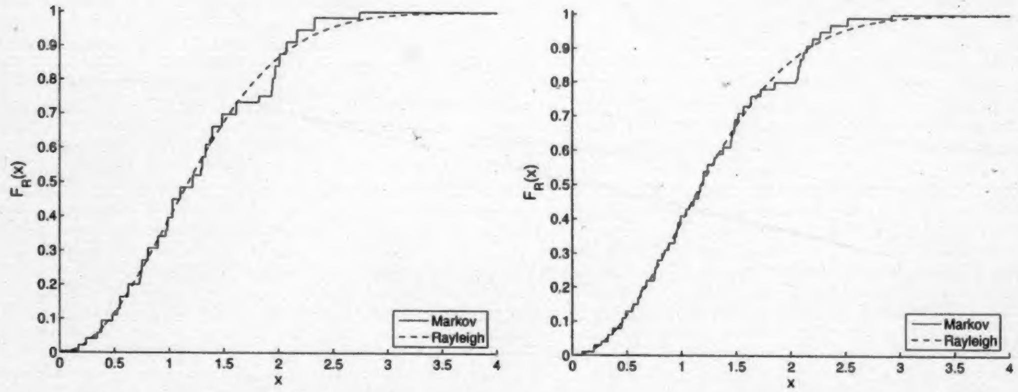

(c) $n = 15$

(d) $n = 20$

Fig. 4.14. The first-order distribution of the Markov chain model of the envelope fading process, based on the Markov chain model of the Gaussian fading process, for various values of n.

distribution is not as good as the modeling of the underlying Gaussian distribution, seen in Fig. 4.1. In general, the modeling of the lower range of the distribution is very good, except for $n = 5$, but for the upper range of the distribution, the modeling is quite poor, even at $n = 20$.

This poor modeling of the upper range of the Rayleigh distribution can be explained by considering the first-order Gaussian distributions in Fig. 4.1. As we pointed out before, although the modeling over most of the support of the distribution is excellent, the use of equiprobable threshold values means that the tails of the Gaussian distribution are not captured well, even for high values of n. This leads to poor modeling of the upper range of the Rayleigh distribution because the large amplitude values represented by the tails of the Gaussian distribution translate to large values of the envelope amplitude.

The Markov chain model of the envelope process will necessarily be invariant if the underlying Gaussian Markov chain model is invariant, which it is, so we will proceed directly to the autocorrelation of the Markov chain model of the ISORA Rayleigh fading envelope process. Figs. 4.15-4.18 show the autocorrelation of the Markov chain model of the ISORA Rayleigh fading envelope process, compared to the theoretical ISORA autocorrelation (2.42). Note that we focus on smaller state-space sizes here than we did in the ISORA Gaussian model analysis earlier, because the envelope transformation causes these models to grow as $(nm)^2$, which means that the transition matrix quickly gets too large for the matrix-power portion of the autocorrelation expression to be practically calculated.

We can immediately see that the oscillatory shape of the Markov chain model autocorrelation has been maintained by the envelope transformation, as has the fact that the oscillation frequency is slower than that of the theoretical function, and it decays faster. Unlike the Markov chain model of the ISORA Gaussian fading, however, we can see that there is a noticeable downward shift in the autocorrelation values as compared to the theoretical. The Markov chain model converges to a value lower than the convergence value of the theoretical. In fact, the value that the autocorrelation function settles at is the square of the mean of the first-order distribution, so this shift in the autocorrelation is actually a consequence of the poor first-order modeling we discussed earlier.

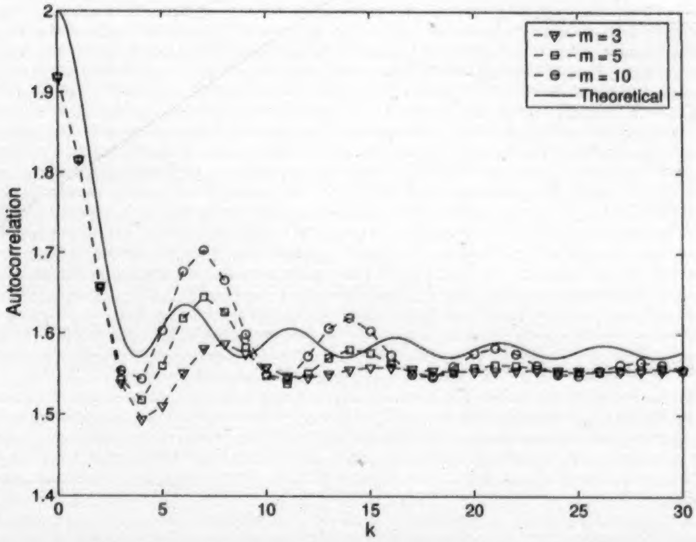

Fig. 4.15. Autocorrelation of the Markov chain model of the ISORA Rayleigh fading envelope process, based on the Markov chain model of the complex Gaussian fading process, for increasing values of m, $n = 10$, and $f_D T = 0.10$.

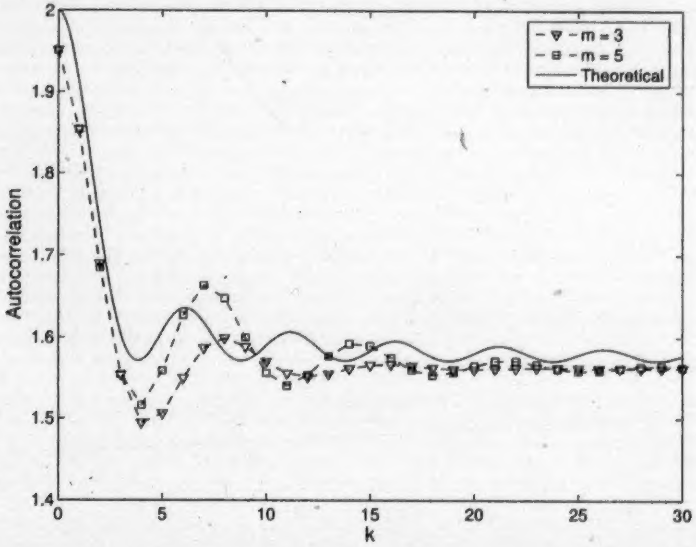

Fig. 4.16. Autocorrelation of the Markov chain model of the ISORA Rayleigh fading envelope process, based on the Markov chain model of the complex Gaussian fading process, for increasing values of m, $n = 15$, and $f_D T = 0.10$.

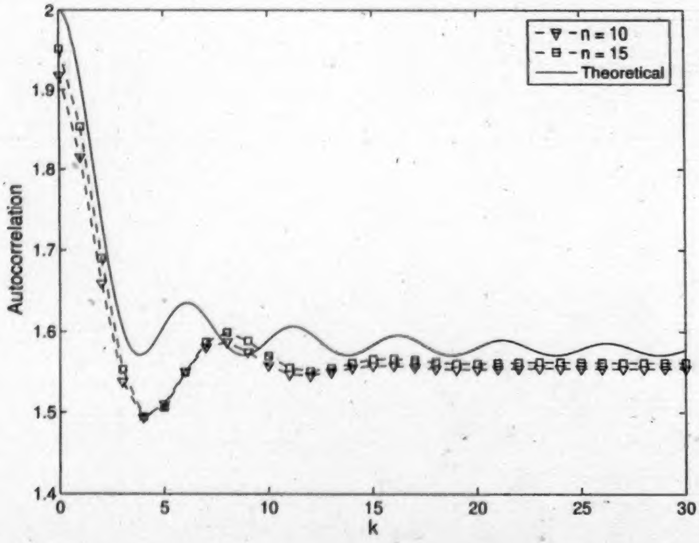

Fig. 4.17. Autocorrelation of the Markov chain model of the ISORA Rayleigh fading envelope process, based on the Markov chain model of the complex Gaussian fading process, for increasing values of n, $m = 5$, and $f_D T = 0.10$.

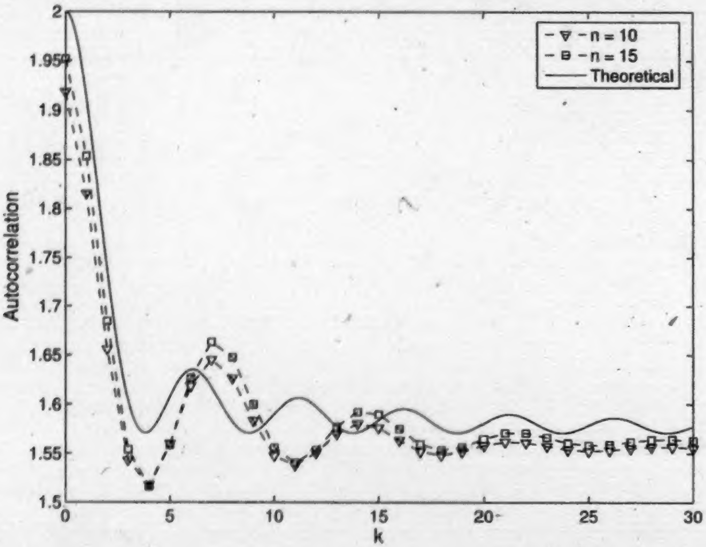

Fig. 4.18. Autocorrelation of the Markov chain model of the ISORA Rayleigh fading envelope process, based on the Markov chain model of the complex Gaussian fading process, for increasing values of n, $m = 10$, and $f_D T = 0.10$.

Figs. 4.15 and 4.16 show the autocorrelation of the Markov chain model for increasing m and constant n. We can see that, like the Markov chain model of the ISORA Gaussian process, increasing m causes an increase in the magnitude of the maxima of the oscillations, but has no significant effect on the oscillation frequency. Increasing m also causes the minima of the oscillations to draw closer to the theoretical, particularly the first minima. Figs. 4.17 and 4.18 show the autocorrelation of the Markov chain model for increasing n and constant m. Unlike the ISORA Gaussian model, where changes to n had no significant effect, the effect of changing n on the Markov chain model of the envelope is more pronounced. In fact, we can see that n affects the amount of downward shift in the Markov chain autocorrelation values. Increasing n causes the autocorrelation function to settle to a value closer to the theoretical. This should be expected because increasing n improves the first-order distribution modeling, which directly effects the mean-squared value that the autocorrelation settles to.

Figs. 4.19-4.21 show the effects of variations in the sample spacing T on the autocorrelation of the Markov chain model of the ISORA Rayleigh fading envelope process. Changes to the sample spacing have basically the same effect on the Markov chain envelope model as they did on the ISORA Gaussian Markov chain model. For larger m, the oscillation maxima increase with decreasing sample spacing, up to the medium sample spacing $T = 0.5\text{e-}3$. Beyond that point, the oscillation maxima decreases with decreasing sample spacing. Alternately, with smaller m, the sample spacing does not have any significant effect on the oscillation maxima for large to medium values of T, but as the sample spacing decreases from medium to small values, the oscillation maxima decreases.

One point that becomes clear from Figs. 4.19-4.21 that was not evident from the ISORA Gaussian Markov chain model analysis is that there is an upper limit to the sample spacing beyond which the sampling of the fading envelope becomes too coarse. By examining the autocorrelation figures, we can see that $T = 1.8\text{e-}3$ appears to be the upper limit on the sample spacing while still maintaining a reasonably smooth sampling of the autocorrelation function. This assertion is supported by Fig. 4.22, which shows a sample fading profile, along with the sampling at $f_D T = 0.18$. Qualitatively, one would expect that a larger

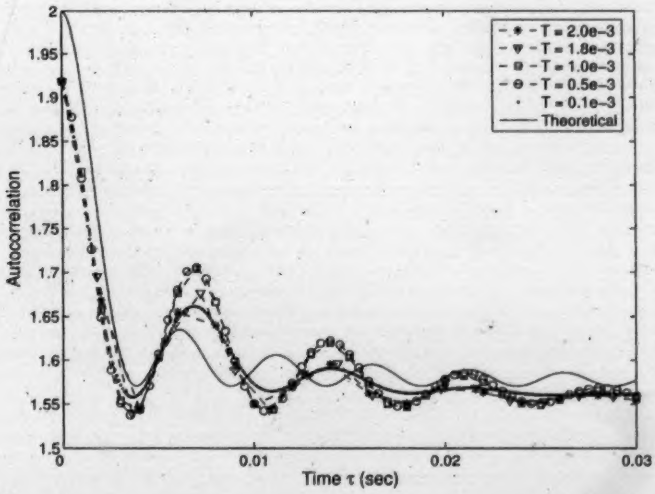

Fig. 4.19. Autocorrelation of the Markov chain model of the ISORA Rayleigh fading envelope process, based on the Markov chain model of the complex Gaussian fading process, for various values of sample spacing T (sec), $n = 10$, $m = 10$, and $f_D = 100$ Hz.

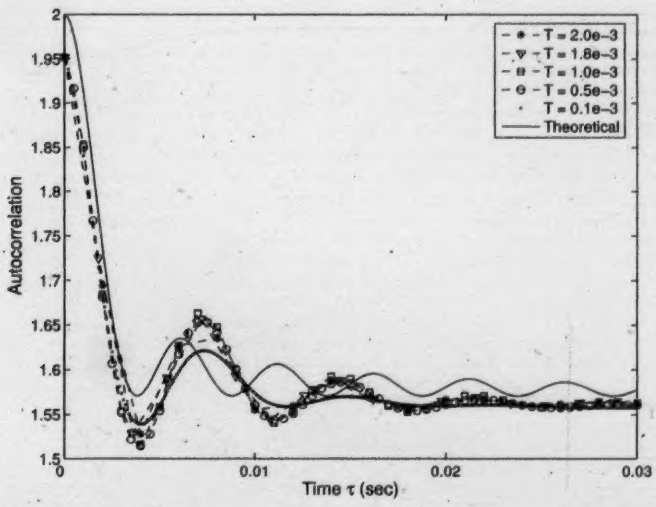

Fig. 4.20. Autocorrelation of the Markov chain model of the ISORA Rayleigh fading envelope process, based on the Markov chain model of the complex Gaussian fading process, for various values of sample spacing T (sec), $n = 15$, $m = 5$, and $f_D = 100$ Hz.

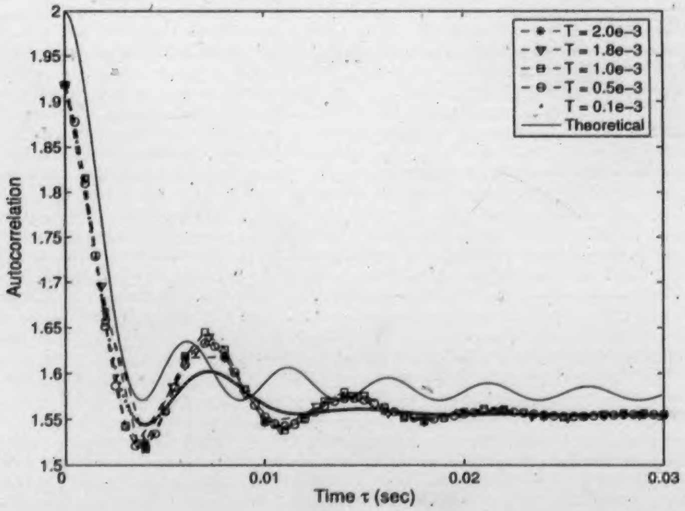

Fig. 4.21. Autocorrelation of the Markov chain model of the ISORA Rayleigh fading envelope process, based on the Markov chain model of the complex Gaussian fading process, for various values of sample spacing T (sec), $n = 10$, $m = 5$, and $f_D = 100$ Hz.

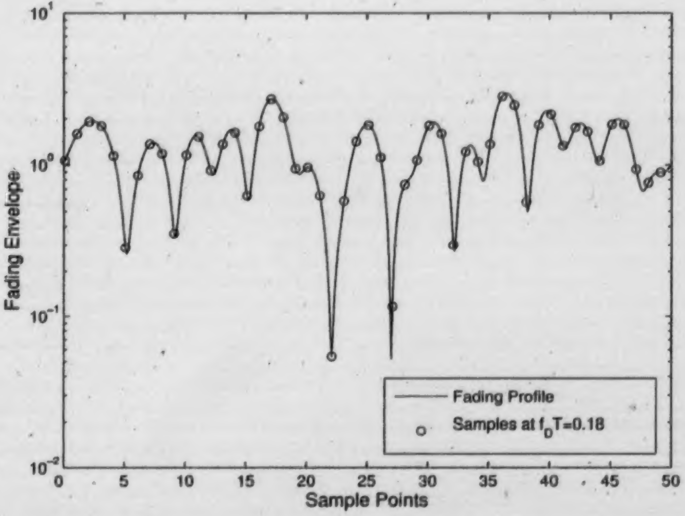

Fig. 4.22. Fading profile showing the sample spacing resulting at $f_D T = 0.18$.

spacing of the samples would miss some fades and crests in the fading amplitude profile.

4.2.6 Conclusion

In this section, we examined a first-order Markov chain model of the ISORA Rayleigh fading channel, based on a state-space made up of the amplitude and rate-of-change of the fading process. This model was defined by first finding a first-order Markov chain model of the underlying complex Gaussian fading process. We found that a first-order Markov chain can effectively model the first-order Gaussian distribution, but has less success with the ISORA autocorrelation function. The new amplitude/rate-of-change state-space resulted in a Markov chain autocorrelation function that exhibited a decaying-oscillatory shape that is much closer to the theoretical function than previous models, however, the Markov chain model autocorrelation decays faster than the theoretical, and has a slower oscillation frequency. Changes to the number of states in the state-space affected the magnitude of the oscillations, but not the decay rate or oscillation frequency.

A method was then described to use this ISORA Gaussian Markov chain model as the basis for a Markov chain model of the ISORA Rayleigh fading envelope process. We saw that the first-order distribution of the envelope Markov chain model was not as good as the Gaussian model, particularly in the upper range of the distribution. The autocorrelation function of the Markov chain model of the ISORA Rayleigh fading envelope was a considerable improvement over previous AFSMC models, displaying a decaying-oscillatory shape that was much closer to the theoretical than the exponential autocorrelation reported by Tan and Beaulieu [6]. However, the limitations of the Gaussian model autocorrelation were maintained during the envelope transformation, specifically, the decay rate was faster than the theoretical and the oscillation frequency was slower. There was also a downward shift in the model autocorrelation values, a result of the errors in the modeling of the first-order distribution.

4.3 Second-Order Markov Chain Model

4.3.1 Introduction

The results of Section 4.2 showed that a Markov chain based on an amplitude/rate-of-change state-space is able to capture the decaying-oscillatory nature of the ISORA autocorrelation function when used to model the Gaussian fading process and then transformed to model the Rayleigh fading envelope process. However, the oscillation frequency is slower than that of the ISORA model, and it decays faster. In this section, we explore a second-order Markov chain model of the ISORA Gaussian fading process, and examine the effects increasing the Markov chain order has on the model.

4.3.2 Computing the Markov Chain Model

Recall that for a first-order Markov chain, the probability of being in a particular state at time k depended only on the state of the chain at time $k-1$. A similar definition applies to second-order Markov chains, except that the probability of being in a particular state at time k depends on the state of the chain at times $k-1$ and $k-2$. Thus, a second-order Markov chain is specified by the same three elements we presented in Section 2.4.2, transition matrix P, initial occupancy vector ϕ_0, and output vector f, but defined over a second-order state-space.

4.3.2.1 Defining the Second-Order State-Space

The definition of a second-order state-space is based on the combination of an underlying first-order state-space at two consecutive time instants. So, the second-order Markov chain state-space is made up of $(nm)^2$ states, labeled $\{w_1, \ldots, w_{(nm)^2}\}$, where $w_d = \{s_{x_d}, s_{y_d}\}$, s_{y_d} being the current first-order state, s_{x_d} being the previous first-order state, with

$$x_d = \text{Mod}(d, nm, 1) \tag{4.17}$$

$$y_d = \text{Quotient}(d, nm, 1) + 1 \tag{4.18}$$

where $\text{Mod}(\cdot,\cdot,1)$ and $\text{Quotient}(\cdot,\cdot,1)$ are defined by (4.2) and (4.1), respectively. The underlying first-order states are defined exactly as in Section 4.2.2, so, the second-order state-space, like the first-order state-space, is completely defined by threshold vectors $\boldsymbol{\delta}$ and $\boldsymbol{\gamma}$.

4.3.2.2 Output Vector f

Since a second-order state is made up of both the current first-order state and the previous first-order state, the output value of a second-order state will be set to the output value of the equivalent current first-order state. Thus, to compute $\mathbf{f}[d]$, we first find the equivalent current first-order state s_{y_d} via (4.18), then find i_{y_d} using (4.1). The output value is found using (4.3), with i_{y_d} replacing i_d.

4.3.2.3 Initial Occupancy Vector $\boldsymbol{\phi}_0$

In the case of a first-order Markov chain, $\boldsymbol{\phi}_0$ was found by integrating the joint distribution of T_c, T_c' over each state in the state-space. For a second-order Markov chain, the state-space consists of two consecutive points, so we will calculate the initial occupancy probabilities by integrating over the joint distribution of two consecutive points, namely $T_{c_1}, T_{c_1}', T_{c_2}$, and T_{c_2}'.

To find $\boldsymbol{\phi}_0[d]$, we first find x_d and y_d with (4.17) and (4.18), which defines the equivalent current and previous first-order states, then find $i_{x_d}, j_{x_d}, i_{y_d}, j_{y_d}$ using (4.1) and (4.2), which defines the amplitude and rate thresholds for the states. If we let $\mathbf{T_c} = [T_{c_1}, T_{c_1}', T_{c_2}, T_{c_2}']$, then

$$\begin{aligned}
\boldsymbol{\phi}_0[d] &= \Pr[Y_k = w_d] \\
&= \Pr[X_k = s_{y_d}, X_{k-1} = s_{x_d}] \\
&= \int_{\gamma_{j_{y_d}-1}}^{\gamma_{j_{y_d}}} \int_{\delta_{i_{y_d}-1}}^{\delta_{i_{y_d}}} \int_{\gamma_{j_{x_d}-1}}^{\gamma_{j_{x_d}}} \int_{\delta_{i_{x_d}-1}}^{\delta_{i_{x_d}}} f_G(T_{c_1}, T_{c_1}', T_{c_2}, T_{c_2}') d\mathbf{T_c}. \qquad (4.19)
\end{aligned}$$

This expression is identical to the numerator of (4.7), and will be similarly computed using the Genz [52] algorithm discussed in Appendix A.

4.3.2.4 Transition Matrix P

The transition matrix for a second-order Markov chain must be computed with some caution, as not all transitions are possible. Consider, for example, that a Markov chain is currently in second-order state w_d, which consists of equivalent current first-order state s_{y_d} and previous first-order state s_{x_d}. We wish to find the probability of the Markov chain making the transition to state w_k, which has equivalent current first-order state s_{y_k} and previous first-order state s_{x_k}. We note that the current first order state of w_d *is* the previous first-order state of w_k, thus, the transition from w_d to w_k is only possible if $s_{y_d} = s_{x_d}$. So, a second-order transition matrix will have a large number of 0 entries because of the many transitions that are not possible.

Let Y_k be a random variable representing the second-order state of the Markov chain at time k. Then, transition matrix P will be calculated as

$$\begin{aligned} P_{qh} &= \Pr[Y_k = w_h | Y_{k-1} = w_q] \\ &= \Pr[X_k = s_{y_h}, X_{k-1} = s_{x_h} | X_{k-1} = s_{y_q}, X_{k-2} = s_{x_q}] \\ &= \begin{cases} \Pr[X_k = s_{y_h} | X_{k-1} = s_{y_q}, X_{k-2} = s_{x_q}], & x_h = y_q \\ 0\,, & \text{otherwise} \end{cases} \end{aligned} \tag{4.20}$$

where x_h, y_h, x_q, y_q are found using (4.17) and (4.18). As was our convention for the first-order Markov chain model, let T_{c_1} and T'_{c_1} represent the amplitude and rate-of-change of the Gaussian fading process at time t, T_{c_2} and T'_{c_2} represent the amplitude and rate at time $t + T$, and T_{c_3} and T'_{c_3} represent the amplitude and rate at time $t + 2T$. If we let $\mathbf{T_c} = [T_{c_1}, T'_{c_1}, T_{c_2}, T'_{c_2}, T_{c_3}, T'_{c_3}]$, then the conditional probability of (4.20) can be computed as

$$\begin{aligned} &\Pr[X_k = s_{y_h} | X_{k-1} = s_{y_q}, X_{k-2} = s_{x_q}] \\ &\quad = \frac{\Pr[X_k = s_{y_h}, X_{k-1} = s_{y_q}, X_{k-2} = s_{x_q}]}{\Pr[X_{k-1} = s_{y_q}, X_{k-2} = s_{x_q}]} \\ &\quad = \frac{\int_{\gamma_{j_{y_h}-1}}^{\gamma_{j_{y_h}}} \int_{\delta_{i_{y_h}-1}}^{\delta_{i_{y_h}}} \int_{\gamma_{j_{y_q}-1}}^{\gamma_{j_{y_q}}} \int_{\delta_{i_{y_q}-1}}^{\delta_{i_{y_q}}} \int_{\gamma_{j_{x_q}-1}}^{\gamma_{j_{x_q}}} \int_{\delta_{i_{x_q}-1}}^{\delta_{i_{x_q}}} f_G(\mathbf{T_c}) d\mathbf{T_c}}{\phi_{\mathbf{o}}[q]}. \end{aligned} \tag{4.21}$$

By extending the discussion of $f_G(T_{c_1}, T'_{c_1}, T_{c_2}, T'_{c_2})$ in Section 2.2.4 to include a third time point, it is clear that $f_G(\mathbf{T_c})$ is a multivariate Gaussian distribution (2.2) where the fading channel correlation structure (2.9), assuming sample spacing T between consecutive points, gives the covariance matrix as

$$\Sigma = \begin{pmatrix} b_0 & 0 & g(T) & g'(T) & g(2T) & g'(2T) \\ 0 & b_2 & -g'(T) & -g''(T) & -g'(2T) & -g''(2T) \\ g(T) & -g'(T) & b_0 & 0 & g(T) & g'(T) \\ g'(T) & -g''(T) & 0 & b_2 & -g'(T) & -g''(T) \\ g(2T) & -g'(2T) & g(T) & g'(T) & b_0 & 0 \\ g'(2T) & -g''(2T) & g'(T) & -g''(T) & 0 & b_2 \end{pmatrix}. \quad (4.22)$$

Like the 4-dimensional version of this joint distribution, there is no closed-form for the numerator of (4.21), but it can be calculated numerically using the Genz [52] algorithm discussed in Appendix A.

4.3.3 Model Analysis

As in the first-order Markov chain model analysis, we focus on threshold vectors δ and γ that result in equiprobable first-order state-spaces. The resulting second-order state-space will not be equiprobable, but this represents no difficulties. The equiprobable state-spaces are used primarily to give a consistent method of calculating values for δ and γ, not because of any model necessity.

There is one state-space calculation issue here that did not merit consideration in the first-order Markov chain model. Because the initial occupancy vector of this model is based on the joint distribution of two consecutive points, some values of ϕ_0 will be extremely small. In fact, because of numerical integration limitations, some values will be 0. Clearly, this is going to cause problems in (4.21), where $\phi_0[q]$ is the denominator of the transition probability expression. To correct this issue, we recognize that, since the Markov chain model is stationary, the initial occupancy vector not only represents the probability of starting in a particular state, but also the probability of being in a particular state at any point in time. Thus, if the initial occupancy probability of a particular state is extremely small, or 0, that state will be visited extremely rarely, or never, and can be removed from

TABLE 4.2

Numerical verification of the stationarity of the second-order Markov chain model of the ISORA Gaussian fading process.

		$\|\phi_1 - \phi_0\|$		
n	m	$f_D T = 0.10$	$f_D T = 0.05$	$f_D T = 0.01$
5	3	9.77×10^{-6}	5.06×10^{-6}	4.07×10^{-6}
5	5	17.09×10^{-6}	18.66×10^{-6}	6.96×10^{-6}
6	3	11.90×10^{-6}	10.51×10^{-6}	5.62×10^{-6}
6	5	17.06×10^{-6}	9.92×10^{-6}	5.08×10^{-6}

the state-space without significantly affecting the statistics of the model. Since the error in the numerical integration calculations is 10^{-6}, as we mention in Appendix A, we remove any state from the state-space that has an initial occupancy value below this error, due to the unreliability of values in this range.

Because the output of a second-order state is the same as the output of the equivalent current first-order state, the first-order distribution of this second-order Markov chain model will be identical to that of the first-order Markov chain model. Also, it is clear from the expression for covariance matrix Σ (4.22) that the marginal distributions $f_G(T_{c_1}, T'_{c_1}, T_{c_2}, T'_{c_2})$ and $f_G(T_{c_2}, T'_{c_2}, T_{c_3}, T'_{c_3})$ of $f_G(\mathbf{T_c})$ are identical to each other as well as to the distribution used to calculate the initial occupancy vector, so the invariance proof we presented in Section 4.2.3.2 is still valid here. In Table 4.2, we show the norm of the difference $\phi_1 - \phi_0$ for a number of model parameters, as we did in Table 4.1 for the first-order analysis. We can see that the differences are, in general, larger than the ones we calculated in the first-order analysis, a consequence of the removal of the low probability states, but the values are still very small, so the second-order Markov chain model can still be considered stationary. Thus, we proceed directly to the autocorrelation analysis.

Because the second-order Markov chain is defined in such a way that it looks like a first-order Markov chain, the autocorrelation expression we derived in Section 2.4.4 can also be used to calculate the autocorrelation function of a second-order Markov chain. Because the second-order Markov chain size increases as $(nm)^2$, we will focus our analysis on smaller values of n and m than in the first-order Markov chain analysis. Figs. 4.23-4.25 show the autocorrelation of the second-order Markov chain model of the ISORA Gaussian fading process for various values of sample spacing T. We also include the autocorrelation of an equivalent first-order Markov chain model to judge the improvement gained by increasing the order of the model. Recall from Figs. 4.8 and 4.9 that for smaller state-space sizes, variations in the sample spacing don't have a significant effect on the first-order Markov chain model autocorrelation function, thus, we only include one first-order comparison plot, for $T = 1.0$e-3. We can see that increasing the Markov chain model order does improve the modeling of the ISORA Gaussian fading process, with the exception of Markov chain models at small sample spacing $T = 0.01$e-3, which appear unaffected. For medium to large sample spacings, increasing the model order increases the autocorrelation oscillation frequency closer to that of the theoretical. The amount by which the oscillation frequency improves appears to depend on the size of the state-space. In Fig. 4.23, which has the smallest state-space size, the oscillation frequency increase is fairly insignificant, with the exception of the largest sample spacing, $T = 1.8$e-3, which is noticeably improved. We saw previously that changes to n do not have much impact on the model autocorrelation function, and Fig. 4.25, which has a state-space in which n is increased by 1, does not appear notably different than Fig. 4.23. In Fig. 4.24, however, in which the model has a larger value of m, the oscillation frequency is noticeably improved for both $T = 1.8$e-3 and $T = 1.0$e-3. In fact, at the largest sample spacing, the Markov chain model autocorrelation well matches the theoretical up to the first maxima, a considerable improvement over the first-order Markov chain models.

The method we presented in Section 4.2.5.1 can be used to find a Markov chain model of the ISORA Rayleigh fading envelope process, based on the second-order Markov chain models of the complex Gaussian fading process we discussed above. Note, however, that the use of this transformation results in a Markov chain whose size increases as $(nm)^4$, which, even for small values of n and m, is impractically large. Fig. 4.26 shows the

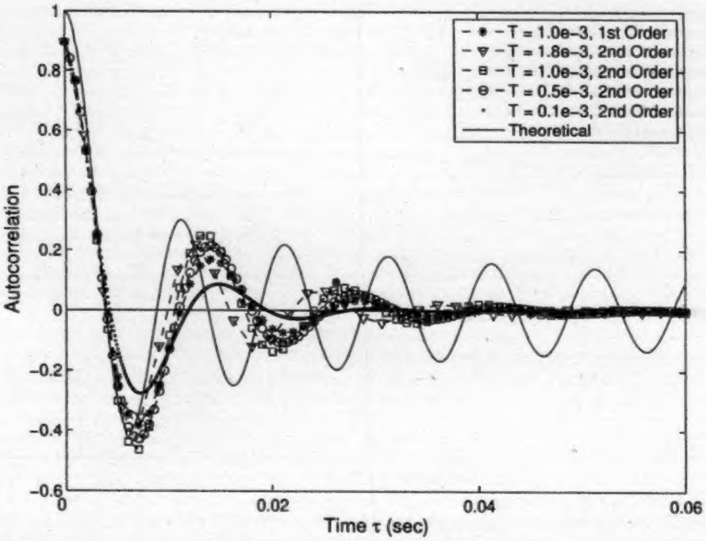

Fig. 4.23. Autocorrelation of the second-order Markov chain model of the ISORA Gaussian fading process for various values of T (sec), $n = 5$, $m = 3$, and $f_D = 100$ Hz.

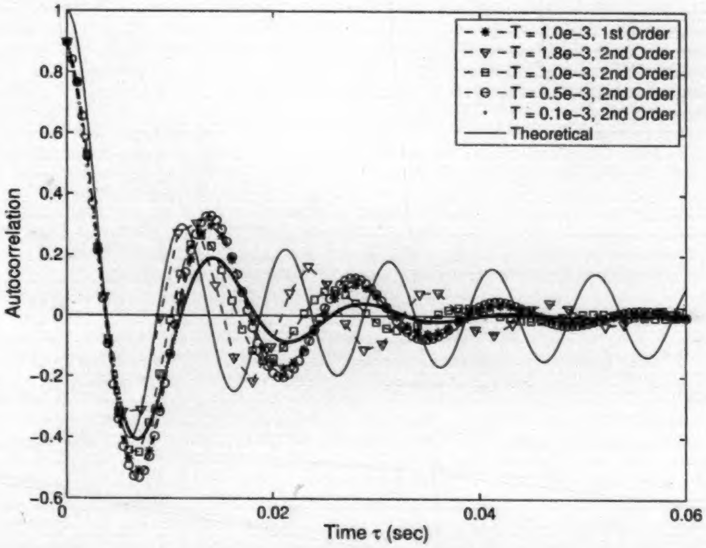

Fig. 4.24. Autocorrelation of the second-order Markov chain model of the ISORA Gaussian fading process for various values of T (sec), $n = 5$, $m = 5$, and $f_D = 100$ Hz.

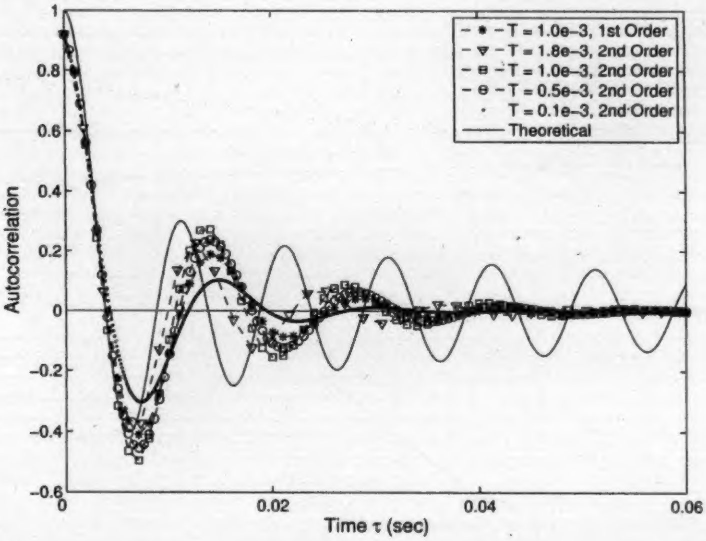

Fig. 4.25. Autocorrelation of the second-order Markov chain model of the ISORA Gaussian fading process for various values of T (sec), $n = 6$, $m = 3$, and $f_D = 100$ Hz.

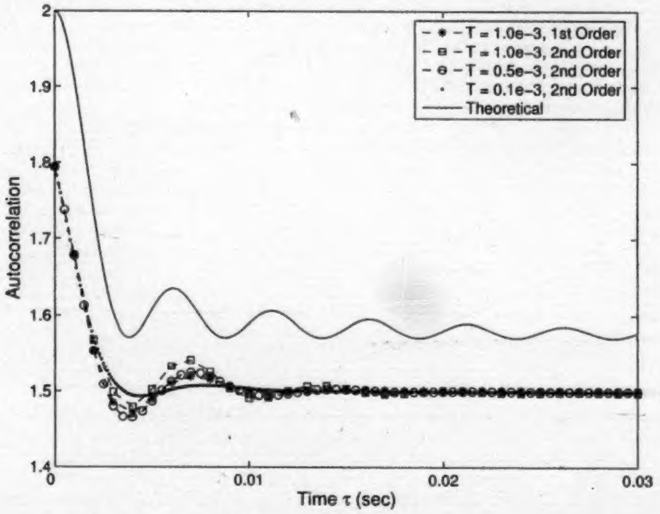

Fig. 4.26. Autocorrelation of the Markov chain model of the ISORA Rayleigh fading envelope process, based on a second-order Markov chain model of the complex Gaussian fading process, for various values of sample spacing T (sec), $n = 5$, $m = 3$, and $f_D = 100$ Hz.

autocorrelation of the second-order Markov chain model of the ISORA Rayleigh fading envelope process for $n = 5$, $m = 3$, which is the largest state-space for which the autocorrelation can be evaluated within a reasonable time frame on an IBM workstation with two 2.2 GHz Intel Xeon processors and 2GB of RAM. We can see that the increase in Markov chain order does improve the autocorrelation slightly, as it did in the ISORA Gaussian fading process model, but $n = 5$ results in a very poor modeling of the first-order distribution of the fading envelope, as we saw in Fig. 4.14(a), which causes the very large downward shift in the autocorrelation values we observe here.

4.3.4 Conclusion

In this section, we studied Markov chain models of the ISORA Rayleigh fading channel, based on second-order Markov chain models of the underlying Gaussian fading process. The elements that specified the second-order Markov chain model were defined much like the elements that specified the first-order model, but with simple extensions.

Though a second-order Markov chain will not model the first-order distribution of the fading channel any better than the first-order Markov chain does, we saw that a second-order Markov chain can noticeably improve the modeling of the ISORA autocorrelation, particularly for larger sample spacings. However, due to the size of a second-order Markov chain, creating a Markov chain model of the ISORA Rayleigh fading process based on a second-order Markov chain model of the underlying Gaussian processes is not practical, since, even for small state-space sizes, the Markov chain envelope model is too large to be analyzed.

4.4 Conclusion

In this chapter, we studied a Markov chain model of the ISORA Rayleigh fading channel based on a Markov chain model of the underlying complex Gaussian process, using a state-space consisting of both the amplitude and rate-of-change of the fading process. In

Section 4.2, we studied first-order Markov chain models. We saw that a first-order Markov chain can well model the first-order Gaussian distribution. By basing the transition matrix on the joint distribution of two consecutive points of the fading process, we also saw that the Markov chain model will necessarily be stationary. When studying the autocorrelation of the Markov chain model, we saw that the amplitude/rate state-space resulted in a decaying-oscillatory autocorrelation function much closer to the theoretical than previous AFSMC models. However, the decay rate of the autocorrelation was faster than that of the theoretical, and the oscillation frequency was slower. Changes to the size of the state-space had no significant effect on either of these observations.

In Section 4.3, we expanded this model to a second-order Markov chain. We saw that increasing the order of the Markov chain can improve its ability to model the ISORA autocorrelation, particularly for larger sample spacings. Though the results suggest that a Markov chain model of the ISORA Rayleigh fading process based on a second-order Markov chain model of the underlying complex Gaussian process could improve on the first-order envelope model, the size of the Markov chain in this case would be impractically large.

Overall, creating a Markov chain model of the ISORA Rayleigh fading process by first modeling the underlying Gaussian process, with a state-space made up of the amplitude and rate-of-change of the process, results in a model that is a considerable improvement over previous Markov chain models. The shape of the autocorrelation function of the new model is much closer to the shape of the ISORA autocorrelation. However, by basing the Rayleigh fading model on a Markov chain model of the underlying Gaussian process, the resulting model of the Rayleigh fading envelope process is impractically large. There are also limitations in the first-order distribution of the Markov chain envelope model. Thus, we are motivated to explore Markov chain models of the ISORA Rayleigh fading process calculated based on the Rayleigh fading envelope statistics directly, which we will examine in the next chapter.

Chapter 5

Markov Chain Modeling of the Rayleigh Fading Envelope Process

5.1 Introduction

In Chapter 4, we proposed and analyzed a Markov chain model of the ISORA Rayleigh fading channel based on a Markov chain model of the underlying complex Gaussian fading process. We observed that the use of a state-space based on the amplitude and rate-of-change of the fading process resulted in a Markov chain model that possessed a decaying-oscillatory autocorrelation function, a considerable improvement over the exponential autocorrelation of previous AFSMC models. However, the process of transforming a Gaussian model into a fading envelope model often resulted in impractically large Markov chain models, especially for second-order Markov chains.

In this chapter, we propose a Markov chain model of the ISORA Rayleigh fading channel, based on a state-space consisting of the amplitude and rate-of-change of the fading process. The model will be calculated based directly on the statistics of the ISORA Rayleigh fading process. In Section 5.2, we examine a first-order Markov chain model of the ISORA Rayleigh fading channel. In particular, we compare its first-order distribution and autocorrelation function to those of the models examined in Chapter 4. In Section 5.3, we extend this model to a second-order Markov chain, and examine the effect of increasing the Markov chain order on the modeling of the ISORA Rayleigh fading channel. Section 5.4 concludes the chapter.

5.2 First-Order Markov Chain Model

5.2.1 Introduction

In this section, we study a first-order Markov chain model of the ISORA Rayleigh fading channel, based on an amplitude/rate-of-change state-space. In Section 5.2.2, we present a method to calculate the three elements of a Markov chain model based directly on the statistics of the ISORA Rayleigh fading process. In Section 5.2.3, we analyze the resulting Markov chain model, in particular, we compare its first-order distribution and autocorrelation function to those of the Markov chain model of the ISORA complex Gaussian envelope fading process, discussed in Chapter 4. Section 5.2.4 concludes this section.

5.2.2 Computing the Markov Chain Model

In this section, we present a method of calculating the three elements of a Markov chain model, namely, transition matrix P, initial occupancy vector ϕ_0, and output vector $\mathbf{f}$, in order to model the ISORA Rayleigh fading process. The method used will be identical to the method employed in Section 4.2, except that the specific statistical distributions used in the calculations will be based directly on the statistics of the fading envelope process, as opposed to the underlying complex Gaussian process.

Recall from Section 2.3.2 that the ISORA Rayleigh fading model has first-order distribution (2.36)

$$f_R(r) = \begin{cases} \frac{r}{b_0} e^{-r^2/2b_0}, & r \geq 0 \\ 0, & r < 0 \end{cases}$$

and autocorrelation function (2.42)

$$R_R(\tau) = \frac{\pi b_0}{2} {}_2F_1\left(-\frac{1}{2}, -\frac{1}{2}; 1; J_0(2\pi f_D \tau)^2\right)$$

where ${}_2F_1(\cdot,\cdot;\cdot;\cdot)$ is the Gaussian Hypergeometric function (2.43). Due to the fact that the state-space under consideration consists of the amplitude and rate-of-change of the Rayleigh fading process, we will be making use of the joint distributions of Rayleigh random variables and their derivatives, which we derived in Section 2.2.4.

5.2.2.1 Defining the State-Space

Since a Rayleigh random variable and its derivative are independent, which we saw in (2.19), the amplitude space and rate space can be partitioned independently, like the state-space of the Gaussian Markov chain model defined in Section 4.2.2.1. In fact, the state-space of this model will be defined in a virtually identical fashion to the previously discussed Gaussian model.

Let the state-space be divided into n amplitude states and m rate states. The n amplitude states are defined by the length $n + 1$ vector $\boldsymbol{\delta} = [\delta_0, \ldots, \delta_n]$ of threshold values, where $\delta_0 = 0$, $\delta_n = \infty$, and $\delta_1, \ldots, \delta_{n-1}$ can be any ascending sequence of real positive numbers. Likewise, the m rate states are defined by a length $m + 1$ vector of threshold values $\boldsymbol{\gamma} = [\gamma_0, \ldots, \gamma_m]$, where $\gamma_0 = -\infty$, $\gamma_m = \infty$, and $\gamma_1, \ldots, \gamma_{m-1}$ is any ascending sequence of real numbers.

Thus, the state-space of this model consists of nm states, where the amplitude and rate thresholds for state s_d are specified by i_d and j_d, calculated using (4.1) and (4.2), respectively. Like the Gaussian Markov chain model of Chapter 4, the state-space of the Markov chain model of the Rayleigh fading process is fully defined by $\boldsymbol{\delta}$ and $\boldsymbol{\gamma}$. The only difference between this state-space definition and that of Section 4.2.2.1 is that here, $\delta_0 = 0$, because the Rayleigh fading amplitude only takes positive values.

5.2.2.2 Output Vector f

Vector **f** represents the output of the Markov chain at each state. As in Section 4.2.2.2, we will choose the elements of **f** to minimize the MSE between the amplitude value of the Markov chain model and the amplitude of the Rayleigh fading process over each state. We saw in Section 4.2.2.2 that the MSE minimizing solution of **f** is the conditional mean of the fading amplitude over each state. Thus, to compute $\mathbf{f}[d]$, we first find i_d using (4.1), which specifies the amplitude thresholds of state s_d, then, the conditional mean for that state can be calculated as

$$\mathbf{f}[d] = \frac{\int_{\delta_{i_d-1}}^{\delta_{i_d}} r f_R(r) dr}{\int_{\delta_{i_d-1}}^{\delta_{i_d}} f_R(r) dr}$$
$$= \begin{cases} \dfrac{\delta_{i_d-1} e^{-\frac{\delta_{i_d-1}^2}{2b_0}} - \sqrt{\frac{\pi b_0}{2}} \mathrm{Erf}\left[\frac{\delta_{i_d-1}}{\sqrt{2b_0}}\right] + \sqrt{\frac{\pi b_0}{2}}}{e^{-\delta_{i_d-1}^2/2b_0}}, & \delta_{i_d} = \infty \\ \dfrac{\delta_{i_d-1} e^{-\frac{\delta_{i_d-1}^2}{2b_0}} - \delta_{i_d} e^{-\frac{\delta_{i_d}^2}{2b_0}} - \sqrt{\frac{\pi b_0}{2}} \mathrm{Erf}\left[\frac{\delta_{i_d-1}}{\sqrt{2b_0}}\right] + \sqrt{\frac{\pi b_0}{2}} \mathrm{Erf}\left[\frac{\delta_{i_d}}{\sqrt{2b_0}}\right]}{e^{-\delta_{i_d-1}^2/2b_0} - e^{-\delta_{i_d}^2/2b_0}}, & \text{otherwise} \end{cases} \tag{5.1}$$

where $\mathrm{Erf}[\cdot]$ is the error function (4.4).

5.2.2.3 Initial Occupancy Vector ϕ_0

The initial occupancy vector defines the distribution of the Markov chain at its starting point. To model the Rayleigh fading process over an amplitude/rate state-space, the initial occupancy vector will be calculated to represent a quantized version of $f_R(r, r')$, which is given in (2.19).

Thus, using (4.1) and (4.2) to find i_d and j_d, $\phi_0[d]$ can be computed as

$$\phi_0[d] = \Pr[X_0 = s_d] = \int_{\gamma_{j_d-1}}^{\gamma_{j_d}} \int_{\delta_{i_d-1}}^{\delta_{i_d}} f_R(r, r') dr dr'$$
$$= \frac{1}{2}\left(e^{-\frac{\delta_{i_d-1}^2}{2b_0}} - e^{-\frac{\delta_{i_d}^2}{2b_0}}\right)\left(\mathrm{Erf}\left[\frac{\gamma_{j_d}}{\sqrt{2b_2}}\right] - \mathrm{Erf}\left[\frac{\gamma_{j_d-1}}{\sqrt{2b_2}}\right]\right). \tag{5.2}$$

5.2.2.4 Transition Matrix P

The transition matrix for the first-order Markov chain model of the ISORA Rayleigh fading process will be found using the joint distribution of two consecutive states, as done in Section 4.2.2.4. If we let r_1 and r_1' represent the amplitude and rate-of-change of the Rayleigh fading process at time t, and let r_2 and r_2' represent the amplitude and rate at time $t + T$, where T is the sample spacing of the model, then we can compute the transition matrix as

$$
\begin{aligned}
P_{qh} &= \Pr[X_k = s_h | X_{k-1} = s_q] \\
&= \frac{\Pr[X_{k-1} = s_q, X_k = s_h]}{\Pr[X_{k-1} = s_q]} && (5.3) \\
&= \frac{\int_{\gamma_{j_h-1}}^{\gamma_{j_h}} \int_{\delta_{i_h-1}}^{\delta_{i_h}} \int_{\gamma_{j_q-1}}^{\gamma_{j_q}} \int_{\delta_{i_q-1}}^{\delta_{i_q}} f_R(r_1, r_2, r_1', r_2') dr_1 dr_1' dr_2 dr_2'}{\phi_0[q]} && (5.4)
\end{aligned}
$$

where i_q, j_q, i_h, j_h are found using (4.1) and (4.2).

Joint distribution $f_R(r_1, r_2, r_1', r_2')$ is the joint distribution of two correlated Rayleigh random variables and their derivatives. We derived an expression for this distribution in Section 2.2.4, where we found that it can be expressed as (2.22). There is no closed-form expression for the numerator of (5.4), so it must be calculated using numerical integration techniques. In this case, we make use of the Monte Carlo method [53] to approximate the integral values, the details of which are given in Appendix B.1.

5.2.3 Model Analysis

To analyze the suitability of a first-order Markov chain in modeling the ISORA Rayleigh fading channel, we compare the statistics of the Markov chain model to those of the ISORA Rayleigh fading model on the basis of the same three properties considered in Chapter 4. These consist of the first-order distribution, model stationarity, and the autocorrelation function.

We continue to focus our analysis on threshold vectors $\boldsymbol{\delta}$ and $\boldsymbol{\gamma}$ that result in equiprobable state-space definitions. Because the amplitude and rate-of-change remain independent when considering the Rayleigh fading process, as we can see from joint distribution (2.19), the amplitude state-space and rate state-space for this model can still be partitioned separately. In particular, we can find $\boldsymbol{\delta}[d]$ by solving

$$
\int_{\delta_{d-1}}^{\delta_d} \frac{r}{b_0} e^{-\frac{r^2}{2b_0}} dr = e^{-\frac{\delta_{d-1}^2}{2b_0}} - e^{-\frac{\delta_d^2}{2b_0}} = \frac{1}{n} \qquad (5.5)
$$

for $d = 1, \ldots, n-1$. Since r' has a Gaussian distribution with variance b_2, $\boldsymbol{\gamma}[d]$ can be found by solving (4.10).

5.2.3.1 First-Order Distribution

Fig. 5.1 shows the first-order distribution of the Markov chain model compared to the Rayleigh distribution function for increasing values of n. The model is quite coarse for smaller values of n, but for $n \geq 10$, the Markov chain model approximates the Rayleigh distribution excellently. Contrast this with the first-order distribution of the Markov chain model of the complex Gaussian envelope fading process, seen in Fig. 4.14. We can see that the modeling of the first-order distribution is vastly improved when the Markov chain is calculated directly from the Rayleigh fading statistics. It is much smoother overall, and does not experience the modeling problems in the upper range of the distribution. Also, considering that the Markov chains examined in Fig. 5.1 have n amplitude states, while the Markov chains examined in Fig. 4.14 have n^2 amplitude states, calculating the Markov chain model directly from the Rayleigh fading statistics not only improves on the modeling of the first-order distribution, but does so with fewer states.

5.2.3.2 Invariance

In Section 4.2.3.2, we proved that a Markov chain model with a transition matrix calculated based on the joint distribution of two consecutive states will be stationary provided that the marginal distributions of the two consecutive states are the same as the distribution used to calculate the initial occupancy vector. The joint distribution of two consecutive states used to calculate the transition matrix of this Markov chain model, $f_R(r_1, r_2, r_1', r_2')$, is given by (2.22). By construction, its marginal distributions $f_R(r_1, r_1')$ and $f_R(r_2, r_2')$ will be identical to each other, as well as to (2.19), which is the distribution used to calculate ϕ_0. Thus, this Markov chain model is stationary.

As we considered in the ISORA Gaussian Markov chain model analysis of Section 4.2.3.2, this proof assumes that the integrals used in the transition matrix calculations are known exactly, which is not true. Thus, to verify the stationarity of the Markov chain model, we numerically compute $\|\phi_1 - \phi_0\|$, the norm of the difference between the Markov chain distributions at two consecutive points, for a number of different model parameters.

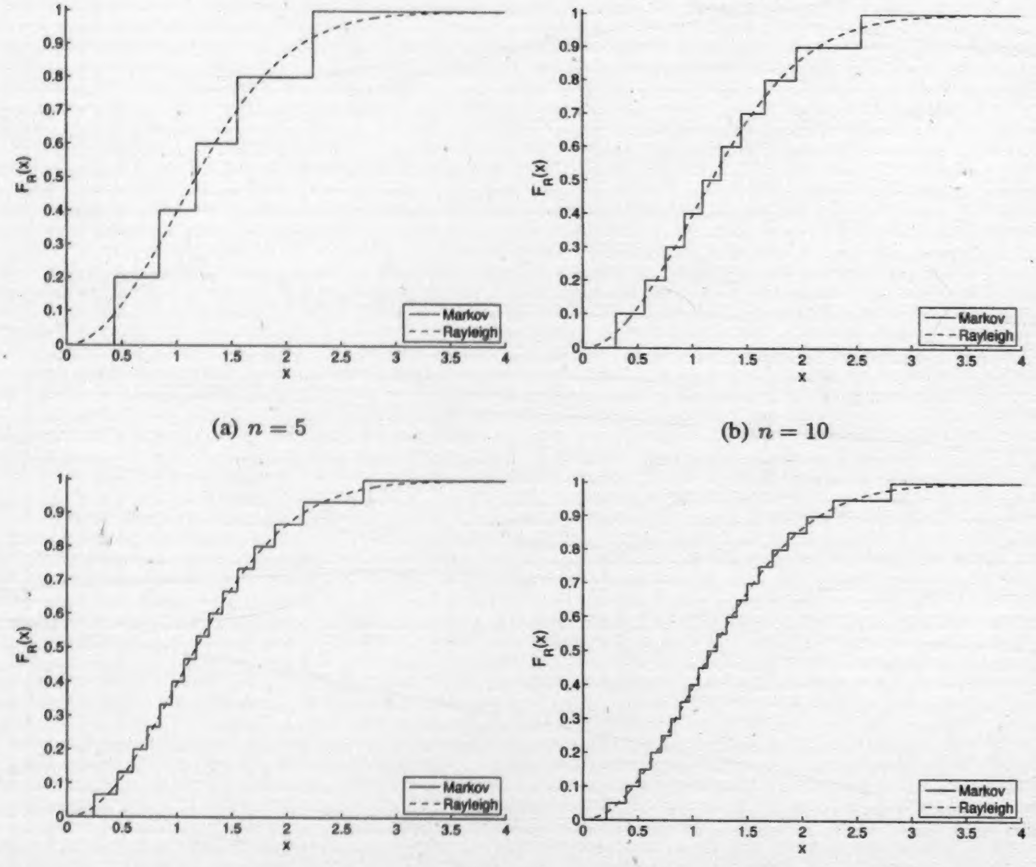

(a) $n = 5$

(b) $n = 10$

(c) $n = 15$

(d) $n = 20$

Fig. 5.1. The first-order distribution of the Markov chain model of the Rayleigh fading process, for various values of n.

TABLE 5.1

Numerical verification of the stationarity of the first-order Markov chain model of the ISORA Rayleigh fading process.

		$\|\phi_1 - \phi_0\|$		
n	m	$f_D T = 0.10$	$f_D T = 0.05$	$f_D T = 0.01$
10	5	3.88×10^{-5}	3.70×10^{-5}	3.79×10^{-5}
10	10	4.12×10^{-5}	4.36×10^{-5}	3.80×10^{-5}
10	15	3.87×10^{-5}	4.20×10^{-5}	3.93×10^{-5}
15	5	4.16×10^{-5}	4.04×10^{-5}	3.67×10^{-5}
15	10	3.61×10^{-5}	3.58×10^{-5}	3.90×10^{-5}
15	15	3.88×10^{-5}	3.88×10^{-5}	3.79×10^{-5}
20	5	3.82×10^{-5}	4.16×10^{-5}	3.55×10^{-5}
20	10	4.18×10^{-5}	3.79×10^{-5}	3.96×10^{-5}
20	15	3.86×10^{-5}	3.93×10^{-5}	3.76×10^{-5}

Table 5.1 shows the results of these calculations. As we saw in Table 4.1, the differences are on the order of the error in the numerical integration values, which, for the case of this model, is 10^{-5}, as we mention in Appendix B.1. Thus, even though the transition matrix for this Markov chain model is calculated with lower accuracy than the models in Chapter 4, it can still be considered stationary.

5.2.3.3 Autocorrelation

Figs. 5.2-5.7 show the autocorrelation of the first-order Markov chain model of the ISORA Rayleigh fading process compared to the theoretical ISORA autocorrelation function (2.42). In Figs. 5.2-5.4, we see the autocorrelation of the Markov chain model for increasing m and constant n, with $f_D T = 0.10$. As with the Markov chain model of the ISORA Gaussian fading process of Chapter 4, we can see that the use of an amplitude/rate-of-change state-space results in a decaying-oscillatory autocorrelation function of similar shape to

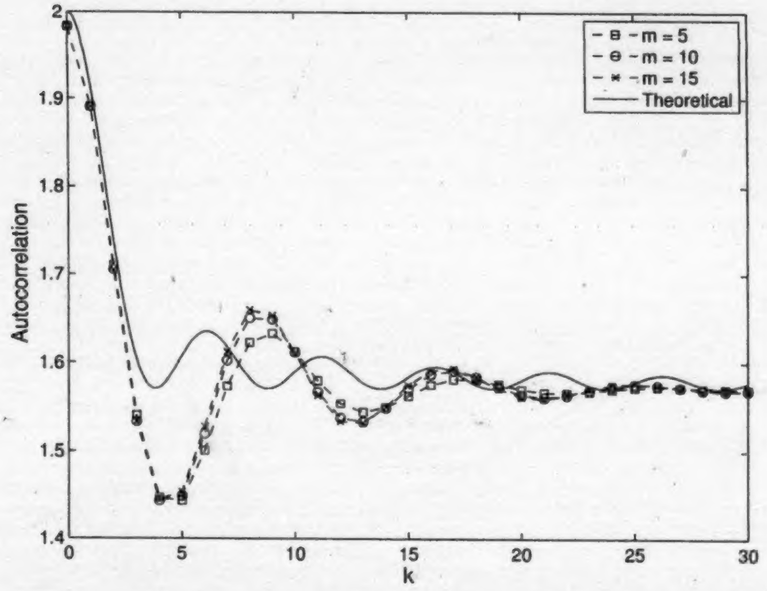

Fig. 5.2. Autocorrelation of the Markov chain model of the ISORA Rayleigh fading process for increasing values of m, $n = 10$, and $f_D T = 0.10$.

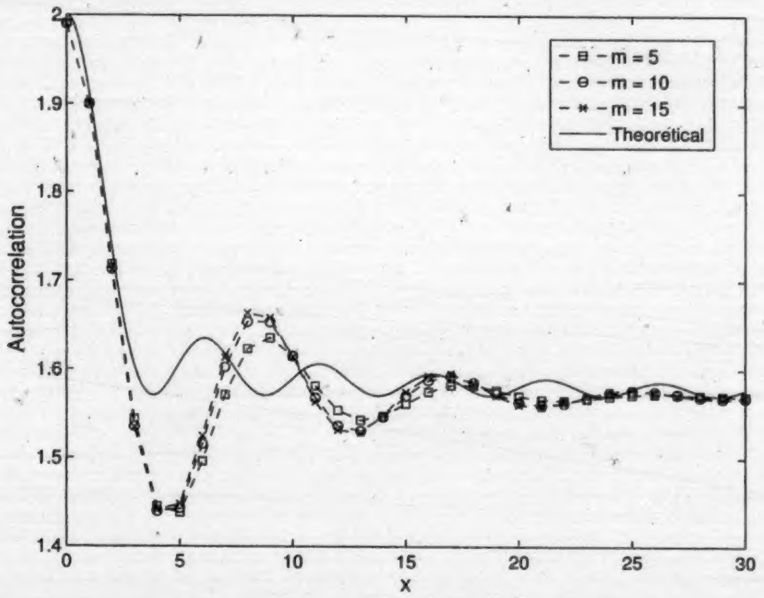

Fig. 5.3. Autocorrelation of the Markov chain model of the ISORA Rayleigh fading process for increasing values of m, $n = 15$, and $f_D T = 0.10$.

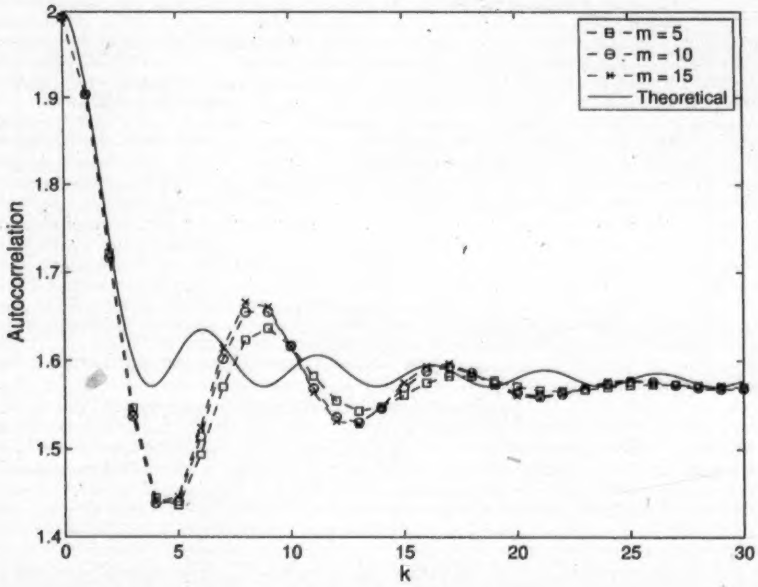

Fig. 5.4. Autocorrelation of the Markov chain model of the ISORA Rayleigh fading process for increasing values of m, $n = 20$, and $f_D T = 0.10$.

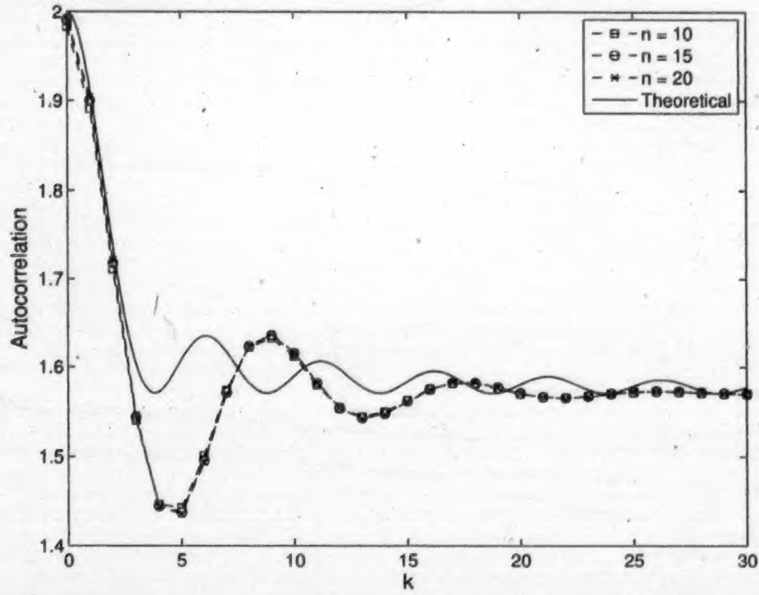

Fig. 5.5. Autocorrelation of the Markov chain model of the ISORA Rayleigh fading process for increasing values of n, $m = 5$, and $f_D T = 0.10$.

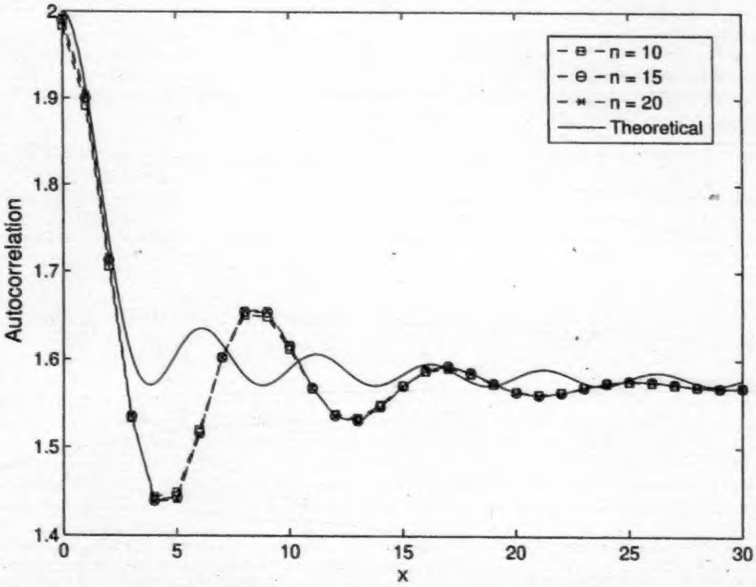

Fig. 5.6. Autocorrelation of the Markov chain model of the ISORA Rayleigh fading process for increasing values of n, $m = 10$, and $f_D T = 0.10$.

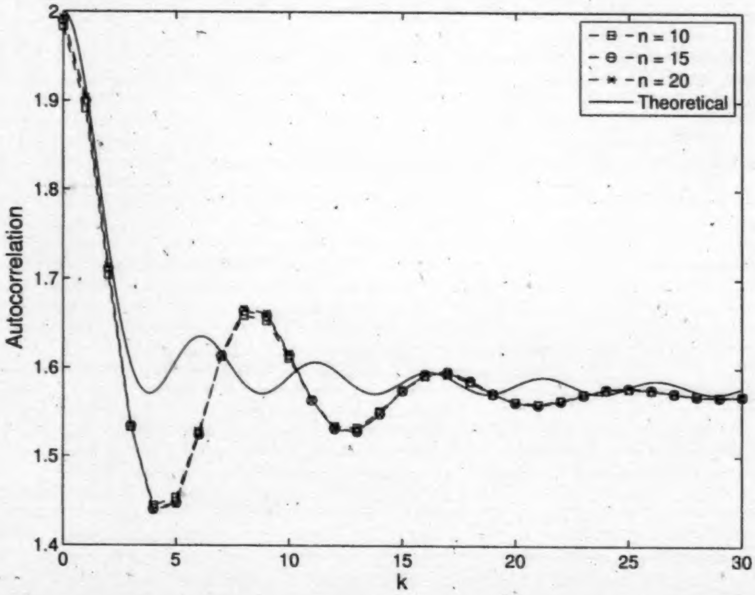

Fig. 5.7. Autocorrelation of the Markov chain model of the ISORA Rayleigh fading process for increasing values of n, $m = 15$, and $f_D T = 0.10$.

the theoretical. Also like the previous Gaussian model, we can see that the Markov chain model autocorrelation function decays faster than the theoretical, and has a slower oscillation frequency. Increasing m has no significant effect on the oscillation frequency or decay rate, but does cause an increase in the extrema of the autocorrelation function, with the exception of the first minima, which remains generally unchanged. We observed this increase in the autocorrelation extrema with increasing m when examining the Gaussian Markov chain model in Figs. 4.2 and 4.3, however, the increases we see here are not as large as the increases we saw for the Gaussian model. Figs. 5.5-5.7 show the same data, but reorganized to show the autocorrelation of the Markov chain model for increasing n and constant m. We can see that n has no significant effect on the autocorrelation, again, like the previous Gaussian Markov chain model.

When contrasting the results in Figs. 5.2-5.7 with the autocorrelation of the Markov chain model of the ISORA complex Gaussian envelope fading process, seen in Figs. 4.15-4.18, some significant differences are evident. First, the autocorrelation of the direct ISORA Rayleigh Markov chain model does not have the downward shift in the autocorrelation values that was seen in the Gaussian envelope model. This can be attributed to the fact that the first-order distribution of the direct Rayleigh Markov chain model is significantly improved over that of the Gaussian envelope model, as we discussed above, so the mean-squared value that the autocorrelation settles to is much closer to the theoretical. Secondly, the value of the first minima of the direct Rayleigh Markov chain model is considerably lower than the theoretical, much more so than the value of the first minima of the Gaussian envelope model. Finally, the fact that the first minima of the Gaussian envelope Markov chain model autocorrelation function is closer to the theoretical than the first minima of the direct Rayleigh model autocorrelation function means that the oscillations of the Gaussian envelope model lag behind the theoretical by a smaller amount than the oscillations of the direct Rayleigh model. Thus, the autocorrelation function of the Gaussian envelope model is closer to the theoretical than the autocorrelation function of the direct Rayleigh model, particularly for larger state-space sizes, despite the downward shift in autocorrelation values.

Figs. 5.8-5.16 show the autocorrelation of the Markov chain model of the ISORA Rayleigh fading process for various values of sample spacing T. As was the case with the autocorrelation of the Markov chain model of the ISORA Gaussian fading process, seen in Figs. 4.6-4.9, the oscillation frequency increases as T is increased, although the increase is much more significant in this case. In the case of the Gaussian Markov chain model, decreasing T from a large sample spacing down to a medium sample spacing caused the oscillation magnitudes to increase. As T was decreased beyond that point, however, the oscillation magnitudes decreased. In the case of the direct ISORA Rayleigh fading Markov chain model, as T is decreased, the oscillation magnitudes increase, for the entire range of T. There is no point where the oscillation magnitudes begin to decrease. The amount by which the magnitudes increase depends on m. As m gets larger, so do the increases in oscillation magnitudes as T decreases. This is most noticeable for the small sample spacing $T = 0.1\text{e-}3$, but it is true for all sample spacings.

When contrasting the results of Figs. 5.8-5.16 with the autocorrelation results for the Markov chain model of the ISORA complex Gaussian fading envelope in Figs. 4.19-4.21, we can see that changes to sample spacing T affect the autocorrelation of the direct Markov chain model of the ISORA Rayleigh fading process much more than they do the Markov chain model of the ISORA complex Gaussian envelope fading process. We previously observed from Figs. 4.19-4.21 that sample spacing $T = 1.8\text{e-}3$ was the largest sample spacing that still resulted in a reasonably smooth sampling of the autocorrelation function, an assertion that was illustrated by the sample fading profile in Fig. 4.22. This same observation can be made from Figs. 5.8-5.16. We can also observe that the autocorrelation that is closest to the theoretical for a first-order Markov chain model of the ISORA Rayleigh fading channel occurs when $T = 1.8\text{e-}3$, for all state-spaces considered. However, it is clear from Figs. 4.19-4.21 that the autocorrelation of a Markov chain model of the ISORA Rayleigh fading channel based on a first-order Markov chain model of the underlying Gaussian process is closer to the theoretical autocorrelation than even the best direct first-order Markov chain model of the ISORA Rayleigh fading channel.

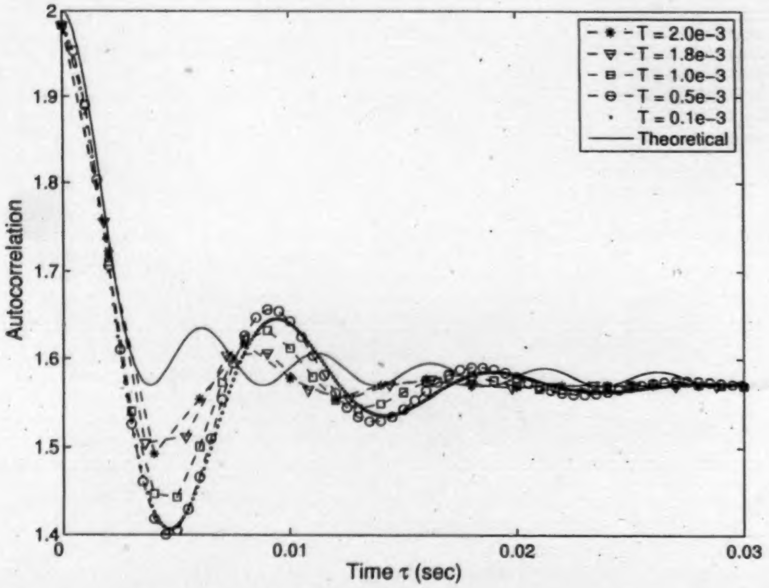

Fig. 5.8. ISORA Rayleigh Markov chain model autocorrelation for various values of sample spacing T (sec), $n = 10$, $m = 5$, and $f_D = 100$ Hz.

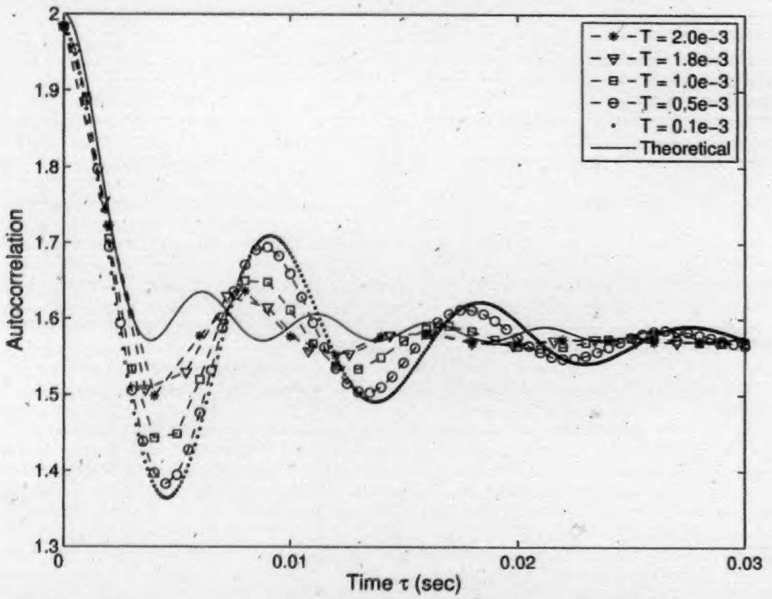

Fig. 5.9. ISORA Rayleigh Markov chain model autocorrelation for various values of sample spacing T (sec), $n = 10$, $m = 10$, and $f_D = 100$ Hz.

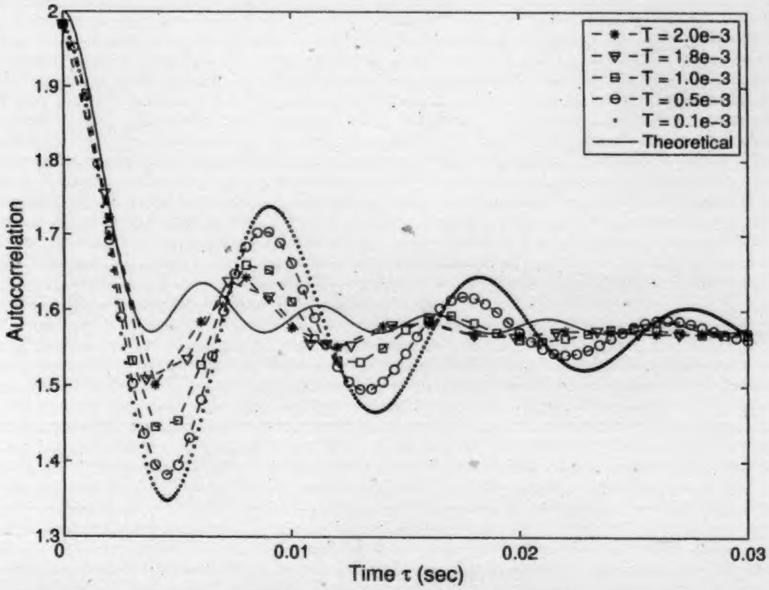

Fig. 5.10. ISORA Rayleigh Markov chain model autocorrelation for various values of sample spacing T (sec), $n = 10$, $m = 15$, and $f_D = 100$ Hz.

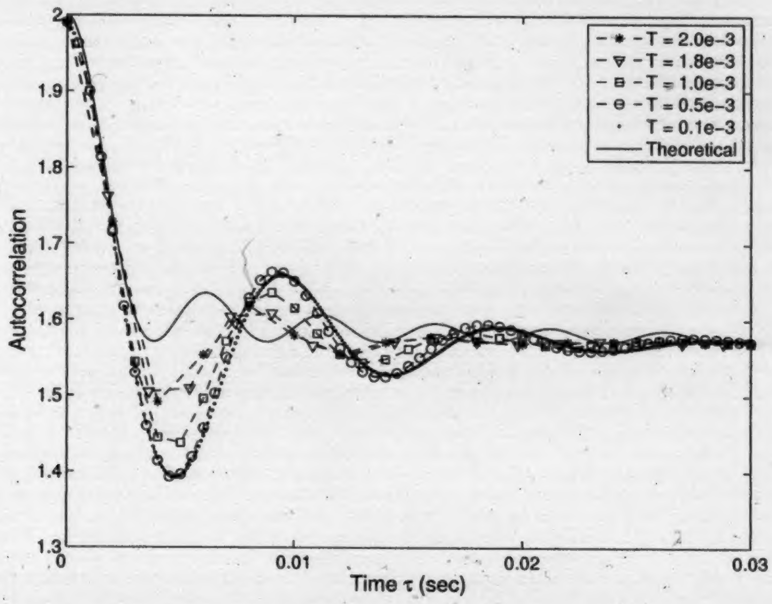

Fig. 5.11. ISORA Rayleigh Markov chain model autocorrelation for various values of sample spacing T (sec), $n = 15$, $m = 5$, and $f_D = 100$ Hz.

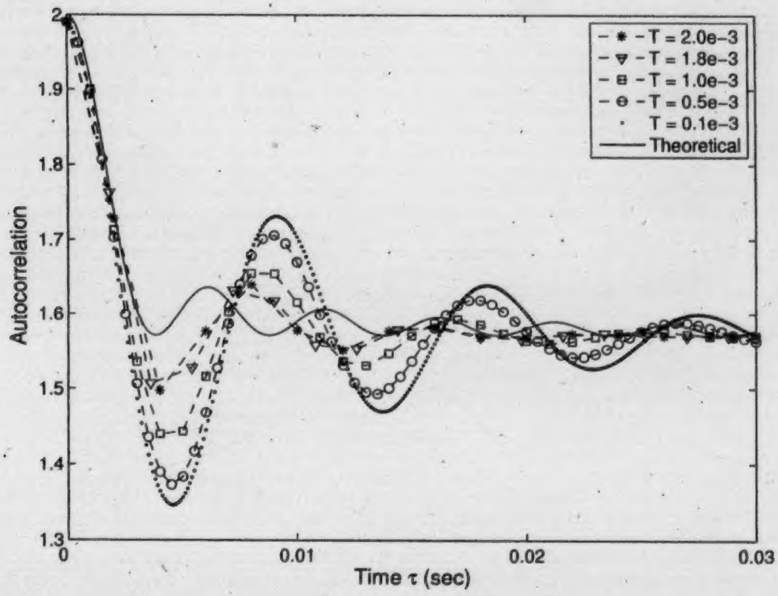

Fig. 5.12. ISORA Rayleigh Markov chain model autocorrelation for various values of sample spacing T (sec), $n = 15$, $m = 10$, and $f_D = 100$ Hz.

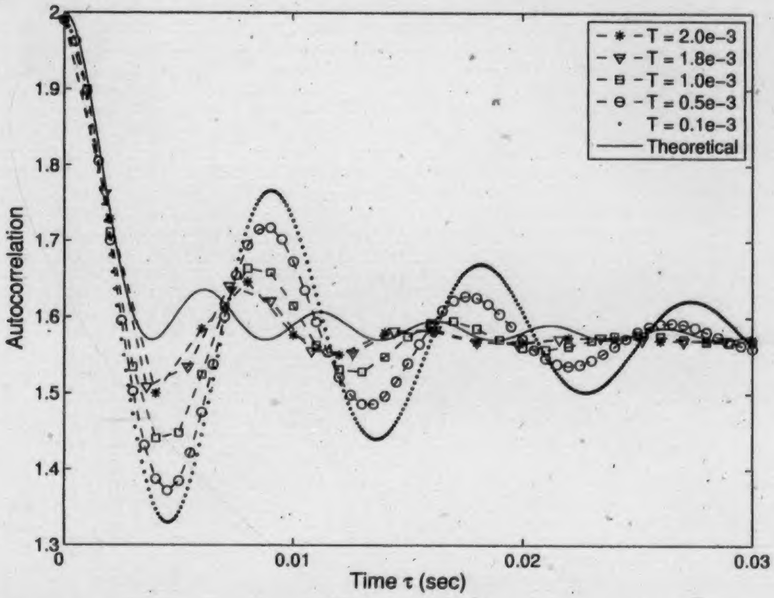

Fig. 5.13. ISORA Rayleigh Markov chain model autocorrelation for various values of sample spacing T (sec), $n = 15$, $m = 15$, and $f_D = 100$ Hz.

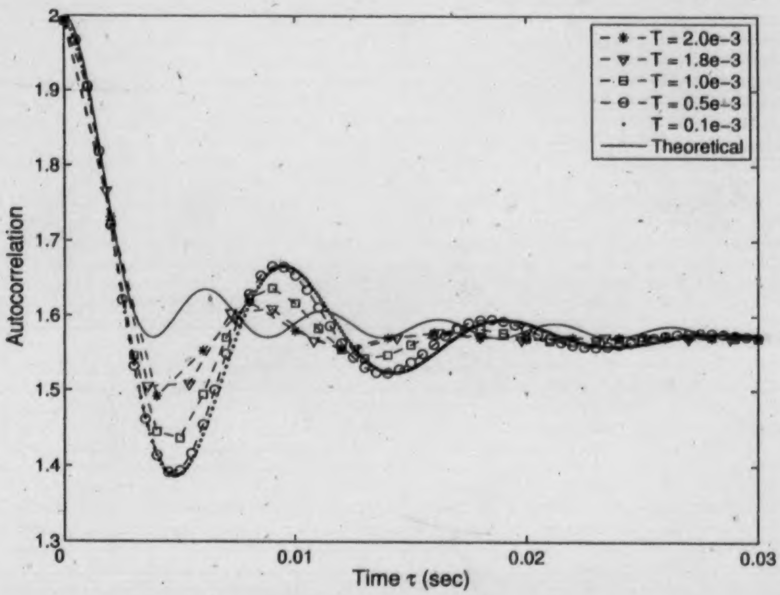

Fig. 5.14. ISORA Rayleigh Markov chain model autocorrelation for various values of sample spacing T (sec), $n = 20$, $m = 5$, and $f_D = 100$ Hz.

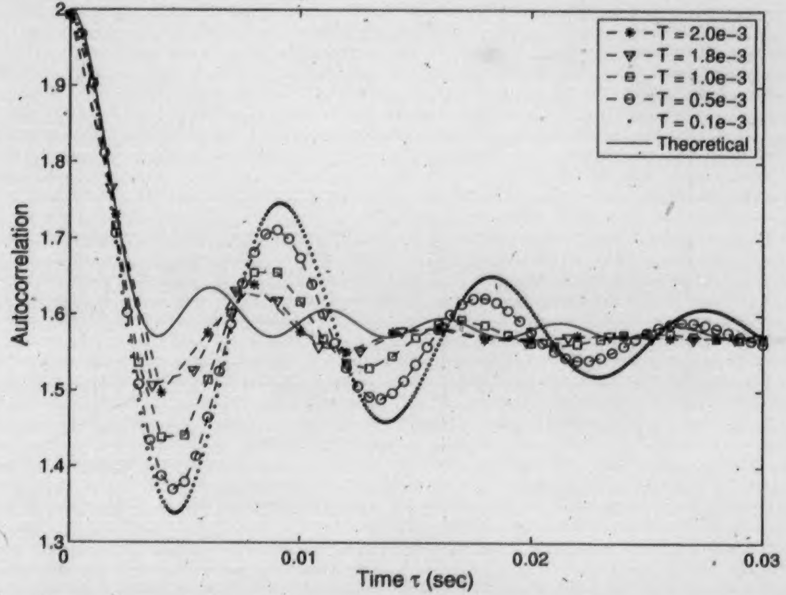

Fig. 5.15. ISORA Rayleigh Markov chain model autocorrelation for various values of sample spacing T (sec), $n = 20$, $m = 10$, and $f_D = 100$ Hz.

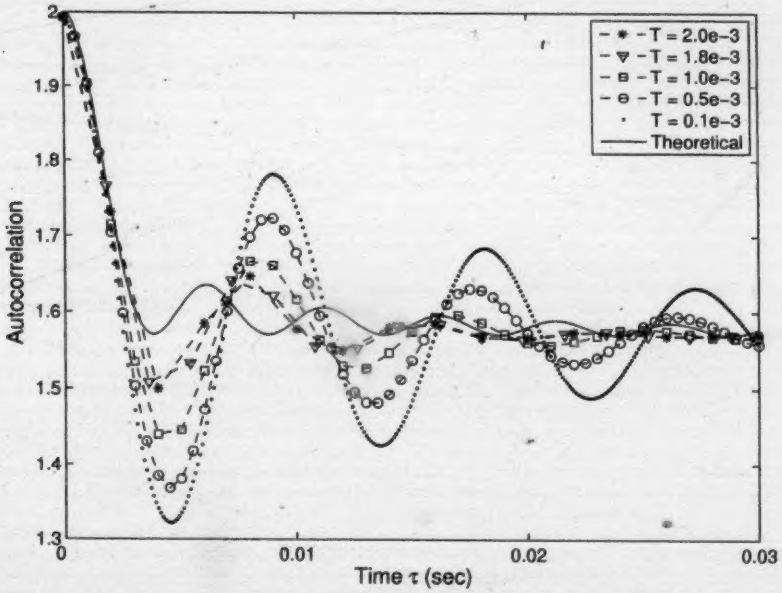

Fig. 5.16. ISORA Rayleigh Markov chain model autocorrelation for various values of sample spacing T (sec), $n = 20$, $m = 15$, and $f_D = 100$ Hz.

5.2.4 Conclusion

In this section, we studied a first-order Markov chain model of the ISORA Rayleigh fading channel, based on an amplitude/rate-of-change state-space, in which the Markov chain model elements were calculated directly from the statistics of the Rayleigh fading process. We found that this direct method resulted in a Markov chain that modeled the first-order distribution of the Rayleigh fading channel better than the Markov chain model of the complex Gaussian envelope fading process studied in Chapter 4. We saw that the amplitude/rate-of-change state-space continued to result in a Markov chain model that displayed a decaying-oscillatory autocorrelation function that was similar in shape to that of the theoretical, though with a slower oscillation frequency and faster decay rate, and we determined that sample spacing $T = 1.8$e-3 resulted in the first-order Markov chain model whose autocorrelation function was closest to that of the theoretical.

It is tempting to claim that a Markov chain model of the ISORA Rayleigh fading channel based on a Markov chain model of the underlying complex Gaussian process is better than a Markov chain model based directly on the ISORA Rayleigh fading statistics, since the Gaussian envelope model's autocorrelation function is closer to the theoretical than the autocorrelation of even the best first-order direct Rayleigh model. However, this is not a fair comparison, since the Gaussian envelope model has size $(nm)^2$, while the first-order direct Rayleigh model has size nm. We would expect that a larger Markov chain would model the fading channel statistics better. In the next section, we will examine a second-order Markov chain model of the ISORA Rayleigh fading channel, based directly on the envelope statistics, to see what improvement an increase in Markov chain order will have on this direct Rayleigh model. Since a second-order Markov chain model will have size $(nm)^2$, it will also make a more appropriate comparison to the first-order Markov chain model of the complex Gaussian envelope fading process from Chapter 4.

5.3 Second-Order Markov Chain Model

5.3.1 Introduction

In Section 5.2, we presented and analyzed a first-order Markov chain model of the ISORA Rayleigh fading channel, based on an amplitude/rate-of-change state-space, where the Markov chain model elements were computed directly from the statistics of the ISORA Rayleigh fading process. We saw that this direct Rayleigh Markov chain model improved on the first-order distribution of the Gaussian envelope model, studied in Chapter 4, but failed to improve on the autocorrelation function, where the Gaussian envelope model autocorrelation was closer to the theoretical than that of the direct Rayleigh model. In this Section, we consider a second-order Markov chain model of the ISORA Rayleigh fading channel, based on an amplitude/rate-of-change state-space, where the elements are computed directly from the Rayleigh fading statistics. We examine the effects of increasing the Markov chain order on the direct Rayleigh fading Markov chain model, as well as compare the resulting model statistics to those of the previous Gaussian envelope Markov chain model.

5.3.2 Computing the Markov Chain Model

In this section, we present a method to calculate the three elements that define a Markov chain model, namely, transition matrix P, initial occupancy vector ϕ_0, and output vector $\mathbf{f}$, for a second-order Markov chain. As in Section 5.2, the Markov chain model elements will be calculated based directly on the statistics of the ISORA Rayleigh fading process, as opposed to the underlying complex Gaussian process.

5.3.2.1 Defining the Second-Order State-Space

The state-space for this second-order Markov chain model will be defined exactly as in Section 4.3.2.1, in which the second-order state-space consists of $(nm)^2$ states, labeled $\{w_1, \ldots, w_{(nm)^2}\}$, where $w_d = \{s_{x_d}, s_{y_d}\}$, s_{y_d} being the current first-order state, with y_d given by (4.18), and s_{x_d} being the previous first-order state, with x_d given by (4.17). The underlying first-order states, s_{y_d} and s_{x_d}, are defined as in Section 5.2.2.1, thus, the second-order state-space is fully specified by threshold vectors $\boldsymbol{\delta}$ and $\boldsymbol{\gamma}$.

5.3.2.2 Output Vector f

As done in Section 4.3.2.2, the output of a second-order state will be set to the output value of the equivalent current first-order state. Thus, to compute $\mathbf{f}[d]$, we first find y_d via (4.18), which specifies the equivalent current first-order state, then find i_{y_d} using (4.1), which specifies the amplitude thresholds of the current first-order state. The value of $\mathbf{f}[d]$ can then be computed using (5.1), with i_d replaced by i_{y_d}.

5.3.2.3 Initial Occupancy Vector ϕ_0

In Section 5.2.2.3, initial occupancy vector ϕ_0 was found by integrating $f_R(r, r')$ over each state in the state-space. As we saw above, the state-space for a second-order Markov chain consists of two consecutive points, so in this case, ϕ_0 will be found by integrating over the joint distribution of these two consecutive points, identified by r_1, r_1', r_2, r_2'.

To calculate $\phi_0[d]$, we first find x_d and y_d with (4.17) and (4.18), then find i_{x_d}, j_{x_d}, i_{y_d}, j_{y_d} with (4.1) and (4.2). Then, the initial occupancy probability of state w_d is

$$\begin{aligned}\phi_0[d] &= \Pr[Y_k = w_d] \\ &= \Pr[X_k = s_{y_d}, X_{k-1} = s_{x_d}] \\ &= \int_{\gamma_{j_{y_d}-1}}^{\gamma_{j_{y_d}}} \int_{\delta_{i_{y_d}-1}}^{\delta_{i_{y_d}}} \int_{\gamma_{j_{x_d}-1}}^{\gamma_{j_{x_d}}} \int_{\delta_{i_{x_d}-1}}^{\delta_{i_{x_d}}} f_R(r_1, r_2, r_1', r_2') dr_1 dr_1' dr_2 dr_2'. \qquad (5.6)\end{aligned}$$

This integral is identical to the numerator of (5.4), and can be similarly approximated using the Monte Carlo method discussed in Appendix B.1.

5.3.2.4 Transition Matrix P

The transition matrix for the second-order Markov chain model of the ISORA Rayleigh fading process will be calculated using a similar method to the one used in Section 4.3.2.4 for the second-order ISORA Gaussian Markov chain model. In that section, we explained that not all transitions in a second-order state-space are possible. Thus, the transition matrix can be expressed as (4.20)

$$\begin{aligned}P_{qh} &= \Pr[Y_k = w_h | Y_{k-1} = w_q] \\ &= \Pr[X_k = s_{y_h}, X_{k-1} = s_{x_h} | X_{k-1} = s_{y_q}, X_{k-2} = s_{x_q}] \\ &= \begin{cases} \Pr[X_k = s_{y_h} | X_{k-1} = s_{y_q}, X_{k-2} = s_{x_q}], & x_h = y_q \\ 0, & \text{otherwise} \end{cases}\end{aligned}$$

where Y_k is a random variable representing the second-order state of the Markov chain at time k, X_k is a random variable representing the first-order state of the Markov chain at time k, and x_h, y_h, x_q, y_q are found using (4.17) and (4.18). Let r_1 and r_1' represent the amplitude and rate-of-change of the Rayleigh fading process at time t, r_2 and r_2' represent the amplitude and rate at time $t + T$, and r_3 and r_3' represent the amplitude and rate at time $t + 2T$. If we let $\mathbf{r} = [r_1, r_1', r_2, r_2', r_3, r_3']$, then the conditional probability above can be computed as

$$\begin{aligned}\Pr[X_k =& s_{y_h} | X_{k-1} = s_{y_q}, X_{k-2} = s_{x_q}] \\ &= \frac{\Pr[X_k = s_{y_h}, X_{k-1} = s_{y_q}, X_{k-2} = s_{x_q}]}{\Pr[X_{k-1} = s_{y_q}, X_{k-2} = s_{x_q}]} \\ &= \frac{\int_{\gamma_{j_{y_h}-1}}^{\gamma_{j_{y_h}}} \int_{\delta_{i_{y_h}-1}}^{\delta_{i_{y_h}}} \int_{\gamma_{j_{y_q}-1}}^{\gamma_{j_{y_q}}} \int_{\delta_{i_{y_q}-1}}^{\delta_{i_{y_q}}} \int_{\gamma_{j_{x_q}-1}}^{\gamma_{j_{x_q}}} \int_{\delta_{i_{x_q}-1}}^{\delta_{i_{x_q}}} f_R(r_1, r_2, r_3, r_1', r_2', r_3') d\mathbf{r}}{\phi_0[q]}. \quad (5.7)\end{aligned}$$

Though we did not derive an expression for joint distribution $f_R(r_1, r_2, r_3, r_1', r_2', r_3')$ in Section 2.2.4, we note that the Monte Carlo method used to numerically integrate joint distribution $f_R(r_1, r_2, r_1', r_2')$, which we discuss in Appendix B.1, does not actually make use of expression (2.22), it only makes use of the transformation of variables that led to that expression. Thus, simple extensions of the method of Appendix B.1, which we discuss in Appendix B.2, can be used to approximate the integral in the numerator of (5.7), even without knowing an actual expression for the joint distribution being integrated.

5.3.3 Model Analysis

As we have done in all previous analyses, we focus on threshold vectors δ and γ that result in equiprobable first-order state-spaces. We also remove any state from the state-space that has an initial occupancy probability below 10^{-6}, for the same reasons we discussed in Section 4.3.3. Since the output of a second-order state is the same as the output of the equivalent current first-order state, the first-order distribution of this second-order Markov chain model will be identical to that of the first-order Markov chain model, seen in Fig. 5.1. By construction, the marginal distributions of $f_R(r_1, r_2, r_3, r_1', r_2', r_3')$, specifically $f_R(r_1, r_2, r_1', r_2')$ and $f_R(r_2, r_3, r_2', r_3')$, are identical to each other and to the distribution used to calculate ϕ_0, so the stationarity proof of Section 4.2.3.2 is valid here. In Table 5.2, we show the norm of the difference $\phi_1 - \phi_0$ for a number of model parameters. As in Table 5.1, which tabulated values of this difference for a first-order Markov chain model, we can see that the differences continue to be on the order of the error in the numerical integration. The values in Table 5.2 are a little larger than those in Table 5.1, a result of removing

TABLE 5.2

Numerical verification of the stationarity of the second-order Markov chain model of the ISORA Rayleigh fading process.

		$\|\phi_1 - \phi_0\|$		
n	m	$f_D T = 0.10$	$f_D T = 0.05$	$f_D T = 0.01$
5	4	5.38×10^{-5}	4.72×10^{-5}	3.20×10^{-5}
5	10	5.13×10^{-5}	5.68×10^{-5}	4.11×10^{-5}
10	4	5.52×10^{-5}	5.19×10^{-5}	3.65×10^{-5}
10	10	5.77×10^{-5}	5.49×10^{-5}	4.32×10^{-5}

the low probability states from the state-space, but they are still small, so the second-order Markov chain model of the ISORA Rayleigh fading channel can be considered stationary. Thus, we proceed to the autocorrelation analysis.

Figs. 5.17-5.20 show the autocorrelation function of the second-order Markov chain model of the ISORA Rayleigh fading channel for various values of sample spacing T. Because the size of the second-order Markov chain increases as $(nm)^2$, we focus our analysis on smaller values of n and m than we did in the first-order Markov chain model analysis of Section 5.2. For comparison purposes, each figure also includes a first-order Markov chain model autocorrelation plot for $T = 1.8\text{e-}3$, which we determined in Section 5.2.3.3 to offer the closest fit to the theoretical for a direct Rayleigh first-order Markov chain model. As we have observed in previous models, changes to n have minimal effect on the autocorrelation function, which we can see here by noticing that Figs. 5.17 and 5.19 look very similar to each other, as do Figs. 5.18 and 5.20. In all cases, we can see that increasing the model order to 2 offers no noticeable benefit at the small sample spacing $T = 0.1\text{e-}3$, a point we also observed when considering the second-order Markov chain model of the ISORA Gaussian fading process in Section 4.3.3. However, the increase in Markov chain order causes a definite improvement at larger sample spacings $T \geq 1.0\text{e-}3$. This can be attributed to the fact that, at small sample spacings, two points don't span a significantly larger area of the theo-

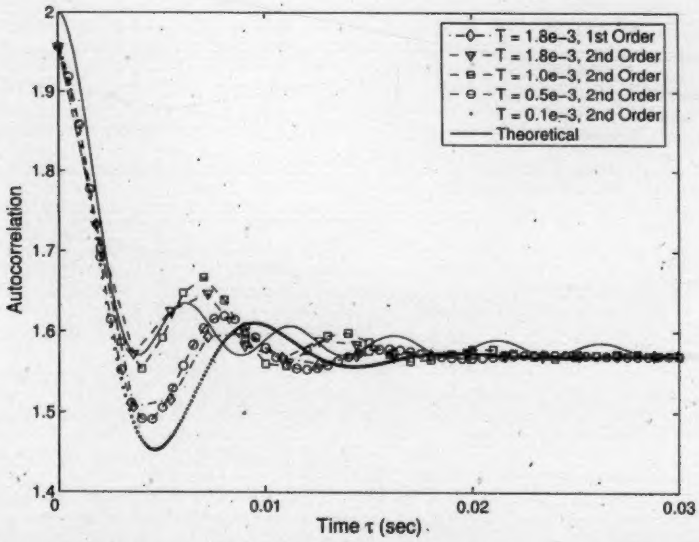

Fig. 5.17. Autocorrelation of the second-order Markov chain model of the ISORA Rayleigh fading channel for various values of T (sec), $n = 5$, $m = 4$, and $f_D = 100$ Hz.

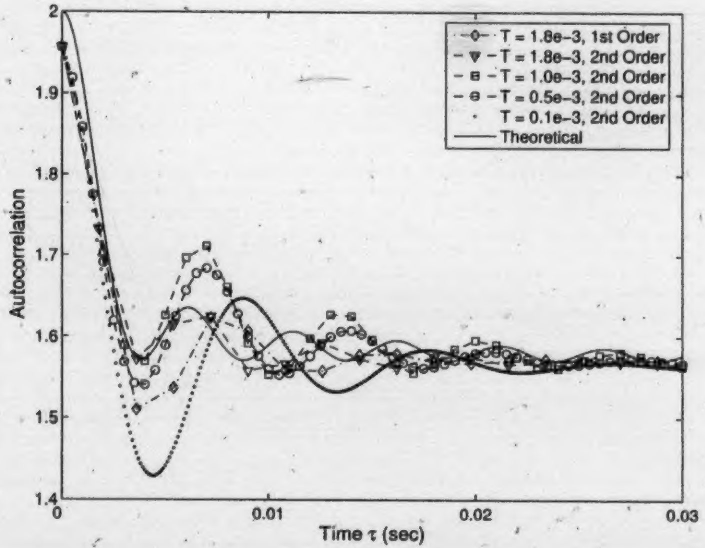

Fig. 5.18. Autocorrelation of the second-order Markov chain model of the ISORA Rayleigh fading channel for various values of T (sec), $n = 5$, $m = 10$, and $f_D = 100$ Hz.

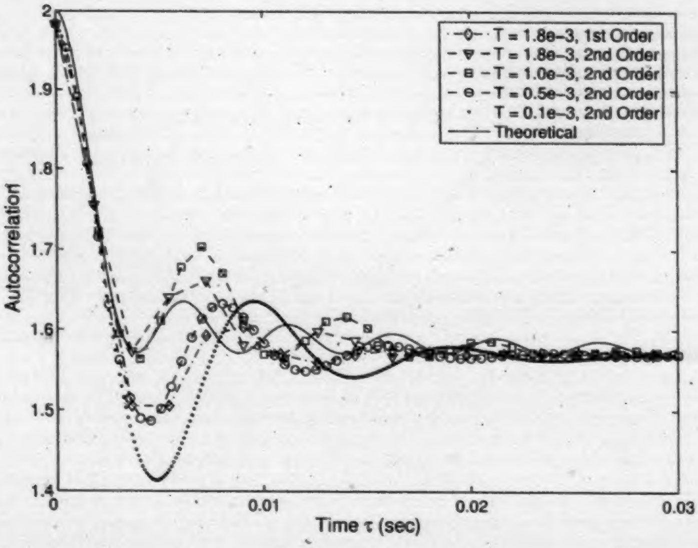

Fig. 5.19. Autocorrelation of the second-order Markov chain model of the ISORA Rayleigh fading channel for various values of T (sec), $n = 10$, $m = 4$, and $f_D = 100$ Hz.

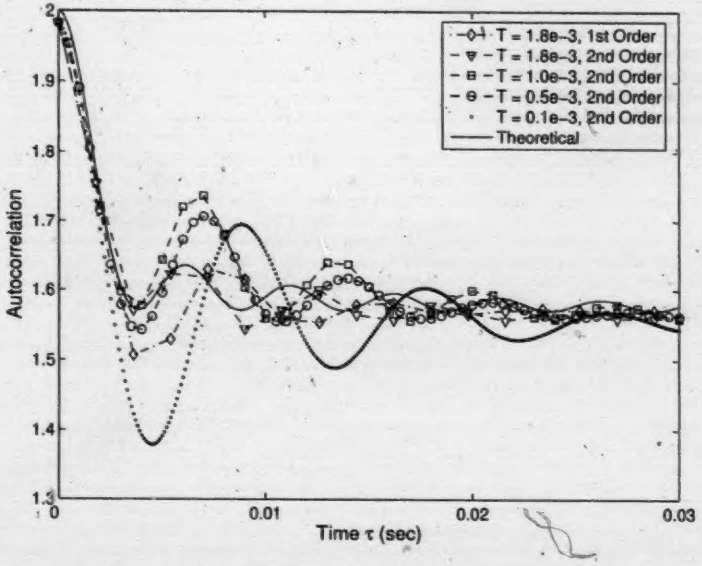

Fig. 5.20. Autocorrelation of the second-order Markov chain model of the ISORA Rayleigh fading channel for various values of T (sec), $n = 10$, $m = 10$, and $f_D = 100$ Hz.

retical function than one point does, but at larger sample spacings, two points span a much larger interval than one point and give much more information about the overall shape of the theoretical autocorrelation function. At the intermediate sample spacing $T = 0.5$e-3, the improvement depends on m. For $m = 10$, there is noticeable improvement beyond the best first-order model, but for $m = 4$, the result is about as close to the theoretical as the first-order model. For the second-order Markov chain models, we can observe that sample spacing $T = 1.8$e-3 continues to result in the closest fit to the theoretical autocorrelation function. In fact, in Figs. 5.18 and 5.20, this sample spacing results in an autocorrelation function that well models the theoretical through to the second minima.

In Section 4.3.3, we saw that a Markov chain model of the ISORA Rayleigh fading process based on a second-order Markov chain model of the underlying complex Gaussian process is too large to be practically analyzed. So, we compare the results in Figs. 5.17-5.20 to those in Figs. 4.19-4.21, which show the autocorrelation of the Markov chain model of the ISORA Rayleigh fading envelope based on a first-order Markov chain model of the underlying complex Gaussian process. This is a fair comparison because the size of both of these Markov chain models grows as $(nm)^2$. For both methods, we can see that, in general, a larger value of m results in better modeling of the theoretical ISORA autocorrelation function than a smaller value of m. When comparing the two methods, we can see that for the large sample spacing $T = 1.8$e-3, the direct Rayleigh second-order Markov chain model results in the autocorrelation function with the best fit to the theoretical. The direct Rayleigh second-order Markov chain model also offers the better fit for sample spacing $T = 1.0$e-3. For medium sample spacing $T = 0.5$e-3, the two methods result in autocorrelation functions with a similar fit to the theoretical for $m = 10$, but the Gaussian envelope model is closer to the theoretical when $m = 4$. For small sample spacing $T = 0.1$e-3, the autocorrelation function of the Gaussian envelope model is considerably closer to the theoretical than that of the direct Rayleigh model.

5.3.4 Conclusion

In this section, we examined a second-order Markov chain model of the ISORA Rayleigh fading channel with an amplitude/rate-of-change state-space, where the Markov chain elements were calculated based directly on the statistics of the ISORA Rayleigh fading process. We saw that a second-order Markov chain models the first-order distribution of the Rayleigh fading channel exactly as well as a first-order Markov chain does. However, we saw that increasing the Markov chain order can offer considerable improvement in the closeness of the Markov chain model autocorrelation to the theoretical ISORA autocorrelation, particularly for large sample spacings. We saw that the second-order Markov chain model that most closely modeled the theoretical ISORA autocorrelation function occurred at sample spacing $T = 1.8\text{e-}3$. We also observed that a direct Rayleigh second-order Markov chain model approximates the theoretical ISORA autocorrelation as well or better than a Markov chain model of the ISORA Rayleigh envelope fading process based on a first-order Markov chain model of the underlying complex Gaussian process, provided m is chosen reasonably large, for medium to large sample spacings. At small sample spacings, however, we saw that the autocorrelation of the Gaussian envelope model is much closer to the theoretical than the direct Rayleigh model.

5.4 Conclusion

In this chapter, we studied a Markov chain model of the ISORA Rayleigh fading channel, based on an amplitude/rate-of-change state-space, in which the Markov chain model elements were calculated based directly on the statistics of the ISORA Rayleigh fading process. In Section 5.2, we examined first-order Markov chain models. We saw that calculating the Markov chain model directly from the Rayleigh fading statistics resulted in significant improvement in the modeling of the first-order Rayleigh distribution over the Gaussian envelope model studied in Chapter 4. The direct Rayleigh Markov chain model had a smoother first-order distribution, and did not exhibit the errors in modeling the upper range of the distribution that we saw in the Gaussian envelope model. When considering the autocorrelation function of the first-order Markov chain model, we saw that the amplitude/rate-of-change state-space resulted in a decaying-oscillatory autocorrelation that was quite similar in shape to the theoretical autocorrelation function, though the decay rate was faster and the oscillation frequency was slower. We saw that the oscillation frequency varies with sample spacing T, and that $T = 1.8\text{e-}3$ resulted in the first-order Markov chain model of the ISORA Rayleigh fading channel whose autocorrelation function was the closest fit to that of the theoretical. However, when comparing the first-order direct Rayleigh Markov chain model to the first-order Gaussian envelope model of Section 4.2, we saw that the autocorrelation function of the Gaussian envelope model was closer to the theoretical than that of the first-order direct Rayleigh model.

In Section 5.3, we considered a second-order Markov chain model of the ISORA Rayleigh fading channel. We saw that increasing the Markov chain order to 2 can significantly improve the modeling of the ISORA autocorrelation, particularly at larger sample spacings, where the increase in order causes a considerable increase in the oscillation frequency, though the decay rate remains largely unaffected. As in the direct Rayleigh first-order Markov chain model, sample spacing $T = 1.8\text{e-}3$ resulted in the second-order Markov chain model whose autocorrelation function was the closest fit to the theoretical. When comparing the direct Rayleigh second-order Markov chain model to the first-order Gaussian envelope model, an appropriate comparison despite the difference in order because they both have size $(nm)^2$, we can see that at large sample spacings, the autocorrelation of the direct Rayleigh model is closer to the theoretical than that of the Gaussian envelope model. At medium sample spacings, the two methods are equally close to the theoretical autocorrelation for large m, but the Gaussian envelope model is closer for small m. Finally, for small sample spacings, the autocorrelation of the Gaussian envelope model is significantly closer to the theoretical than that of the direct Rayleigh model.

Chapter 6

Conclusions

6.1 Introduction

In this thesis, we examined Markov chain models of the ISORA Rayleigh fading channel based on a state-space that consisted of both the amplitude and rate-of-change of the fading process. We considered two approaches to defining the Markov chain model. First, we obtained a Markov chain model of the ISORA Rayleigh fading process by transforming a Markov chain model of the underlying complex Gaussian process. Second, we obtained a Markov chain model of the ISORA Rayleigh fading process by calculating the Markov chain model elements directly from the ISORA Rayleigh fading envelope statistics. Within both approaches, we considered first- and second-order Markov chains.

In all cases, we observed that the use of an amplitude/rate-of-change state-space resulted in a Markov chain model with a decaying-oscillatory autocorrelation function of similar shape to the theoretical ISORA autocorrelation, a significant improvement over the exponential autocorrelation possessed by AFSMC models. However, the decay rate was faster than the theoretical, and the oscillation frequency was slower. Increasing the Markov chain order improved the oscillation frequency in some cases, particularly for large sample spacings, but the improved oscillation frequency was still too slow for the Markov chain model to be considered a good general model of the ISORA Rayleigh fading channel.

6.2 Review of Contributions

1. We proposed a Markov chain model of the ISORA complex Gaussian fading process, based on an amplitude/rate-of-change state-space. We saw that a first-order Markov chain can effectively model the first-order distribution of the Gaussian fading process, and that the use of an amplitude/rate-of-change state-space resulted in a decaying-oscillatory autocorrelation function of similar shape to that of the theoretical ISORA autocorrelation. However, the decay rate was faster than the theoretical, and the oscillation frequency was slower. Changes to the number of amplitude states in the state-space were seen to affect the goodness of the first-order distribution of the Markov chain model, but had little effect on the autocorrelation function. In contrast, changes to the number of rate states in the state-space had no effect on the first-order distribution of the model, but affected the size of the extrema of the oscillations of the autocorrelation function. Though changes to the state-space size had no significant effect on the decay rate or oscillation frequency of the autocorrelation function, changes to the sample spacing of the model were seen to have a very slight effect on the oscillation frequency. We then observed that increasing the Markov chain order to 2 caused an increase in the oscillation frequency of the autocorrelation function, particularly for larger state-space sizes and large sample spacings.

2. We proposed a method to transform Markov chain models of the ISORA Gaussian fading process into Markov chain models of the ISORA Rayleigh fading process. As a result of this transformation, the size of the Markov chain model of the Rayleigh fading process was the square of the size of the model of the Gaussian process. This meant that the transformation could not practically be applied to second-order Markov chain models of the Gaussian fading process because the resulting Rayleigh fading models were too large to be analyzed, except for very small state-space sizes. When the transformation was applied to first-order Markov chain models of the Gaussian process, we observed that the first-order distribution of the resulting envelope models exhibited errors in the upper range of the distribution, a result of coarseness

in the tails of the first-order distribution of the Markov chain model of the Gaussian fading process. These errors in the first-order distribution of the model resulted in a downward shift of the Markov chain model autocorrelation values as compared to the theoretical ISORA autocorrelation. The transformed Markov chain model autocorrelation function was seen to have a similar decaying-oscillatory shape to that of the theoretical, though with a faster decay rate and slower oscillation frequency. Changes to the sample spacing had no significant effect, but changes to the number of rate states affected the lag between the Markov chain model autocorrelation extrema and those of the theoretical. For a large number of rate states, the Markov chain model autocorrelation was seen to be quite close to the theoretical up to the first maxima, despite the downward shift. We also determined that sample spacing $T = 1.8\text{e-}3$ was the largest sample spacing that still resulted in a reasonably smooth sampling of the autocorrelation function.

3. We gave precise analytical expressions for the elements of a Markov chain model of the ISORA Rayleigh fading channel, with an amplitude/rate-of-change state-space, based directly on the statistics of the ISORA Rayleigh fading process. The analytical expressions cannot be found in closed-form, so we developed a numerical method to approximate the values.

4. We performed a detailed analysis of a first-order Markov chain model of the ISORA Rayleigh fading channel with an amplitude/rate-of-change state-space, in which the Markov chain model elements were calculated directly from the ISORA Rayleigh fading statistics. We saw that the direct calculation method resulted in a Markov chain model whose first-order distribution closely matched the theoretical Rayleigh distribution, without exhibiting the errors in the upper range of the distribution that were observed in the Gaussian envelope model. We observed that the amplitude/rate-of-change state-space continued to result in a decaying-oscillatory autocorrelation function similar in shape to the theoretical ISORA autocorrelation function, though with a faster decay rate and slower oscillation frequency. The direct Rayleigh cal-

culation method also removed the downward shift in autocorrelation values that was seen in the Gaussian envelope model. Changes to the number of amplitude states in the state-space affected the goodness of the first-order distribution of the Markov chain model, but had no significant effect on the autocorrelation function. In contrast, changes to the number of rate states had no effect on the first-order distribution, but affected the size of the extrema of the oscillations of the autocorrelation function, as well as slightly affecting the oscillation frequency. Changes to the sample spacing were seen to have a significant effect on the oscillation frequency, as well as the size of the extrema. As the sample spacing was increased, the oscillation extrema decreased, and the oscillation frequency drew closer to that of the theoretical. We determined that sample spacing $T = 1.8$e-3 was the largest sample spacing that maintained a reasonably smooth sampling of the autocorrelation function, and saw that it also resulted in the Markov chain model of the Rayleigh fading channel whose autocorrelation function was closest to that of the theoretical.

5. We proposed a second-order Markov chain model of the ISORA Rayleigh fading channel with an amplitude/rate-of-change state-space, in which the Markov chain model elements were calculated directly from the ISORA Rayleigh fading statistics. We observed that the increase in Markov chain order caused a definite improvement in the Markov chain model autocorrelation function, causing it to draw much closer to the theoretical ISORA autocorrelation function, particularly for larger sample spacings. We observed that the second-order Markov chain model whose autocorrelation function was closest to that of the theoretical occurred at sample spacing $T = 1.8$e-3. Finally, we observed that, for large sample spacings $T \geq 1.0$e-3, the direct Rayleigh second-order Markov chain model autocorrelation function was closer to that of the theoretical than the autocorrelation function of the Gaussian envelope model. For medium sample spacing $T = 0.5$e-3, we saw that the autocorrelation functions of the direct Rayleigh and Gaussian envelope models were similarly close to the theoretical, assuming a large enough number of rate states, so the direct Rayleigh model was

again preferable due to the improved first-order distribution. At small sample spacings, however, the autocorrelation function of the Gaussian envelope model was seen to be considerably closer to the theoretical, in spite of the limitations in the first-order distribution of that model.

6. We derived an expression for the joint distribution of two correlated Rayleigh random variables and their derivatives, $f_R(r_1, r_2, r_1', r_2')$.

6.3 Suggestions for Future Work

An important result obtained in this thesis is that increasing the Markov chain model order can improve the closeness of its autocorrelation function to that of the theoretical. This suggests that a high enough order Markov chain could effectively act as a general model of the ISORA Rayleigh fading channel. Unfortunately, we have seen that we need a reasonably large number of amplitude states to effectively model the first-order distribution of the channel, and a reasonably large number of rate states generally improves the modeling of the autocorrelation function. Thus, even a second-order Markov chain can quickly become too large to practically use. High-order Markov chains have been modeled with the mixture transition distribution model, discussed by Berchtold and Raftery [54], and an autoregressive model, discussed by Pegram [55]. Both of these models approximate high-order Markov chains, but with a smaller number of parameters, and are worth examining as models of the ISORA Rayleigh fading channel that may improve on the autocorrelation results seen in this thesis.

In Section 4.2.5, we saw that transforming a Markov chain model of the ISORA Gaussian fading process into a Markov chain model of the ISORA Rayleigh fading envelope process resulted in a poor modeling of the first-order Rayleigh distribution, due to coarseness in the tails of the model of the first-order Gaussian distribution. This coarseness was a result of defining the amplitude thresholds to result in an equiprobable state-space, since the tails of the Gaussian distribution are low probability. Selecting the amplitude thresholds to force a better modeling of the Gaussian tails could result in improved modeling of the envelope Rayleigh distribution. We suggest examining different methods of determining the amplitude thresholds and studying whether the first-order distribution of the transformed Gaussian Markov chain model can be improved.

In Chapter 5, we observed that the closeness of the autocorrelation function of the direct Markov chain model of the ISORA Rayleigh fading channel to that of the theoretical improved as the sample spacing was increased, for both first- and second-order Markov chains. It would be desirable to have a Markov chain model whose autocorrelation accurately approximates the theoretical autocorrelation through to the second minima, as we saw for the direct Rayleigh second-order Markov chain model in Figs. 5.18 and 5.20 for $T = 1.8\text{e-}3$, but for smaller values of the sample spacing. Because the autocorrelation function of the Markov chain models for smaller values of T are accurate over only a limited number of samples, we suggest exploring a two-tiered Markov chain model of the ISORA Rayleigh fading channel. The top level of this model would consist of a Markov chain model for a large sample spacing, while the second level would consist of a Markov chain model for a smaller sample spacing that would fill in the time points between the large time instants. This could potentially exploit both the closeness of the large sample spacing model autocorrelation to the theoretical, and the accuracy of smaller sample spacing models over a limited number of points. An example of this transition scheme is shown in Fig. 6.1, where P_1 indicates the Markov chain model transition matrix for large sample spacing T_1, while P_2 indicates the Markov chain model transition matrix for smaller sample spacing T_2. It is not immediately clear whether a Markov chain model using this two-tiered system would be stationary, but it merits examination.

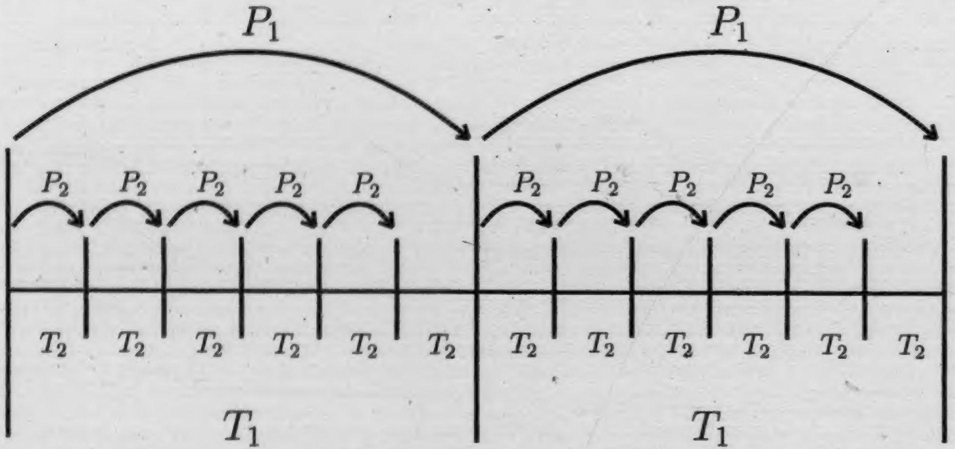
P_1
P_1
P_2
P_2
P_2
P_2
P_2
P_2
P_2
P_2
P_2
P_2
T_2
T_2
T_2
T_2
T_2
T_2
T_2
T_2
T_2
T_2
T_2
T_2
T_1
T_1

Fig. 6.1. Example of the proposed two-tiered Markov chain model transition scheme.

Appendix A

Numerical Integration of Multivariate Gaussian Distributions

To integrate the numerator of (4.7), we make use of the algorithm proposed by Genz [52] to perform numerical integration of the multivariate Gaussian distribution with arbitrary covariance matrix Σ over a hypercube. His algorithm consists of a series of three transformations that have the effect of placing the multivariate Gaussian distribution in a form better suited to typical multivariate numerical integration routines. We sketch the algorithm transformations here.

The multivariate Gaussian integral over a hypercube has the general form

$$I = \frac{1}{\sqrt{(2\pi)^m \Delta_\Sigma}} \int_{a_1}^{b_1} \int_{a_2}^{b_2} \cdots \int_{a_m}^{b_m} e^{-\frac{1}{2}\mathbf{x}^T \Sigma^{-1} \mathbf{x}} d\mathbf{x} \tag{A.1}$$

where $\mathbf{x} = [x_1, x_2, \ldots, x_m]^T$, Σ is the covariance matrix, and Δ_Σ is the determinant of Σ. The integration limits can be finite or infinite values.

The first transformation is a simple Cholesky decomposition transformation, $\mathbf{x} = C\mathbf{y}$, where $CC^T = \Sigma$. Thus, $\mathbf{x}^T \Sigma^{-1} \mathbf{x} = \mathbf{y}^T C^T C^{-1^T} C^{-1} C \mathbf{y} = \mathbf{y}^T \mathbf{y}$, and $d\mathbf{x} = \Delta_C d\mathbf{y} = \Delta_\Sigma^{1/2} d\mathbf{y}$, giving the transformed multivariate Gaussian integral as

$$I = \frac{1}{\sqrt{(2\pi)^m}} \int_{a'_1}^{b'_1} e^{-\frac{y_1^2}{2}} \int_{a'_2(y_1)}^{b'_2(y_1)} e^{-\frac{y_2^2}{2}} \cdots \int_{a'_m(y_1,\ldots,y_{m-1})}^{b'_m(y_1,\ldots,y_{m-1})} e^{-\frac{y_m^2}{2}} d\mathbf{y} \tag{A.2}$$

where $a'_i(y_1, \ldots, y_{i-1}) = (a_i - \sum_{j=1}^{i-1} c_{ij} y_j)/c_{ii}$ and $b'_i(y_1, \ldots, y_{i-1}) = (b_i - \sum_{j=1}^{i-1} c_{ij} y_j)/c_{ii}$.

This implies an obvious second transformation, $y_i = \Phi^{-1}(z_i)$, where

$$\Phi(y) = \frac{1}{\sqrt{2\pi}} \int_{-\infty}^{y} e^{-\frac{1}{2}x^2} dx \tag{A.3}$$

is the Gaussian distribution function. This transformation gives the multivariate Gaussian integral as

$$I = \int_{d_1}^{e_1} \int_{d_2(z_1)}^{e_2(z_1)} \cdots \int_{d_m(z_1,\ldots,z_{m-1})}^{e_m(z_1,\ldots,z_{m-1})} d\mathbf{z} \tag{A.4}$$

where

$$d_i(z_1,\ldots,z_{i-1}) = \Phi((a_i - \sum_{j=1}^{i-1} c_{ij}\Phi^{-1}(z_i))/c_{ii})$$

$$e_i(z_1,\ldots,z_{i-1}) = \Phi((b_i - \sum_{j=1}^{i-1} c_{ij}\Phi^{-1}(z_i))/c_{ii}).$$

The final transformation simplifies the integration limits. By using the transformation $z_i = d_i + w_i(e_i - d_i)$, the final form of the multivariate Gaussian integral is given by

$$I = (e_1 - d_1) \int_0^1 (e_2 - d_2) \cdots \int_0^1 (e_m - d_m) \int_0^1 d\mathbf{w} \tag{A.5}$$

where

$$d_i = \Phi((a_i - \sum_{j=1}^{i-1} c_{ij}\Phi^{-1}(d_j + w_j(e_j - d_j)))/c_{ii}) \tag{A.6}$$

$$e_i = \Phi((b_i - \sum_{j=1}^{i-1} c_{ij}\Phi^{-1}(d_j + w_j(e_j - d_j)))/c_{ii}). \tag{A.7}$$

The integral over w_m can be performed immediately because d_m and e_m don't depend on w_m, so these transformations have the added bonus of reducing the integration dimension by one.

The final version of the multivariate Gaussian integral may look much more complicated than the initial version, but the new expression can be numerically integrated using standard integration methods to much better accuracy than the original version. In [52], Genz finds that a simple Monte Carlo method will give reasonably accurate results in a short time period for reasonably small-dimensioned problems. For larger problems, an adaptive algorithm [56], [57] gives better results.

The particular implementation of this algorithm that we make use of in Chapter 4 is the QSIMVNV software package, which implements this algorithm with a quasi-random number-theoretic integration method [58], [59]. This package is available at Genz's website (http://www.math.wsu.edu/faculty/genz/homepage). The use of QSIMVNV permits efficient performance of the many multivariate Gaussian integrations we need, with an error of 10^{-6}.

Appendix B

Numerical Integration of the Joint Distribution of Correlated Rayleigh Random Variables and Their Derivatives

B.1 Two Correlated Rayleigh Random Variables

We encountered the integration of the joint distribution of two correlated Rayleigh random variables and their derivatives, $f_R(r_1, r_2, r_1', r_2')$, in the numerator of (5.4), as well as (5.6). We derived an expression for this joint distribution in Section 2.2.4, where we found that it can be expressed as (2.22). However, attempts to numerically integrate this expression using numerical cubature rules given by Stroud [60], as well as the adaptive algorithms of van Dooren and de Ridder [56], and Genz and Malik [57], fail to approximate the integral to a reasonable accuracy. In fact, the accuracy of the results is generally so poor that the values attained using these methods are useless. Instead, we note from the derivation of distribution (2.22) that it was obtained via a reasonably simple transformation of variables applied to a multivariate Gaussian distribution. Thus, we will approximate the integral of the joint distribution of two correlated Rayleigh random variables and their derivatives using the Monte Carlo method [53].

The desired integral can be well approximated by the empirical average

$$\frac{1}{N}\sum_{q=1}^{N} I_D(R_q) \tag{B.1}$$

where the R_q are independent samples with distribution $f_R(r_1, r_2, r_1', r_2')$, $I_D(\cdot)$ is the indicator function

$$I_D(R) = \begin{cases} 1\,, & R \in D \\ 0\,, & R \notin D \end{cases} \tag{B.2}$$

and D is the region of integration. Thus, the integration problem is reduced to one of generating N independent samples with distribution $f_R(r_1, r_2, r_1', r_2')$.

To generate a sample with this distribution, we recall from Section 2.2.4 that (2.22) was derived by forming the multivariate Gaussian distribution

$$f_G(T_{c_1}, T_{c_1}', T_{c_2}, T_{c_2}', T_{s_1}, T_{s_1}', T_{s_2}, T_{s_2}') \tag{B.3}$$

and applying the transformation of variables (2.21). Thus, we can generate a sample with distribution $f_R(r_1, r_2, r_1', r_2')$ by generating a sample with distribution (B.3) and transforming it.

Define random vectors $\mathbf{T_c} = [T_{c_1}, T_{c_1}', T_{c_2}, T_{c_2}']^T$ and $\mathbf{T_s} = [T_{s_1}, T_{s_1}', T_{s_2}, T_{s_2}']^T$. In Section 2.2.4, we saw that these are independent Gaussian random vectors, each with covariance matrix

$$\Sigma = \begin{pmatrix} b_0 & 0 & g(T) & g'(T) \\ 0 & b_2 & -g'(T) & -g''(T) \\ g(T) & -g'(T) & b_0 & 0 \\ g'(T) & -g''(T) & 0 & b_2 \end{pmatrix} \tag{B.4}$$

where $g(\tau) = b_0 J_0(2\pi f_D \tau)$, and T is the spacing between the time instants indicated by subscripts 1 and 2. So, we can generate a sample with distribution (B.3) by generating samples of Gaussian vectors $\mathbf{T_c}$ and $\mathbf{T_s}$. To do this, we first generate samples of random variables $X_1, \ldots, X_8$, which are all independent, unit variance Gaussian random variables. This can be done using the well-known Box-Muller transform [61]. First, we generate samples of U_1 and U_2, which are random variables uniformly distributed between 0 and 1.

Then, we form $V_1 = 2U_1 - 1$, $V_2 = 2U_2 - 1$, and $S = V_1^2 + V_2^2$. If $S > 1$, then we start over by regenerating U_1 and U_2, otherwise, we form

$$X_1 = \sqrt{\frac{-2\log S}{S}}V_1, \quad X_2 = \sqrt{\frac{-2\log S}{S}}V_2 \tag{B.5}$$

so X_1 and X_2 will be independent, unit variance Gaussian samples. This process is repeated until we have sample values for $X_1, \ldots, X_8$, then, we form Gaussian sample vectors $\mathbf{X_1} = [X_1, X_2, X_3, X_4]^T$ and $\mathbf{X_2} = [X_5, X_6, X_7, X_8]^T$. Finally, we can transform $\mathbf{X_1}$ and $\mathbf{X_2}$ into Gaussian sample vectors with covariance matrix (B.4) by first finding the matrix C such that $\Sigma = CC^T$. Then, samples of Gaussian vectors $\mathbf{T_c}$ and $\mathbf{T_s}$ are formed via the linear transformations [62]

$$\mathbf{T_c} = C\mathbf{X_1}, \quad \mathbf{T_s} = C\mathbf{X_2}. \tag{B.6}$$

We can rewrite the transformation of variables (2.21) as

$$r_1 = \sqrt{T_{c_1}^2 + T_{s_1}^2} \tag{B.7a}$$

$$r_2 = \sqrt{T_{c_2}^2 + T_{s_2}^2} \tag{B.7b}$$

$$r_1' = \frac{T_{c_1}T_{c_1}' + T_{s_1}T_{s_1}'}{\sqrt{T_{c_1}^2 + T_{s_1}^2}} \tag{B.7c}$$

$$r_2' = \frac{T_{c_2}T_{c_2}' + T_{s_2}T_{s_2}'}{\sqrt{T_{c_2}^2 + T_{s_2}^2}}. \tag{B.7d}$$

By applying this transformation to the Gaussian sample vectors $\mathbf{T_c}$ and $\mathbf{T_s}$, we get a single sample with distribution $f_R(r_1, r_2, r_1', r_2')$.

After generating a large number of these samples, we estimate the integral of joint distribution $f_R(r_1, r_2, r_1', r_2')$ using (B.1), which is essentially the fraction of sample points that are within the integration limits. An added benefit of this method is that all integration values over the partitioned space can be approximated from the same data set. It should be noted that during actual implementation, we used $N = 6.5 \times 10^8$ points, which gives a confidence interval of 10^{-5}, 99% of the time.

B.2 Three Correlated Rayleigh Random Variables

We encountered the integration of the joint distribution of three correlated Rayleigh random variables and their derivatives, $f_R(r_1, r_2, r_3, r_1', r_2', r_3')$, in the numerator of (5.7). This integral will be performed using the Monte Carlo method, in much the same way as we described in Appendix B.1. The integral can be well approximated by the empirical average (B.1), so the integration problem reduces to one of generating independent samples with distribution $f_R(r_1, r_2, r_3, r_1', r_2', r_3')$. This can be done using simple extensions of the method described in Appendix B.1.

Define $\mathbf{T_c} = [T_{c_1}, T_{c_1}', T_{c_2}, T_{c_2}', T_{c_3}, T_{c_3}']^T$ and $\mathbf{T_s} = [T_{s_1}, T_{s_1}', T_{s_2}, T_{s_2}', T_{s_3}, T_{s_3}']^T$. From the correlation structure of the ISORA Rayleigh fading channel (2.9), we know that these are independent Gaussian random vectors, each with covariance matrix

$$\Sigma = \begin{pmatrix} b_0 & 0 & g(T) & g'(T) & g(2T) & g'(2T) \\ 0 & b_2 & -g'(T) & -g''(T) & -g'(2T) & -g''(2T) \\ g(T) & -g'(T) & b_0 & 0 & g(T) & g'(T) \\ g'(T) & -g''(T) & 0 & b_2 & -g'(T) & -g''(T) \\ g(2T) & -g'(2T) & g(T) & g'(T) & b_0 & 0 \\ g'(2T) & -g''(2T) & g'(T) & -g''(T) & 0 & b_2 \end{pmatrix}$$

where $g(\tau) = b_0 J_0(2\pi f_D \tau)$, and T is the spacing between the time instants indicated by subscripts 1, 2, and 3. We can generate samples of random vectors $\mathbf{T_c}$ and $\mathbf{T_s}$ using the Gaussian random vector generating method described in Appendix B.1. We can then transform these Gaussian samples to get a sample with distribution $f_R(r_1, r_2, r_3, r_1', r_2', r_3')$ by applying the transformation

$$r_3 = \sqrt{T_{c_3}^2 + T_{s_3}^2} \tag{B.8a}$$

$$r_3' = \frac{T_{c_3} T_{c_3}' + T_{s_3} T_{s_3}'}{\sqrt{T_{c_3}^2 + T_{s_3}^2}} \tag{B.8b}$$

in addition to transformation (B.7).

After generating a large number of these samples, we estimate the integral of joint distribution $f_R(r_1, r_2, r_3, r_1', r_2', r_3')$ using (B.1). As we mentioned in Appendix B.1, using this method allows us to approximate the values of all integrations over a partitioned space from the same data set.

References

[1] H.-P. Lin and M.-J. Tseng, "Two-layer multistate Markov model for modeling a 1.8GHz narrow-band wireless propagation channel in urban Taipei city," *IEEE Transactions on Vehicular Technology*, vol. 54, no. 2, pp. 435–446, Mar. 2005.

[2] M. Rossi, L. Badia, and M. Zorzi, "SR ARQ delay statistics on N-state Markov channels with non-instantaneous feedback," *IEEE Transactions on Wireless Communications*, vol. 5, no. 6, pp. 1526–1536, June 2006.

[3] T. S. Rappaport, *Wireless Communications Principles and Practice*, 2nd ed. Upper Saddle River, NJ: Prentice-Hall, 2002.

[4] P. Bergamo, D. Maniezzo, A. Giavanardi, G. Mazzini, and M. Zorzi, "Improved Markov model for Rayleigh fading envelope," *Electronics Letters*, vol. 38, no. 10, pp. 477–478, May 2002.

[5] F. Swarts and H. C. Ferreira, "Markov characterization of channels with soft decision outputs," *IEEE Transactions on Communications*, vol. 41, no. 5, pp. 678–682, May 1993.

[6] C. C. Tan and N. C. Beaulieu, "On first-order Markov modeling for the Rayleigh fading channel," *IEEE Transactions on Communications*, vol. 48, no. 12, pp. 2032–2040, Dec. 2000.

[7] R. H. Clarke, "A statistical theory of mobile-radio reception," *Bell System Technical Journal*, vol. 47, pp. 957–1000, 1968.

[8] A. Papoulis and S. U. Pillai, *Probability, Random Variables and Stochastic Processes*, 4th ed. New York, NY: McGraw-Hill, 2002.

[9] W. C. Jakes, *Microwave Mobile Communications*. New York, NY: John Wiley & Sons, 1974.

[10] M. Abramowitz and I. A. Stegun, *Handbook of Mathematical Functions with Formulas, Graphs, and Mathematical Tables*, 9th ed. New York, NY: Dover Publications, 1972.

[11] S. O. Rice, "Mathematical analysis of random noise," *Bell System Technical Journal*, vol. 23, pp. 282–332, 1944.

[12] D. Middleton, *An Introduction to Statistical Communication Theory*. New York, NY: IEEE Press, 1996.

[13] S. O. Rice, "Distribution of the duration of fades in radio transmission: Gaussian noise model," *Bell System Technical Journal*, vol. 37, pp. 581–635, 1958.

[14] W. B. Davenport Jr. and W. L. Root, *An Introduction to the Theory of Random Signals and Noise*. New York, NY: IEEE Press, 1958.

[15] R. H. Clarke and W. L. Khoo, "3-D mobile radio channel statistics," *IEEE Transactions on Vehicular Technology*, vol. 46, no. 3, pp. 798–799, Aug. 1997.

[16] J. D. Parsons, *The Mobile Radio Propagation Channel*, 2nd ed. New York, NY: John Wiley & Sons, 2000.

[17] S. O. Rice, "Statistical properties of a sine wave plus random noise," *Bell System Technical Journal*, vol. 27, pp. 109–157, 1948.

[18] Y. Chen and N. C. Beaulieu, "Maximum likelihood estimation of the K factor in Ricean fading channels," *IEEE Communications Letters*, vol. 9, no. 12, pp. 1040–1042, Dec. 2005.

[19] K. K. Talukdar and W. D. Lawing, "Estimations of the parameters of the Rice distribution," *Journal of the Acoustical Society of America*, vol. 89, pp. 1193–1197, Mar. 1991.

[20] L. J. Greenstein, D. G. Michelson, and V. Erceg, "Moment-based estimation of the Ricean K-factor," *IEEE Communications Letters*, vol. 3, pp. 175–176, June 1999.

[21] G. Azemi, B. Senadji, and B. Boashash, "Ricean k-factor estimation in mobile communication systems," *IEEE Communications Letters*, vol. 8, pp. 617–619, Oct. 2004.

[22] M. Nakagami, "The m-distribution, a general formula of intensity distribution of rapid fading," in *Statistical Methods in Radio Wave Propagation*, W. G. Hoffman, Ed., pp. 3–36. Pergamon Press, Oxford, England, 1960.

[23] H. Suzuki, "A statistical model for urban radio channel model," *IEEE Transactions on Communications*, vol. 25, pp. 673–680, 1977.

[24] J. Cheng and N. C. Beaulieu, "Maximum-likelihood based estimation of the Nakagami m parameter," *IEEE Communications Letters*, vol. 5, no. 3, pp. 101–103, Mar. 2001.

[25] A. Abdi and M. Kaveh, "Performance comparison of three different estimators for the Nakagami m parameter using Monte Carlo simulation," *IEEE Communications Letters*, vol. 4, pp. 119–121, Apr. 2000.

[26] J. G. Kemeny and J. L. Snell, *Finite Markov Chains*. New York, NY: Springer, 1976.

[27] J. G. Kemeny, J. L. Snell, and A. W. Knapp, *Denumerable Markov Chains*. New York, NY: Springer, 1976.

[28] S. Karlin and H. M. Taylor, *A Second Course in Stochastic Processes*. New York, NY: Academic Press, 1981.

[29] P. Brémaud, *Markov Chains: Gibbs Fields, Monte Carlo Simulation, and Queues*. New York, NY: Springer, 1999.

[30] E. N. Gilbert, "Capacity of a burst-noise channel," *Bell System Technical Journal*, vol. 39, no. 9, pp. 1253–1265, Sept. 1960.

[31] E. O. Elliott, "Estimates of error rates for codes on burst-noise channels," *Bell System Technical Journal*, vol. 42, no. 9, pp. 1977–1997, Sept. 1963.

[32] B. D. Fritchman, "A binary channel characterization using partitioned Markov chains," *IEEE Transactions on Information Theory*, vol. 13, no. 2, pp. 221–227, 1967.

[33] L. R. Rabiner and B. H. Juang, "An introduction to hidden Markov models," *IEEE ASSP Magazine*, vol. 3, pp. 4–16, Jan. 1986.

[34] A. C. Atkinson and M. C. Pearce, "The computer generation of beta, gamma and normal random variables," *Journal of the Royal Statistical Society*, vol. 139, pp. 431–461, 1976.

[35] G. L. Stüber, *Principles of Mobile Communications*, 2nd ed. Boston, MA: Kluwer, 2001.

[36] H. S. Wang and N. Moayeri, "Finite-state Markov channel - a useful model for radio communication channels," *IEEE Transactions on Vehicular Technology*, vol. 44, no. 1, pp. 163–171, 1995.

[37] W. C. Y. Lee, *Mobile Communications Engineering*. New York, NY: McGraw-Hill, 1982.

[38] M. F. Pop and N. C. Beaulieu, "Limitations of sum-of-sinusoids fading channel simulators," *IEEE Transactions on Communications*, vol. 49, no. 4, pp. 699–708, Apr. 2001.

[39] H. S. Wang and P.-C. Chang, "On verifying the first-order Markovian assumption for a Rayleigh fading channel model," *IEEE Transactions on Vehicular Technology*, vol. 45, no. 2, pp. 353–357, May 1996.

[40] R. G. Gallager, *Information Theory and Reliable Communication*. New York, NY: Wiley, 1968.

[41] M. Zorzi, R. R. Rao, and L. B. Milstein, "ARQ error control for fading mobile radio channels," *IEEE Transactions on Vehicular Technology*, vol. 46, no. 2, pp. 445–455, May 1997.

[42] A. S. Tanenbaum, *Computer Networks*. Englewood Cliffs, NJ: Prentice-Hall, 1989.

[43] J. C.-I. Chuang, "Comparison of two ARQ protocols in a Rayleigh fading channel," *IEEE Transactions on Vehicular Technology*, vol. 39, pp. 367–373, Nov. 1990.

[44] J. I. Marcum, "A statistical theory of target detection by pulsed radar," *IEEE Transactions on Information Theory*, vol. 6, no. 2, pp. 59–267, Apr. 1960.

[45] Q. Zhang and S. A. Kassam, "Finite-state Markov model for Rayleigh fading channels," *IEEE Transactions on Communications*, vol. 47, no. 11, pp. 1688–1692, Nov. 1999.

[46] M. R. Hueda and C. E. Rodríguez, "A new information theoretic test of the Markov property of block errors in fading channels," *IEEE Transactions on Vehicular Technology*, vol. 54, no. 2, pp. 425–434, Mar. 2005.

[47] T. Cover and J. Thomas, *Elements of Information Theory*. New York, NY: Wiley, 1991.

[48] H. Liu and M. E. Zarki, "Performance of H.263 video transmission over wireless channels using hybrid ARQ," *IEEE Journal on Selected Areas in Communications*, vol. 15, no. 9, pp. 1775–1786, Dec. 1997.

[49] F. Babich, "Performance of hybrid ARQ schemes for the fading channel," *IEEE Transactions on Communications*, vol. 50, no. 12, pp. 1882–1885, Dec. 2002.

[50] L. Galluccio, F. Licandro, G. Morabito, and G. Schembra, "An analytical framework for the design of intelligent algorithms for adaptive-rate MPEG video encoding in

next-generation time-varying wireless networks," *IEEE Journal on Selected Areas in Communications*, vol. 23, no. 2, pp. 369–384, Feb. 2005.

[51] M. Rossi, L. Badia, and M. Zorzi, "Exact statistics of ARQ packet delivery delay over Markov channels with finite round-trip delay," in *Proceedings of IEEE Globecom 2003*, vol. 6, pp. 3356–3360.

[52] A. Genz, "Numerical computation of multivariate normal probabilities," *Journal of Computational and Graphical Statistics*, vol. 1, pp. 141–149, 1992.

[53] C. P. Robert and G. Casella, *Monte Carlo Statistical Methods*. New York, NY: Springer-Verlag New York, Inc., 1999.

[54] A. Berchtold and A. E. Raftery, "The mixture transition distribution model for high-order Markov chains and non-Gaussian time series," *Statistical Science*, vol. 17, no. 3, pp. 328–356, 2002.

[55] G. G. S. Pegram, "An autoregressive model for multilag Markov chains," *Journal of Applied Probability*, vol. 17, pp. 350–362, 1980.

[56] P. van Dooren and L. de Ridder, "An adaptive algorithm for numerical integration over an n-dimensional cube," *Journal of Computational and Applied Mathematics*, vol. 2, no. 3, pp. 207–210, 1976.

[57] A. C. Genz and A. A. Malik, "An adaptive algorithm for numerical integration over an N-dimensional rectangular region," *Journal of Computational and Applied Mathematics*, vol. 6, no. 4, pp. 295–298, 1980.

[58] H. Niederreiter, "On a number-theoretical integration method," *Aequationes Mathematicae*, vol. 8, pp. 304–311, 1972.

[59] R. Cranley and T. N. L. Patterson, "Randomization of number theoretic methods for multiple integration," *SIAM Journal on Numerical Analsis*, vol. 13, pp. 904–914, 1976.

[60] A. H. Stroud, *Approximate Calculation of Multiple Integrals*. Englewood Cliffs, NJ: Prentice-Hall, 1971.

[61] S. M. Ross, *Simulation*, 3rd ed. San Diego, CA: Academic Press, 2002.

[62] M. C. Jeruchim, P. Balaban, and K. S. Shanmugan, *Simulation of Communication Systems: Modeling, Methodology, and Techniques*, 2nd ed. New York, NY: Kluwer Academic/Plenum Publishers, 2000.